Polymorphism in Bacterial Flagella Suspensions

A Dissertation

Presented to

The Faculty of the Graduate School of Arts and Sciences

Brandeis University

Martin A. Fisher School of Physics

Zvonimir Dogic, Martin A. Fisher School of Physics, Advisor

In Partial Fulfillment

of the Requirements for the Degree

Doctor of Philosophy

by

Walter J. Schwenger

February, 2017

This dissertation, directed and approved by Walter J. Schwenger's committee, has been accepted and approved by the Graduate Faculty of Brandeis University in partial fulfillment of the requirements for the degree of:

DOCTOR OF PHILOSOPHY

Eric Chasalow, Dean of the Graduate School of Arts & Sciences

Dissertation Committee:

Zvonimir Dogic, Martin A. Fisher School of Physics, Chair

Benjamin Rogers, Martin A. Fisher School of Physics

Jeffrey Urbach, Department of Physics, Georgetown University

Acknowledgments

The years I have spent as a graduate student have simultaneously been some of the most rewarding and challenging of my life. There are too many individuals that have contributed to my work and well being during this time to name them all. I would first and foremost like to thank my advisor, Zvonimir Dogic for his patience, understanding, and scientific flexibility.

I would also like to thank the other members of the Dogic lab. The environment in the lab was always friendly, helpful, and genuinely fun. I would particularly like to thank Sevim Yardimci for taking me under her wing and teaching me the ropes in how to work with bacterial flagella and always being available to provide insight and experience.

Finally, I would like to thank all of my friends and family for their continued support and understanding. My parents, Walter and LuAnn, as well as my brother, Paul, have always been there when I needed them most. Most importantly, I would like to thank my girlfriend, Erica, for all her love and patience during my time in graduate school. I feel truly honored to be in the company of the great people I have had the opportunity to experience in my life during this time and I will never forget any of you.

Thank you for everything,

Walter

Abstract

Polymorphism in Bacterial Flagella Suspensions

A dissertation presented to the Faculty of
the Graduate School of Arts and Sciences of
Brandeis University, Waltham, Massachusetts

by Walter J. Schwenger

Bacterial flagella are a type of biological polymer studied for its role in bacterial motility and the polymorphic transitions undertaken to facilitate the run and tumble behavior. The naturally rigid, helical shape of flagella gives rise to novel colloidal dynamics and material properties. This thesis studies methods in which the shape of bacterial flagella can be controlled using *in vitro* methods and the changes the shape of the flagella have on both single particle dynamics and bulk material properties. We observe individual flagellum in both the dilute and semidilute regimes to observe the effects of solvent condition on the shape of the filament as well as the effect the filament morphology has on reptation through a network of flagella. In addition, we present rheological measurements showing how the shape of filaments effects the bulk material properties of flagellar suspensions. We find that the individual particle dynamics in suspensions of flagella can vary with geometry from needing to reptate linearly via rotation for helical filaments to the prevention of long range diffusion for block copolymer filaments. Similarly, for bulk material properties of flagella suspensions, helical geometries show a dramatic enhancement in elasticity over straight filaments while block copolymers form an elastic gel without the aid of crosslinking agents.

Contents

List of Figures

Chapter 1

Introduction

Many everyday physical systems are based on colloidal systems, both biological and artificial. Colloidal interactions are important for understanding systems such as inks [1], dyed plastics [2], foods [3–5], and the interior of cells [6, 7] can all be described as colloidal in nature. In general, colloidal suspensions consist of a mixture of two types of material in which one material are microscopic particles that are insoluble in the other. One of the most common types of colloidal solutions, in which a solid material is dispersed in a liquid medium is referred to as a sol. Solid colloidal particles need to be a sufficiently small size so that Brownian motion is a strong enough force to prevent sedimentation. For this reason, colloidal particles typically range in size from 10 nm to 10 µm [8].

Colloidal suspensions have been of interest in biological systems due to their prevalence [9–13]. The cytosol is a dense suspension of a wide array of assorted proteins, polymers, organelles, vesicles, etc. In particular, biopolymers are key ingredients for many of the vital functions cells perform for continued survival and replication. Biopolymers like actin and microtubules create a network of entangled polymers that help to provide structural rigidity to cells as well as the means by which motor proteins transport cargo around the cell.

Another biopolymer, DNA, contains the genetic information necessary for protein synthesis and is organized into densely packed chromosomes that, when unpacked, entangle with one another inside the cell nucleus.

These biopolymers are typically classified into one of three categories by the ratio of their persistence length, L_p, to their contour length, L as shown in Figure 1.1 [14]. The persistence length gives a length over which thermal energy can significantly bend the filament whereas the contour length is simply the full length of the polymer if it were stretched straight [15, 16]. If $L_p/L \ll 1$, the filament is in the flexible regime such as is the case with DNA [17]. If $L_p/L \gg 1$, the filament is in the stiff regime such as is the case with microtubules [18]. Finally, if $L_p/L \sim 1$, the filament is considered semi-flexible such as actin filaments [18]. In polymer solution studies, these three different filaments are very important, not only because of the biological role they serve, but also because they are relatively easy to purify and study *in vitro*.

Here we review the work done on these three different types of biological polymer systems. We will pay particular attention to the material properties that arise due to the differences in stiffness at the single particle level. We will then introduce a fourth type of filament, bacterial flagella, that will be the focus of the rest of this thesis.

1.1 Flexible Polymers, DNA

DNA plays a vital role in the cell, carrying the information necessary for cell growth, reproduction, and survival from one generation of cells to the next. In eukaryotic cells, almost all the DNA is confined to the nucleus. This means that within the nucleus, the concentration of DNA can reach quite high levels [20]. The dynamics of how a dense DNA suspension behaves as a material, in addition to being a model for flexible polymer solutions, is also a

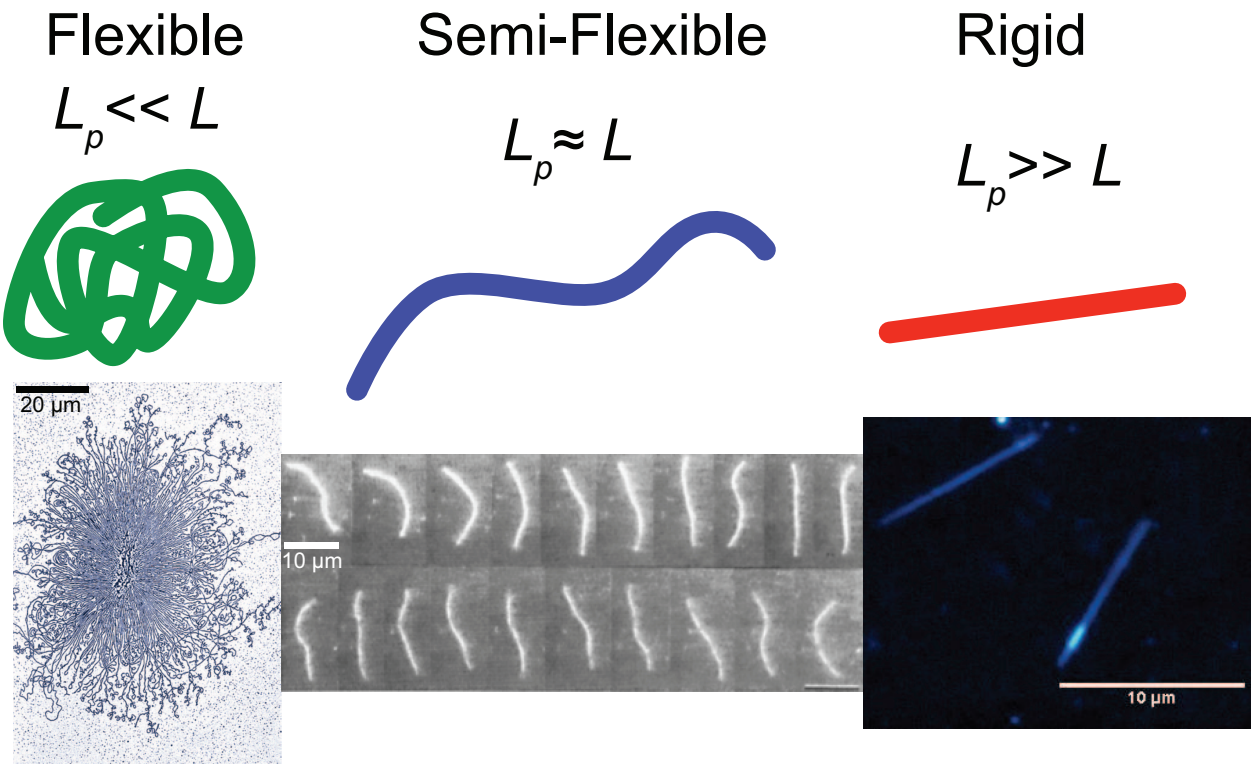

Figure 1.1: Illustration showing the three different types of biopolymers as determined by the persistence length. From left to right: electron micrograph showing DNA that burst forth from a lysed E. coli. [19], fluorescent images showing a time series of thermal fluctuations in an actin filament [18], darkfield image of a microtubule.

question of biological importance. DNA has a persistence length of 50 nm [17], whereas its contour length can be on the order of tens of centimeters. This means that DNA is firmly in the flexible limit because $L_p/L \ll 1$. The way that flexible polymers can get entangled and give rise to non-trivial bulk behavior was described by de Gennes as the reptation model and later refined by Doi and Edwards [21, 22].

The viscoelastic nature of flexible polymers is due to the way that each filament can become entangled with its nearest neighbors [23]. Flexible filaments are able to wrap around neighboring filaments but because they are unable to pass through them, take time to break free via diffusion. These entanglements last only for a time scale given by the properties of the flexible polymers. This is due to the fact that as a polymer is diffusing through a dense network, the volume in which it can freely diffuse is given by a tube around the contour of the polymer that extends out as far as the nearest neighbor as shown in Figure 1.2. The shape and size of this tube helps determine how long the filament will take to diffuse out of the tube. The single molecule dynamics of reptation in flexible filaments have experimentally been shown using fluorescently labeled λ-phage DNA in a dense suspension of unlabeled DNA [24]. The DNA was observed to undergo a random walk motion and the measured diffusion coefficient is consistent with the predictions of reptation theory.

DNA provides an excellent model system with which to study the behavior of flexible filament suspensions because biological systems produce it in great quantities and it is relatively easy to purify and isolate. Rheological studies of DNA suspensions show clear viscoelastic behavior [26, 27]. In order to quantify viscoelastic material properties, two quantities are typically measured: the loss modulus (alternatively G'' or viscous modulus) and the storage modulus (alternatively G' or elastic modulus). When the loss modulus is greater than the storage modulus, the material behaves more similarly to a viscous fluid than it does an elastic solid. Similarly, when the storage modulus is greater than the loss modulus, the

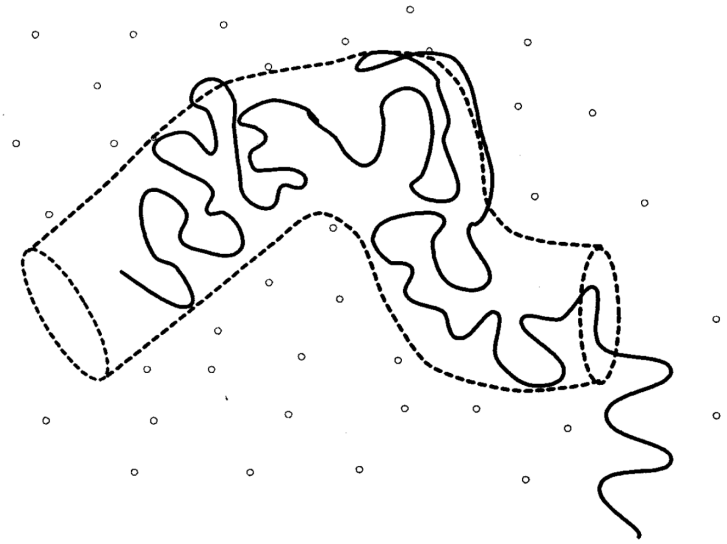

Figure 1.2: Schematic representation of a flexible polymer (solid line) confined inside a tube (dashed line) defined by the nearest neighbors of the polymer (small circles). Figure reprinted from [25].

material responds more like an elastic solid than it does a viscous fluid. In most real-world materials, the rate at which a sample is sheared changes the way in which it responds to that deformation meaning that G' and G'' are frequency dependent.

In a typical polymer solution like DNA, small oscillatory deformations that happen on a time scale much shorter than the average entanglement time of the system lead to a response that is dominated by the loss modulus. This means that, similar to a viscous fluid, energy is dissipated through viscous flow rather than stored via elastic deformation like in a solid. For small oscillatory deformations that happen at a time scale much longer than the average entanglement time of the system, the response is dominated by the loss modulus again. This is because the DNA polymers have time to relax and find a new equilibrium with the applied strain at such long time scales, essentially being able to flow like a liquid. However, for intermediate timescales between the two extremes, the response of the material is dominated by the storage modulus. This means that the suspension is behaving similarly

to a more solid material, able to react elastically in opposition to attempted deformations [28].

1.2 Semi-Flexible Polymers, Actin Filaments

Actin filaments are important structural elements to many kinds of cells. In addition to providing structural rigidity through network formation, actin filaments also serve many other purposes in different types of cells; aiding in processes such as endocytosis, cytokinesis, and morphogenesis [29]. Filamentous actin (F-actin) polymers in cells typically have contour lengths ranging from 1-10 µm [30]. This is on the same order as the persistence length of F-actin, 17.7 µm, meaning that actin filaments are classified as semi-flexible polymers [31]. This is especially the case for in vitro experiments where typical contour lengths are around 20 µm for F-actin [18, 32, 33]. Semi-flexible polymer solutions still undergo similar entanglements as that of flexible polymers, though not to the same degree [34, 35]. Because the persistence length of actin filaments is larger, it is easier to image the conformations that filaments assume when in a concentrated solution. This enables direct visualization of semi-flexible filaments undergoing reptation as shown in Figure 1.3 [34, 35].

In a cellular environment, there is a class of proteins called actin binding proteins (ABPs) that bind to actin and can act as crosslinkers, joining actin filaments at a certain point [36–38]. Rheological studies performed on actin filaments *in vitro* show that crosslinking can make a large difference in the elasticity of the actin network. Actin solutions without ABPs still show viscoelasticity like the flexible filament solutions of DNA. However, with the introduction of ABPs crosslinking the filaments, the elasticity of the network is increased dramatically [39]. The ability for actin filaments to significantly deform without breaking combined with the crosslinking properties provided by ABPs means that actin networks

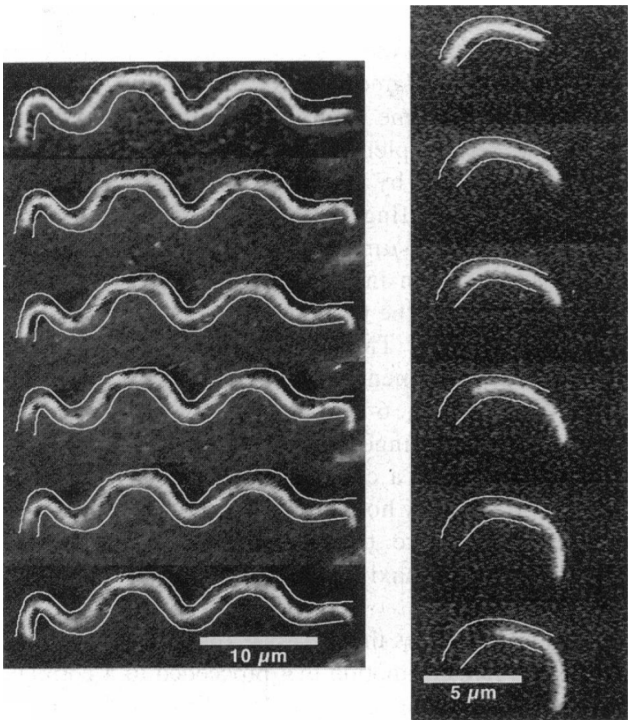

Figure 1.3: Fluorescently labeled actin filaments undergoing reptation in a concentrated solution of unlabeled filaments. The thin white lines are added to indicated the extents of the tube inside which the filaments can diffuse freely. Both time sequences represent a total elapsed time of 48 s. The filament on the left has a total contour length of 40 µm while the filament on the right has a contour length of 6.9 µm. This time series shows how much faster the shorter filament can reptate through the network as compared to the longer filament. Images taken from [35].

provide more elasticity than other cytoskeletal components such as microtubules and intermediate filaments, rigid and flexible polymers respectively. This is borne out of experimental results that show the storage modulus of crosslinked actin networks grows with filament concentration according to a power law with an exponent of $v = 2.2\text{-}2.5$ compared with just $v = 1.4$ for non-crosslinked filaments [39–41].

1.3 Stiff Polymers, Microtubules

Microtubules, like actin filaments, are one of the key ingredients of the cytoskeleton that provide cells with rigidity as well as provide a scaffold for cellular transport. However, microtubules are not semi-flexible like actin filaments. Despite the potentially very long contour lengths of microtubules in cells, up to the order of 10 µm, the persistence length for these filaments is much larger, on the order of one millimeter [18, 31]. This separation of scales satisfies the requirement for microtubules to be considered a stiff polymer, so that thermal energies are insufficient to cause significant bending. Like actin filaments, there are proteins that act as crosslinkers in microtubule networks [42, 43]. These microtubule-associated proteins (MAPs) can significantly change the material properties of the microtubule network.

Rheological measurements of microtubule systems show clear viscoelasticity arising from microtubule suspensions [44]. The effect of introducing crosslinkers also clearly shows an increase in the elastic modulus of microtubule networks. The results show that even though microtubules behave viscoelastically, they differ from the theoretical predictions by Doi and Edwards by a significant amount. This has been attributed to weak interactions between microtubule neighbors [44]. Similarly to actin networks, microtubule networks see the elastic modulus grow with increasing concentration according to a power law. For microtubules that are not crosslinked, the exponent is similar to actin, $v = 1.4$, whereas for crosslinked

networks, $v = 1.6\text{-}1.8$ as compared to actin which was $v = 2.2\text{-}2.5$ [39, 44].

1.4 Thesis Outline

All the previous systems discussed are, nominally, straight biopolymers that are bent via thermal fluctuations and entropy from that straight shape. The persistence length of the different filaments dictates how much of an effect the thermal bending has on how bent or straight the biopolymers. DNA is a model system of a flexible filament in which the contour length is much longer than the persistence length. Flexible filaments are able to become highly entangled in solution by being able to form loops and wrap around neighboring filaments [16, 22]. Filamentous actin is an example of a semi-flexible biopolymer in which the persistence length is on the same order as the contour length. These filaments are able to entangle with one another through bending around neighbors [39]. Microtubules are an excellent model system for rigid biopolymers and have an extensive body of work surrounding their research. However, microtubules are straight rigid rods. The restriction that rigid molecules can only have a straight shape is a restriction that is not necessary for natural systems.

In this thesis, we present experiments conducted with bacterial flagella; a rigid biopolymer that can have a straight shape, but also several different types of helical shape. In the second chapter we discuss the structure of flagella and many of the methods by which flagella are purified, manipulated, and visualized in order to carry out in vitro experiments with the helical structures. The third chapter discusses the methods used to change the shape of flagella using different environmental conditions. In this chapter, we also discuss the shape phases that we observe as flagella are subjected to changes in solvent condition, temperature, and pH. In chapter four, we discuss the behavior of flagella in dense solutions of other flagella.

First, we discuss the way in which flagella reptate through these networks and how the flagella shape impacts diffusion. Then, we present bulk rheological results of flagella suspensions, illustrating how the filament shape can impact the macroscopic material properties of the flagella suspension. Finally, we discuss an alternative way to measure material properties using microscopic tracer particles called microrheology. Differences are observed between bulk and microrheology results, and we discuss possible origins of these differences.

Chapter 2

Bacterial Flagella as a Model Colloid

2.1 Introduction

Bacterial flagella are a biopolymer utilized by prokaryotic organisms to provide motility [45, 46]. Fully assembled, flagella are typically on the order of several micrometers in length and protrude from the cellular membrane where they are attached to a motor protein complex. In wild type strains of bacteria, flagella normally assume a rigid left-handed helical shape [47]. The motor complex rotates, driven by a proton gradient across the cell membrane, causing the helical flagella to rotate and produce thrust, driving the cell through the surrounding medium [48]. The helical nature of flagella is vital for bacteria to provide thrust in the extremely low Reynolds Number limit in which they exist [49, 50].

This study focuses on the flagellar filaments of Salmonella typhimurium, which has many flagella on its membrane. These bacteria move via a run and tumble type of behavior as illustrated in Figure 2.1. They will travel very rapidly in one direction for a time (run), then will suddenly stop, randomly reorient themselves in a new direction (tumble), and then proceed to run in that new orientation [46]. The switching between run and tumble

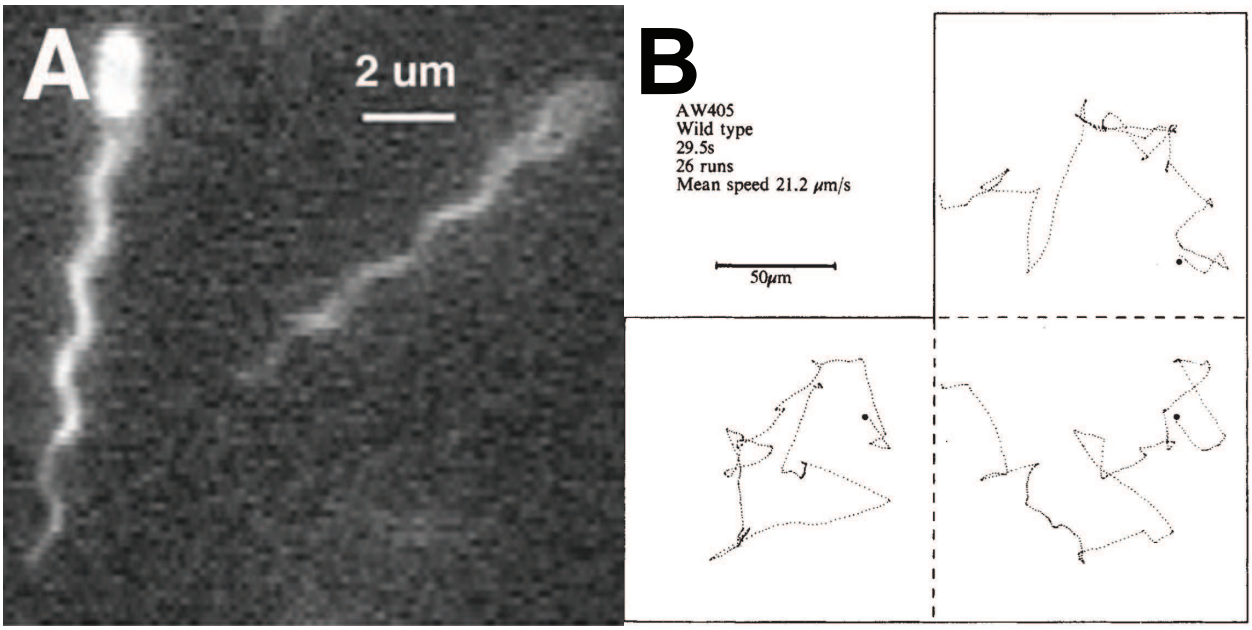

Figure 2.1: A shows a fluorescent image of E. coli during a run phase of motion with a flagellar bundle clearly visible. Image reprinted from [51]. B shows trajectories of individual bacteria tracked in three dimensions. The two phases of motion are clear as run phases are motion directed in very nearly a straight line where the tumble phase occurs when the bacteria reorients before the next run phase. Image reprinted from [46].

behavior is controlled via a vast array of sensing pathways, but it is generally used to try to propel bacteria in a direction with more favorable conditions. Bacteria will tumble more often if they are traveling into an area with less favorable conditions compared to where they just came from to effectively turn themselves around. Conversely, if they are heading in a direction in which conditions are improving, they will run for longer periods of time and tumble less frequently.

When in a run phase, the flagellar motors rotate in a counter-clockwise direction from the perspective of the distal end of the flagella [52]. When exhibiting this run behavior, hydrodynamic interactions between the multiple flagella of the bacterium cause the flagella to form a bundle, cooperating with one another to propel the cell in one direction [53–55].

When the cell switches to a tumble phase of motion, one or more of the flagellar motors change the rotation direction, moving in a clockwise fashion [56]. This causes hydrodynamic interactions between filaments that drives apart the bundle of flagella. During this phase, flagella assume random positions and orientations around the bacterium. To further add to the random motions caused by the switch to tumbling behavior, some flagella can be induced to change their helical shape in this process as shown in Figure 2.2 [51]. The torque acting on each filament as its motor switches rotation direction can be enough to drive some filaments to assume other helical forms including right-handed helical forms [57–60]. Once the tumble phase of motion ends, the flagellar motors once again all assume a counter-clockwise rotation and the flagella bundle is reformed for the next run phase.

In this chapter, we detail the characteristics of flagella relevant to its use as a colloidal particle. First, we will discuss in detail the structure of flagellar filaments and discuss how changes in the conformation of flagellin monomers give rise to a range of possible shapes for the flagella to assume. Also, we explain the procedure of growing and purifying flagella for study as well as how to polymerize flagella *in vitro* and chemically modify flagella once purified. Finally, we detail different techniques used to visualize flagellar filaments so that individual filaments can be studied.

2.2 Flagella as a Helical Colloid

Filamentous and rod-like colloidal particles have widely been studied both experimentally and theoretically [61–64]. Flagella represent a new type of colloidal particle, a stiff biopolymer with a preferred helical shape. The important difference in the shape of flagella from that of other biomolecule colloids is that while other biopolymers like DNA, actin, and microtubules have a helical structure at the molecular scale, they typically dont have any

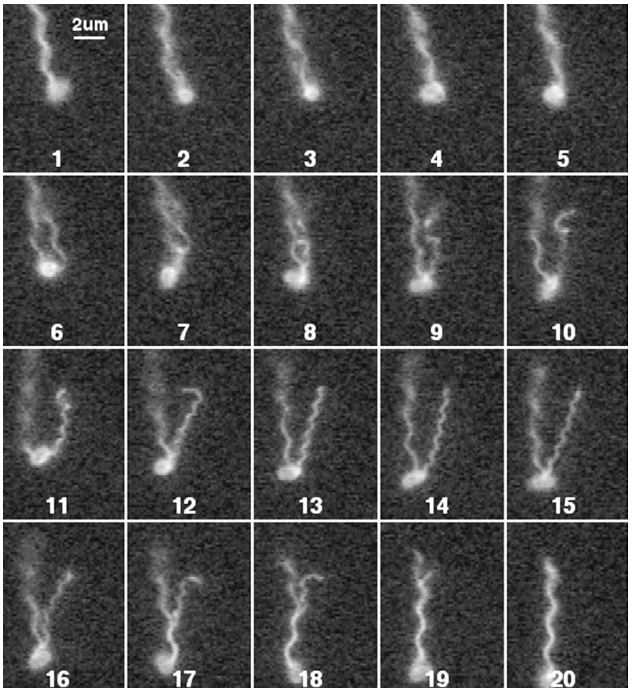

Figure 2.2: Time series of images of a fluorescently labeled E. coli undergoing a tumble phase of motion and inducing a polymorphic transition in a flagellum. Frames 1-5 show a cell ending a run phase and transitioning to a tumble phase. Frames 6-15 show one of the flagellum undergoing a polymorphic transition from a normal helical state to a curly morphology. Frames 16-20 show the transition reversing itself as the cell transitions back into a run phase of motion. Image reprinted from [51].

regular helical structure at the filament scale. Meanwhile, flagellar filaments also have a helical structure at the molecular level, but at the filament scale, this helix of monomers is supercoiled into a larger helix. DNA can exhibit supercoiled states, but only flagella have a natural state of nonzero curvature as a supercoiled helix is the ground state for wild type flagellar filaments.

In addition to having a preferred helical state, flagella can exhibit multiple different helical forms (and two straight forms) based on the specific conformation of the monomers in the filament (discussed in more detail in section 2.3 of this chapter). This means that not only do flagella have nonzero curvature, but the curvature is tunable depending on the shape of flagella used in the experiment. Finally, filaments can undergo transitions between these helical states driven by changes in the external environment. Specifically, we present experiments in chapter three showing that changes in pH and temperature can drive flagella to transition into new helical shapes. Temperature is particularly nice for experiments since it is easily changed on most experimental apparatus and in a non-intrusive way to cause changes to occur in samples.

There are other helical colloid particles that have been synthetically manufactured shown in Figure 2.3 [65–67], and have the advantage of having complete experimental control over the helical shape, length, and handedness of individual filaments. However, natural flagella exhibit several key advantages over synthetic variants. First, bacterial flagella can be produced in large quantities simply by growing a large quantity of bacteria from which to harvest filaments. With modern bioreactors, bacteria can be produced at industrial scale and flagella purification can be adapted to such an environment [68]. Another key advantage of natural flagella is the ability to change helical shape in response to environmental stimuli. The bi-stable nature of flagellin monomers and their ability to switch conformations between two different folded states [69–71] allows natural flagella to be used in dynamic colloidal ex-

periments that change with an external experimentally controlled variable. Without this switching ability, synthetic flagella lack the ability to reproduce a vital function for bacterial motility.

2.3 Structure of Flagella

On a molecular level, flagella are polymers consisting almost entirely of copies of a single protein, flagellin. The flagellin monomers are approximately 50 kDa in mass and are arranged helically into a tube 23 nm in diameter with a central hollow region approximately 2 nm in diameter [73, 74]. While there is some variation in different species, flagella from Salmonella Typhimurium have 11 monomers of flagellin in each turn of the helix and a helical pitch at the monomer scale of approximately 5 nm. The monomers, when fully assembled into a filament are organized into 11 protofilaments that run along the longitudinal axis of the flagellum as shown in Figure 2.4 [75]. These protofilaments are formed due to very cooperative binding among monomers that are neighbors directly in line with the long axis of the filament.

Flagellin monomers naturally assume one of two conformations given the names R and L. When a monomer is in the R conformation, it is 1.5% shorter in length than when in the L conformation [76]. Also, due to the strongly cooperative binding within protofilaments, every monomer within a single protofilament will assume the same conformation, either R or L [69]. Neighboring protofilaments that are different conformations will elastically deform to maintain proper binding site alignment. This elastic deformation causes bending in the overall flagellar filament which manifests itself as a curvature. This curvature is what defines the helical shape of the flagellar filament. The shorter R protofilaments are grouped together on the interior of the supercoiled helix to make their binding sites line up with the longer neighboring L protofilaments.

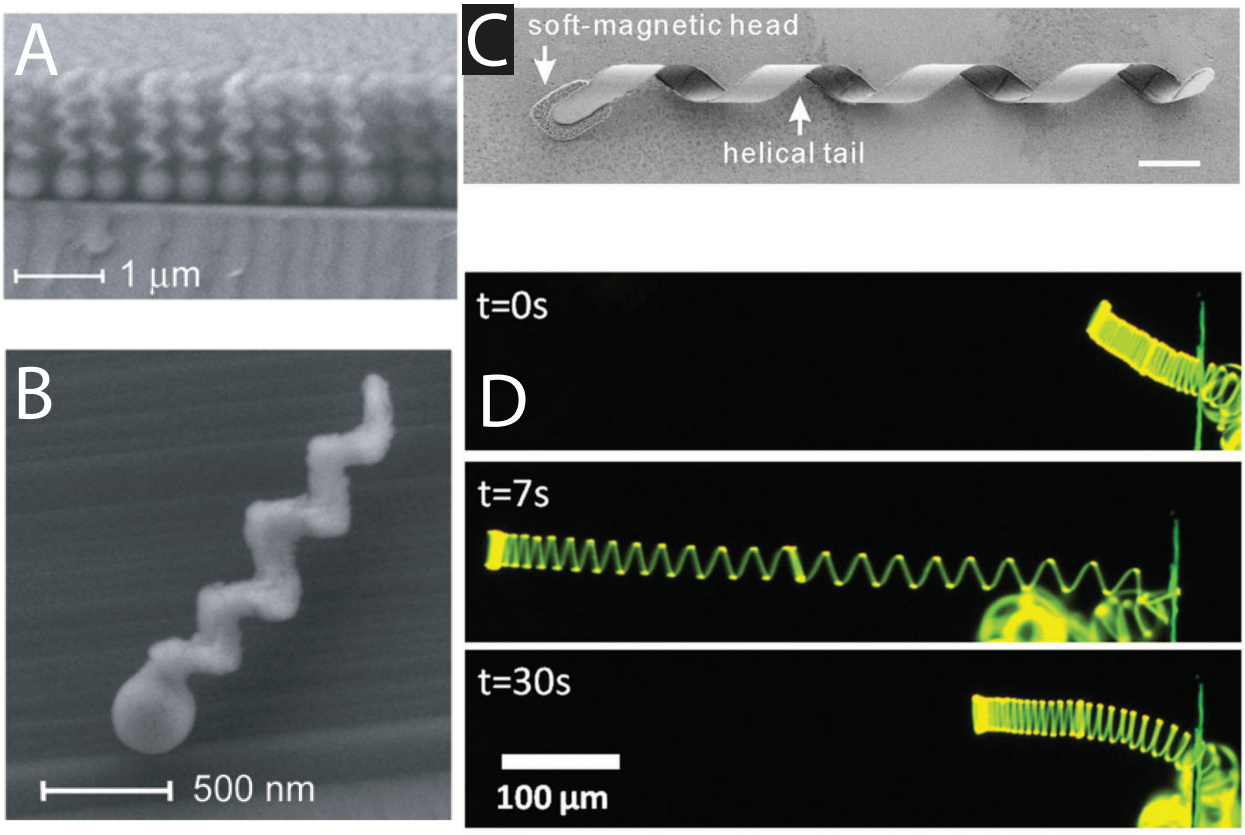

Figure 2.3: Examples of artificial helical particles. A) SEM image of a wafer in which glass helical nanopropellors have been fabricated using glancing angle deposition. B) SEM image of a single glass helical particle made using the same process as A. C) Artificial bacterial flagella made by scrolling strained bilayers. A magnetic head is attached to one end in order to provide for magnetically controlling rotation and therefore motility. D) Time series images showing deformation to an artificially manufactured helix due to fluid flow. Helices were fabricated from CdSe Quantum Dots and gold nanoparticles. Images reprinted from A,B) [72] C) [65] D) [67].

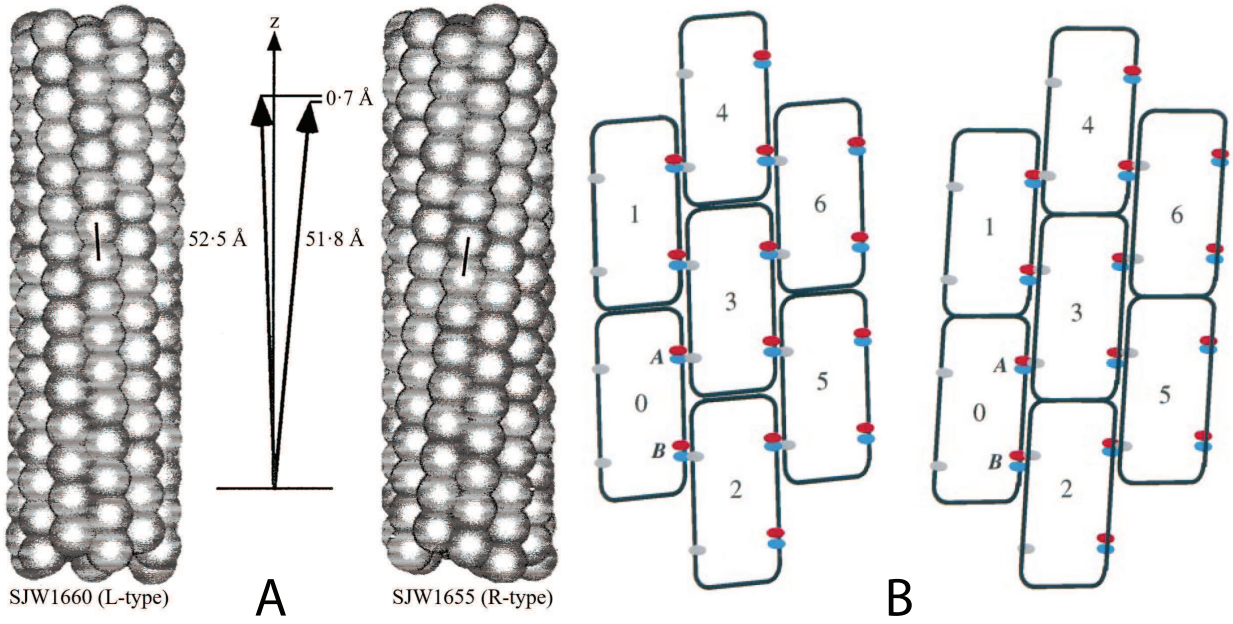

Figure 2.4: A) Comparison between assembled L and R type flagellum. The tilt angle of the 11-start helix is marked on each filament to show the different handedness of the two filaments. Vectors representing the spacing between adjacent monomers are shown in the center, illustrating that the L-type filament is slightly longer than the R-type. B) A schematic of the Calladine model of flagella polymorphism showing how differently spaced binding sites leads to a change in packing arrangement [69]. L-type monomers use the blue binding sites to bind to nearest neighbors, where the R-type monomers use the red binding sites. The slight difference in distance between the binding sites at point A and B for the red and blue active sites is what leads to the slight length difference. Images reprinted from [77] and [73].

Since the R protofilaments are always grouped together on the flagella and there are only 11 protofilaments in total, only 12 possible configurations for the protofilaments can be constructed. These shapes are typically defined through the number of protofilaments that are of the R conformation, n. The two extreme configurations, $n = 0$ and $n = 11$, are both straight filaments that do not exhibit any helical curvature. This is easily understood because there is no need for the filament to bend to align the binding sites of neighboring protofilaments because all the protofilaments are the same length. Wild-type flagella during the run phase of bacterial motion are in the $n = 2$ shape, often given the name normal because of its commonness in nature [78]. The reason this helical shape is preferred for bacterial motility is because it is the most hydrodynamically efficient of any of the polymorphic shapes that flagella can assume [79].

In total, there are twelve possible shapes that bacterial flagella can assume, ranging from $n = 0$ to $n = 11$, illustrated in Figure 2.5. Not all twelve shapes have been experimentally observed, but Calladine [69–71] has outlined a model by which the dimensions of any of the twelve polymorphic states can be accurately predicted [73]. Other notable polymorphic states that appear naturally in the tumble phase are the $n = 5$ and $n = 6$, or, Curly (I) and Curly (II) helices respectively. These two helices are right-handed, opposite of the normal shape; thus, when the flagellar motor reverses direction of rotation, they still provide propulsion directed toward the cell body, but will be impacted by the reduced hydrodynamic efficiency of the curly shapes as compared to the normal shape. Ultimately, this polymorphism serves a biological purpose in that it helps to drive apart the flagellar bundle formed during a run phase and helps the bacteria to better tumble in place to achieve a new, random orientation [53, 54, 80].

The causes of polymorphism in bacterial flagella have been studied extensively in the past and many different factors have been found to contribute. Perhaps the most biologically re-

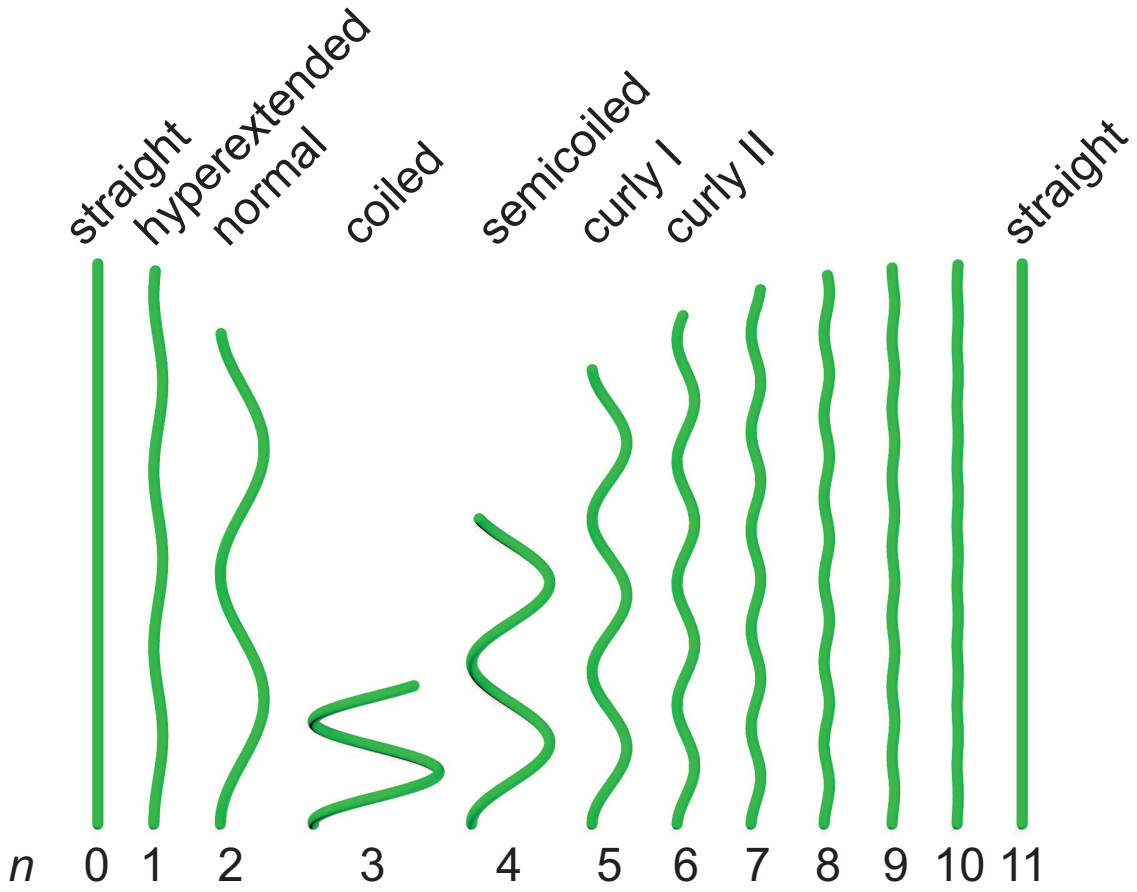

Figure 2.5: Possible polymorphic shapes of bacterial flagella. The polymorphism number, n, is the number of protofilaments that are in the R conformation. Conventional names of different polymorphic shapes that are commonly observed in experiment are given. Contour length of each filament is 5 µm. All morphologies with $n \leq 3$ are left-handed helices while $n > 3$ are right-handed.

levant factor that has been shown to cause polymorphic transitions is that of mechanical torque exerted on the filaments [57–60]. Similarly, mechanical force, via extension and contraction, has also been shown to be able to cause polymorphic transitions in individual filaments [81, 82]. More relevant to this study are findings that show changes in pH, ionic strength, and temperature can induce polymorphic transitions [47, 83, 84]. Solvent changes, such as the introduction of sugars and alcohols have also been shown to induce these changes [85, 86]. In this study, we will focus on chemically induced polymorphic transitions using organic solvents such as ethylene glycol and dimethyl-sulfoxide as well as temperature induced transitions that operate via changing the pH of the solvent as a function of temperature.

The final way in which the shape of flagella can be controlled is by changing the structure of the flagellin monomer through mutation. Three different *S. typhimurium* strains were used for these experiments. The wild-type strain, SJW 1103, exhibits flagella that are naturally of the normal polymorphic state (9L/2R). The L-type variant, SJW 1660, differs from 1103 by a point mutation in flagellin, G426A [76]. Mutants of the 1660 strain only grow flagellin in the L conformation, meaning that the flagellar filaments are straight rather than helical, rendering the bacteria immotile. The final strain used was an R-type variant, SJW 1655. This mutant differs from 1103 by the point mutation in flagellin of A449V [76]. Making only flagellin in the R conformation, this mutant also produces straight flagella and is immotile. Unless otherwise noted, all experimental techniques and protocols are identical between different mutants.

2.4 Flagella Purification

To study bacterial flagellar filaments in vitro, it is first necessary to purify flagella and separate them from the bacteria hosts. In this study, we used *Salmonella typhimurium* and

several mutants as host cells to grow flagella with SJW 1103 being the wild type strain. We use a modified procedure from that of Asakura in order to purify flagellar filaments separate from the bacterial hosts [87]. The first steps of the process are to streak out LB-agar plates with a frozen glycerol stock of the desired strain and incubate these plates overnight at 37°C. The next day, scrape a single colony of bacteria from the plate and culture this in 3 ml of sterile 2XYT media for at least 12 hours at 37°C while being shaken. Multiple 3 ml tubes can be used to scale up production for later steps. After this growth period, the small tubes should allow *Salmonella typhimurium* to reach the maximum cell density allowed in the medium. From the small culture tubes, 1 ml of the bacteria solution should be added to shake flasks containing 1 L of sterile 2XYT media. These shake flasks should be incubated at 37°C and shaken for approximately four hours. This will allow the bacteria to multiply to an OD_{600} of ~ 1.4.

With the bacteria grown in the shake flasks, the next step is to concentrate the cellular bodies, complete with the flagella. The media from the shake flasks should be centrifuged at 11,000 g for 12 minutes to pellet the flagella. The apparatus we utilized is a Beckman Coulter JA.10 rotor spun at 8,000 rpm for 12 minutes to pellet the bacteria bodies. The resulting supernatant from this spin can be discarded. Centrifuge tubes can be refilled and spun again with a pellet from a previous spin remaining in the bottom of the tube without damaging the resulting flagella for this step. After the bacterial cell bodies have been pelleted, a small amount of 20 mM potassium phosphate buffer with a pH of 7.0 should be added to the pellets and, using a pipette, the bacteria pellet should be suspended in the phosphate buffer. The volume of phosphate buffer that needs to be added is dependent on the number of bacteria present. Ultimately, the concentration of bacteria in phosphate buffer should be ~ 150 times higher than before it was spun down. Achieving such high concentrations is vital for the next step where the flagellar filaments are removed from the bacterial cell bodies.

To remove flagella from the bacteria, the concentrated bacterial solution must be shaken vigorously and chaotically for approximately 8 minutes. This was achieved by utilizing a Vortex mixer set to the highest setting. However, instead of mixing the tube on the Vortex mixer while upright, the tube was instead turned onto its side and manually held down to the mixer, creating a chaotic flow in the bacterial solution. At such high concentrations, this is enough of a shear flow as to cause flagella to separate from the bacterial cell body, but not so much that flagella are being destroyed in the process. The flagellar filaments separate at the hook portion of the filament; meaning that they still possess the capping protein on the distal end of the filament while also keeping several hook associated proteins (HAPs) on the proximal end of the filament [88, 89].

Cell bodies and flagellar filaments are separated through centrifugation at 12,000 x g for 20 minutes to pellet the bacteria and preserve the supernatant containing flagellar filaments. Next, the flagella are pelleted via centrifugation at 64,000 x g for 60 minutes and then resuspended in storage buffer (10 mM phosphate buffer pH 7.0). The volume of storage buffer to use for resuspension should be small enough so that after this step the solution has a concentration of above 1 mg/ml flagellin. To this suspension, a volume of PEG solution (20% w/w PEG MW 8000, 2.5 M NaCl) equivalent to 20% of the volume of the suspension is added to introduce an osmotic pressure. This causes the long, thin flagellar filaments to bundle together due to a depletion interaction. The solution is then centrifuged at 28,000 x g for 15 minutes to pellet these flagellar filament bundles. The supernatant is discarded and the flagella are resuspended in storage buffer once more. To make sure any excess PEG is removed, the flagella are centrifuged a final time at 64,000 x g for one hour. After this final spin, the flagella can be resuspended in storage buffer and kept refrigerated. Kept at 4°C, the filaments can be preserved for up to six months. To preserve filaments for a longer span of time, 15% v/v glycerol can be added and the filaments can be stored at -80°C.

2.5 *In Vitro* Polymerization

2.5.1 Procedure

When flagella are purified from *S. typhimurium* following the above procedure, there is no means to control the average length or shape of flagellar filaments. To experimentally control these parameters of flagella, we developed an *in vitro* procedure to polymerize flagellar filaments from monomeric solutions. The nucleation barrier for flagellin monomers in solution to form a polymerized filament is too high for spontaneous growth to occur, so a seeded growth is needed. Through this seeded polymerization, we experimentally control the average length of filaments as well as gain the ability to create more complicated shapes through multiple types of flagellin.

When flagellar filaments are purified through the procedure detailed in the previous section, in addition to the filament that consists of polymerized flagellin, there is a capping protein on the distal end of the flagellum as well as several hook associated proteins on the proximal end of the filament [90]. Previous studies that have polymerized flagella *in vitro* have depolymerized flagellar filaments into monomeric flagellin and then combined this with flagellar fragments created through sonication of fully assembled filaments [81, 87, 91]. This procedure, though effective in re-constituting flagellar filaments, is limited by the presence of capping proteins and hook associated proteins in the monomeric solution. When these proteins bind to a filament, they effectively block new monomers in solution from binding to the end of the flagellum by directly binding to the flagellin monomers at either end of the filament. To polymerize filaments without this limitation, flagellin monomers need to be purified so that any non-flagellin proteins in the monomeric solution are removed. To this end, we have made use of ion exchange chromatography to purify flagellin monomers

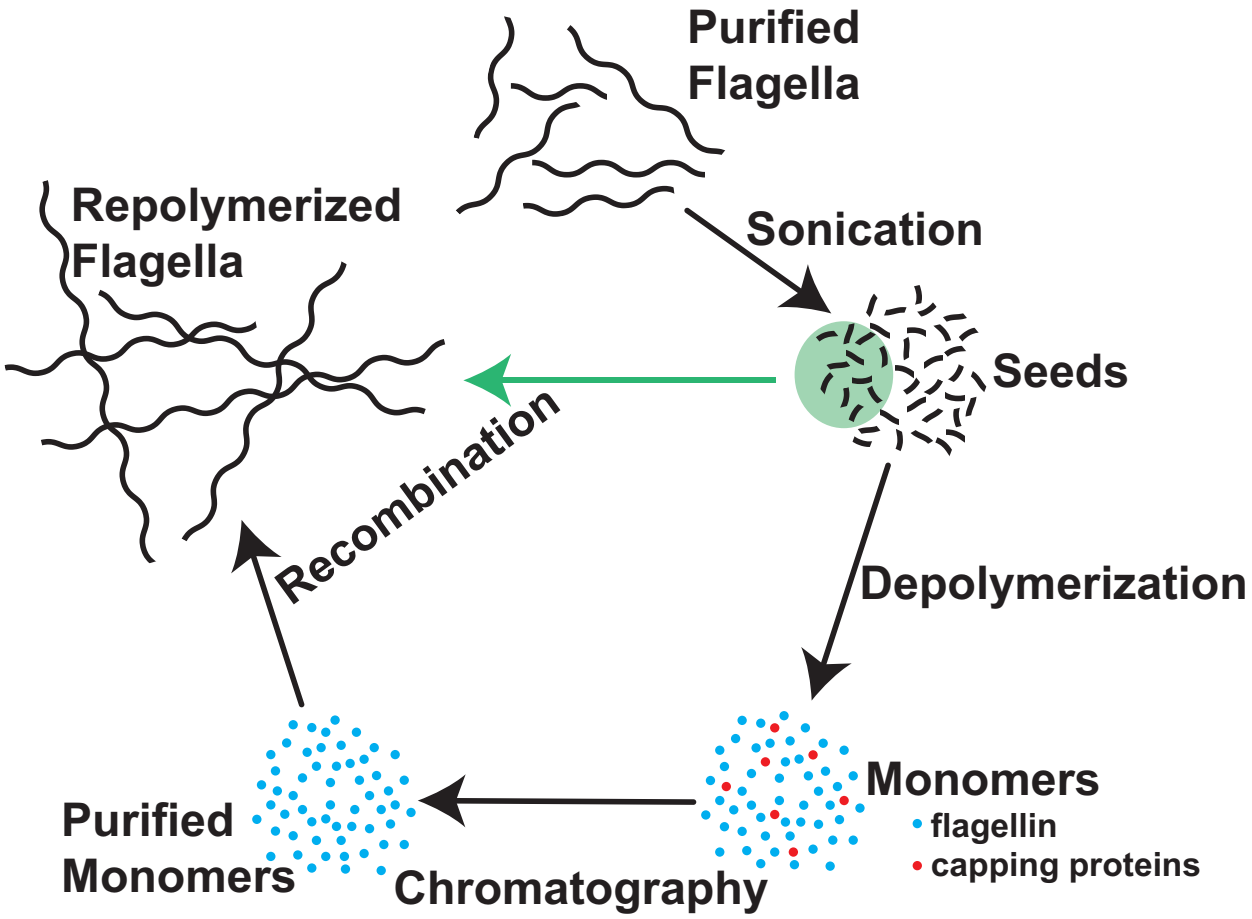

Figure 2.6: Schematic of the *in vitro* polymerization process. This process enables polymerization free from capping proteins from inhibiting continued growth.

for polymerization (Figure 2.6).

To polymerize filaments *in vitro*, filaments were diluted to 4 ml of an 8 mg/ml solution in a 5 mM phosphate buffer pH 7.0 and then breaking the filaments into small pieces through tip sonication. The resulting flagellar fragments, called seeds, have a small amount set aside for later use but the rest are then heated at 65°C for 15 minutes to depolymerize the filaments entirely. This monomeric solution is then centrifuged at 347,000 x g for 30 minutes to pellet any flagella that failed to depolymerize or protein aggregates. The preserved supernatant is loaded into an anion exchange chromatography column (Mono Q 5/50 GL GE Healthcare

Product 17-5166-01) using a low salt buffer (5 mM phosphate buffer pH 7.0). To elute the flagellin monomers, an ionic strength gradient is run by increasing the concentration of a high salt buffer (10 mM phosphate buffer, 0.5 M NaCl, pH 7.0) from 0 to 100% over the course of 90 minutes. The absorbance peak that corresponds to flagellin should prominently stand out compared to the other proteins associated with flagellar filaments mainly due to the much higher quantity of flagellin as shown in Figure 2.7. The collected monomers are dialyzed in the high salt buffer for two hours to increase the ionic strength to help polymerization. This monomer solution is then combined with a certain mass percentage of the seed fragments and left to sit in room temperature overnight. The purified monomers will bind to the seed fragments, growing flagellar filaments.

Different flagella strains have different efficiencies with which they polymerize. With the wild type SJW 1103 monomers, typically about a 33-50% of the initial protein mass loaded onto the chromatography column will end up in repolymerized filaments. The all L straight type mutant SJW 1660 typically results in 20-33% of the initial protein in the polymerized filaments. Lastly, SJW 1655 is the least efficient of the strains used. It usually results in only about 5-20% of the protein polymerizing into filaments at the end of the procedure.

2.5.2 Length Control

The resulting filaments are polydisperse in length, but the average length can be controlled by changing the amount of seeds used to nucleate polymerization. Representative length distributions for both purified and polymerized filaments of several seed concentrations can be seen in Figure 2.8. After the filaments polymerize overnight, they are then centrifuged at 110,000 x g for 45 minutes to pellet the polymerized filaments. The supernatant containing free monomeric flagellin that failed to polymerize is discarded. Remaining filaments are

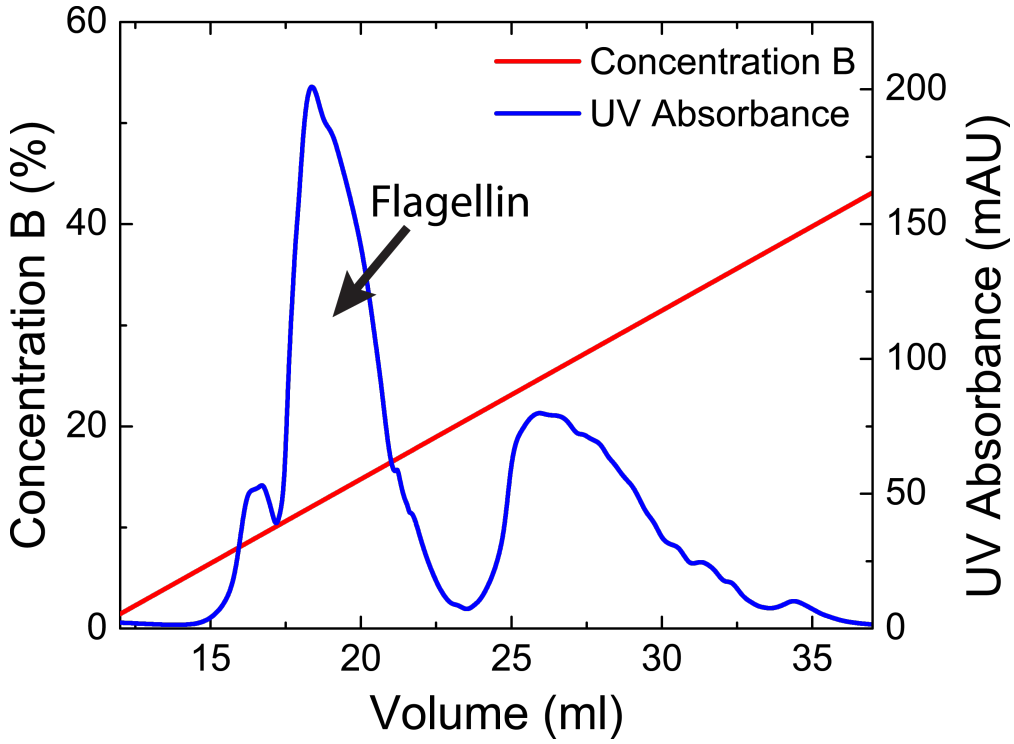

Figure 2.7: Chromatogram from ion exchange chromatography purifying SJW 1660 monomers. The absorbance peak indicating flagellin monomers is indicated. Other peaks represent capping proteins and hook associated proteins (HAPs) that elute as well. This purification began with 4 ml of 8 mg/ml flagella and resulted in a total of 3 ml of 2.5 mg/ml monomer. The gradient used was a 120 minute gradient at a flow rate of 0.5 ml/min.

resuspended in storage buffer and refrigerated for later use.

2.5.3 Block Copolymers

Utilizing in vitro polymerization, block copolymer filaments can be assembled that consist of more than one mutant strain of flagellin in a single filament [90]. Block copolymer filaments are assembled by performing the polymerization multiple times, once for each strain of flagellin to be included in the final block copolymer. The first polymerization proceeds as above with the exception that the filaments, after polymerization overnight, are resuspended in a high salt buffer (10 mM phosphate buffer, 0.5 M NaCl, pH 7.0) instead of storage buffer. The second strain of flagellin to be included in the block copolymer is purified via chromatography using the same method as the first strain. However, instead of using seeds created through sonication to nucleate polymerization, the filaments from the first strain that were polymerized are used as the seeds for the second strain.

By changing the ratio at which the filaments from the first strain are combined with the monomers of the second strain, the average relative length of each side of the block copolymer can be controlled. This mixture should sit out at room temperature overnight to allow for polymerization to occur. After polymerization is complete, the block copolymer filaments are centrifuged at 110,000 x g for 45 minutes. The supernatant is discarded and the pelleted block copolymers are resuspended in storage buffer and refrigerated for later use.

2.6 Flagella Modification

For flagella to be a useful colloidal particle in a wide range of applications, it is necessary to develop a suitable range of surface modification procedures so that experimental control can

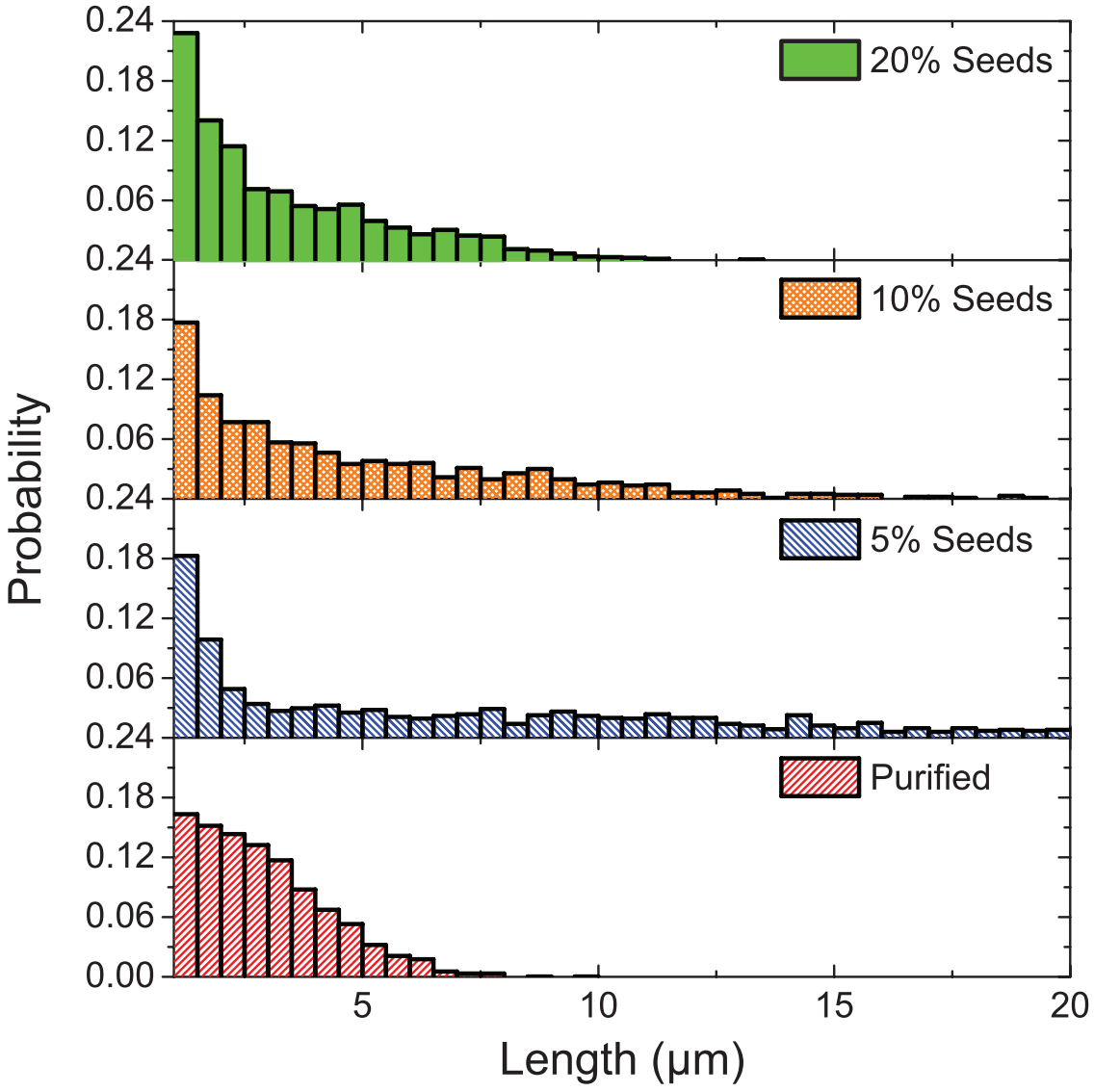

Figure 2.8: Length distributions for polymerized flagellar filaments with different initial seed amounts as well as for purified filaments that have not undergone *in vitro* polymerization. A 20% seed content produces a sample of flagella with an average length of 3.37 ± 0.06 μm with $N = 1346$. Polymerizaton with seed contents of 10% and 5% produces flagella with average lengths of 4.8 ± 0.1 μm and 7.2 ± 0.2 μm with $N = 972$ and $N = 1144$ respectively. Purified filaments were found to have a mean length of 2.89 ± 0.03 μm with $N = 2032$.

be tuned. To this end, we have developed a range of modifications we can make to flagella post-synthesis due to the amino groups on the exterior of assembled filaments. These amino groups enable the use of NHS attachment chemistry for things such as fluorescent dyes or other attachment chemistries. In this section, we will describe the methods used to chemically modify flagella after purification or polymerization.

As mentioned, the flagellar filament has exposed amino groups on the exterior and can be labeled with an amine-reactive rhodamine dye (Sigma-Aldrich, SKU 21955) by mixing the dye for 2 hours with the flagella in labeling buffer (10 mM potassium phosphate, 100 mM sodium bicarbonate pH 8.7, 1-5 mg/ml flagella final concentration). Any amine-reactive dye can be used, but we found the Rhodamine to be the most intensely fluorescent as well as photostable of any dyes tested. The dye solution is a 1 mg/ml solution of dye in a DMSO solvent that can be stored at -80°C. For each 0.5 ml of the flagella and labeling buffer solution, 20 µl of rhodamine solution can be added. To achieve 100% labeling of amine sites, a 40-1 dye-flagellin ratio should be used.

To remove excess rhodamine dye, a 60% v/v glycerol and labeling buffer solution is added to a centrifuge tube and the dye-flagella mixture is layered on top. The contents are then centrifuged at 347,000 x g for 20 minutes to pellet the labeled flagella. The excess dye and glycerol mixture supernatant is removed while the labeled filaments are resuspended in storage buffer and refrigerated until use. Rhodamine dye was found to be very photostable when bound to flagellin. Without antioxidants, fluorescent exposure can exceed 20 minutes in phosphate buffer pH 7.0. With antioxidants, exposures of an hour or more can be observed with reduced, but still visible fluorescence. Freezing labeled filaments with 15% v/v added glycerol at -80°C will preserve the labeled filaments for very long periods of time and maintain the fluorescent properties upon thawing.

In addition to fluorescent dyes, the exterior amino groups on flagella can be used to

attach other attachment chemistry molecules. A biotin-streptavidin link is often used in optical tweezer experiments that use streptavidin coated beads and biotin labeled molecules of interest or vice versa due to the strong, non-covalent bond between biotin and streptavidin [92]. Using a similar technique to above, flagella can be labeled with an amine reactive biotin marker (ThermoFisher Catalog Number 21330) for use in optical tweezers experiments such as the one shown in Figure 2.9. First, 2 mg of biotin is measured out and dissolved in 170 µl degassed, deionized water. The flagella are diluted into the labeling buffer like before and 4 µl of the biotin solution is added to each 500 µl of the flagella solution. At this time, any other amine-reactive procedures can be run concurrently on the flagella.

The flagella mixture is then allowed to mix via rotation in room temperature for at least two hours before being moved into a 4°C refrigerator and mixed there overnight. To remove excess reactants, a solution that is 60% v/v glycerol 40% labeling buffer is added to a centrifuge tube and the flagella solution is layered on top. After centrifuging at 347,000 x g for 20 minutes, the supernatant is discarded while the pelleted flagella are suspended in storage buffer for use. Like rhodamine dye, adding glycerol to the flagellar solution at a concentration of 15% v/v and freezing the sample at -80°C will preserve the filaments for long-term use. Upon thawing, flagella will remain fluorescent if labeled with dye and the biotin label remains functional for use with streptavidin bonds along the entire length of the filament.

For some experiments, having the entire filament labeled with biotin may be undesirable. In this situation, we have developed a procedure which enables a small section of the filament that is usually located at one end of the filament to be labeled with biotin but not the rest of the filament. This procedure only works with filaments that were polymerized from monomeric solutions, rather than purified filaments. First, flagella are polymerized, following the procedure detailed above, with a seed content of 20%. This creates, on average, short

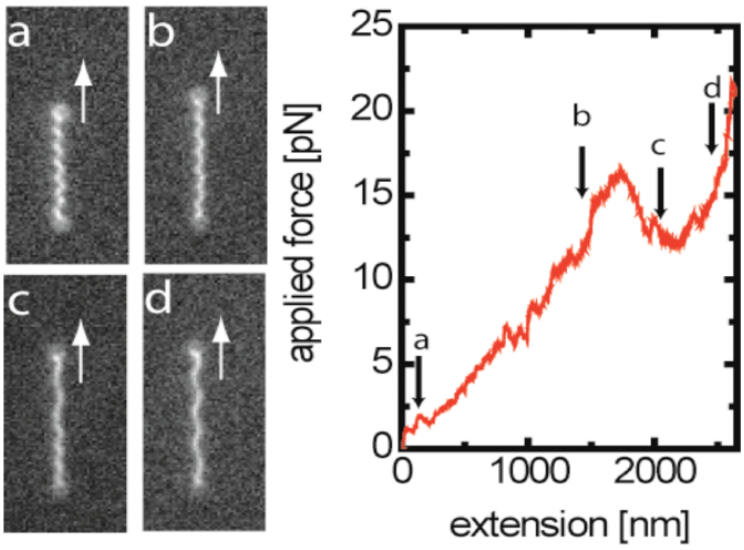

Figure 2.9: Optical tweezer experiment with a single biotin and fluorescently labeled filament being stretched by two streptavidin coated microspheres, one at either end. The force required for extension is measured and plotted, showing that the polymorphic transition that occurs corresponds with a drop in required force.

filaments that then get labeled with biotin (and any other amine-reactive molecules desired) following the procedure listed above with the exception that the biotin solution (and other amine-reactives) should be diluted by a factor of 10 to prevent an excess of biotin blocking flagellin binding sites. After these short segments are labeled with biotin, they are used as seeds for a second round of flagellin polymerization. The ratio of these filaments to the monomers is a way to experimentally control the average length of the resulting filaments.

After the second polymerization, the fully assembled filaments can also be labeled with any surface modification desired such as a rhodamine dye. The result of this procedure is flagella that only have a subsection of the filament that is labeled with biotin while the entire filament can be labeled with another molecule of interest. The biotin labeled portion is most often located at one end of the final filament. This can partially be explained by a possible presence of a capping protein or hook associated protein on the seed used for the

first polymerization, which would only allow polymerization from one end of the filament. Likewise, if there were biotin that bound in a flagellin-flagellin binding location on one end of the filament, it would prevent further polymerization from that side. This is supported by the fact that if the biotin labeling fraction is too high, the biotin labeled short filaments fail to polymerize any further.

Lastly, it is possible to modify flagella so that alternative attachment chemistries can be used. For example, using an amine-reactive azide (Fisher Scientific Catalog No. P126130) and labeling flagella using the same protocol as biotin or rhodamine, it is possible to utilize click-chemistry protocols. For example, it is possible to attach DNA oligos to flagella in this manner. First, flagella need to be fully labeled with the amine-reactive azide so that there are no free amino groups. Then, DNA oligos that are modified with an amino group on either the $5'$ or the $3'$ end are mixed with an amine-reactive DBCO (Sigma-Aldrich SKU 764019) to attach the DBCO to the end of the DNA. After removing excess DBCO from the oligo solution either through centrifugation or dialysis, the labeled oligos can be mixed with the azide labeled flagella in a 1x PBS buffer and mixed for 24 hours at room temperature.

2.7 Visualization of Flagella

An important aspect of any colloidal system is the ability to visualize individual particles to better understand the dynamics of the macroscopic system through microscopic interactions. In this work, we have primarily utilized optical microscopy techniques when observing flagellar systems. While it is possible to image flagella with a brightfield contrast enhancing technique such as differential interference contrast (DIC) [93], the techniques we employed the most were darkfield microscopy and fluorescence microscopy [94].

Darkfield microscopy is a technique with which unmodified flagella can be imaged under

a microscope. The small diameter of flagella (23 nm) makes standard brightfield techniques very difficult if not impossible due to the negligible amount of light that is absorbed by such a small molecule. Darkfield circumvents this restriction by instead scattering light off the particle of interest and imaging only the scattered light and not the light used for illuminating the sample. This technique requires only minor changes from a standard brightfield microscope as shown in Figure 2.10. In darkfield, the light source used to illuminate the sample is a very bright (> 1000 W) white light source. The intensity is needed for flagella because such a small fraction of that light is imaged by the detector. The other main difference in darkfield is that there is a light blocking element placed immediately prior to the condenser in the light path. The purpose of this is to block the illuminating light in the center of the back focal plane. This causes the sample to only be illuminated by light that is at an extreme incident angle upon the sample rather than the more direct light in line with the light path. The objective used in darkfield must have either an adjustable numerical aperture or a low enough numerical aperture that incident light on the sample is coming in at an angle too great to be focused onto the image sensor.

The goal of this arrangement is to create conditions in which, if there is nothing in the sample to scatter light, none of the light from the illumination pathway will be imaged onto the image sensor, creating a dark image, thus the name darkfield. If there is something in the sample that can scatter light, then the scattered light from the sample is radiated in all directions, meaning that some of the resulting scattered light will be directed into the objective and imaged. This technique enables visualizing flagella that are completely unmodified because the flagellar filaments scatter light effectively. Additionally, because the intensity scales as the square of the scattering cross-section, darkfield can be very useful when studying bundling of flagellar filaments. For example, a bundle of two flagella would be four times as intense as a single flagellum in darkfield, but using another technique

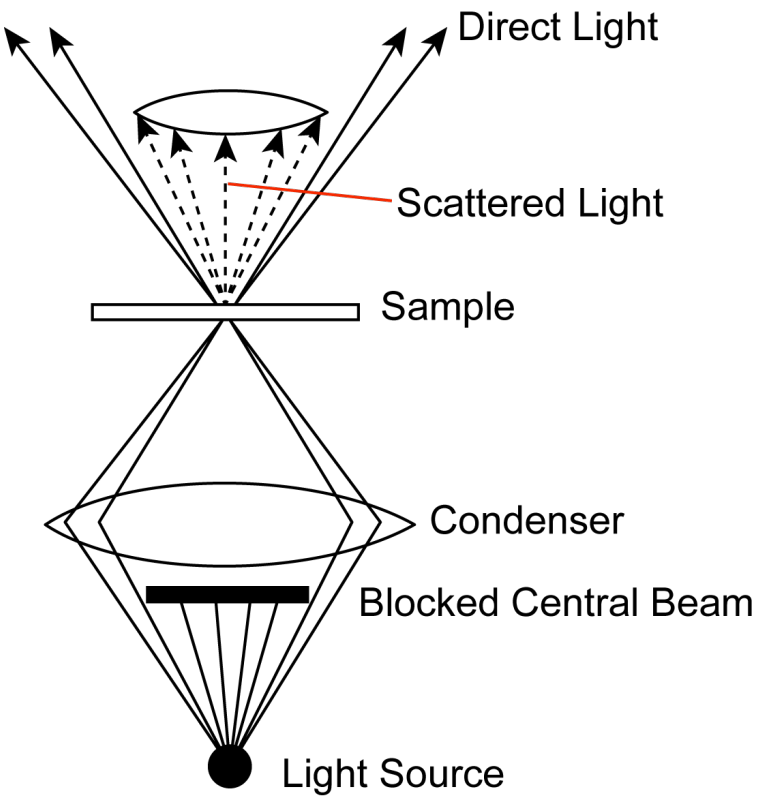

Figure 2.10: Schematic illustrating the basic ray optics of darkfield microscopy. Only the light scattered from the sample is collected by the objective while the direct light is incoming at too large an incident angle to be directly imaged.

such as fluorescence, the bundle would only be twice as bright since it scales linearly with fluorophore concentration. However, the drawbacks of this technique are that anything in your sample, including impurities in the solvent and defects in the glass slides, will also scatter light and appear quite bright in images. Also, because all flagella scatter light, if the flagella concentration is too high, then individual filaments can no longer be discerned from one another. Additionally, this technique prevents looking at flagellar filaments while still attached to bacteria to look at in vivo behavior because the cell body scatters so much light compared to flagella, that they cannot be resolved.

To complement darkfield imaging, fluorescence microscopy was used to observe flagella

in solution. This microscopy technique can only be performed on modified flagellar filaments that have been labeled with a fluorescent dye. The dye we found to work best with bacterial flagella was a Rhodamine based dye that has an excitation wavelength of 554 nm and emission wavelength of 584 nm in phosphate buffer. The optical apparatus is arranged so that a light source (either a wavelength specific laser a broad spectrum, very intense white light source) is focused onto a dichroic mirror that reflects the excitation wavelength of the dye of interest (Figure 2.11). This reflected light is used to illuminate the sample and excite the fluorophores. These then relax back into a ground state and emit a photon in the process with energy equivalent to a light wave with a wavelength equal to the emission wavelength of the dye. The direction of the emitted light is completely random, but that means that some of the emitted light is directed toward the microscope objective, opposite the direction of the excitation light. This emitted light then travels through the dichroic mirror and to the image sensor.

One of the advantages of this technique is that it allows for extremely specific imaging. Only very specific wavelengths will be allowed to be incident upon the sample or allowed through to the image sensor due to the specificity of the dichroic mirror. This contrasts with darkfield imaging where any part of the sample that scatters light will be imaged, whether it is of interest or not. Also, fluorescent imaging allows for imaging individual filaments at high flagella concentrations. Labeling a small fraction of the filaments with the fluorescent dye, only those filaments that are labeled will be visible to the image sensor while the rest of the unlabeled filaments will not appear. Also, fluorescence enables visualizing living bacterial cells with attached flagella [51].

The risks of fluorescence microscopy compared to darkfield are that fluorophores will photobleach over time, lowering the intensity of a flagellar filament until it no longer fluoresces. The choice of dye molecule is the primary driver of photobleaching. Rhodamine

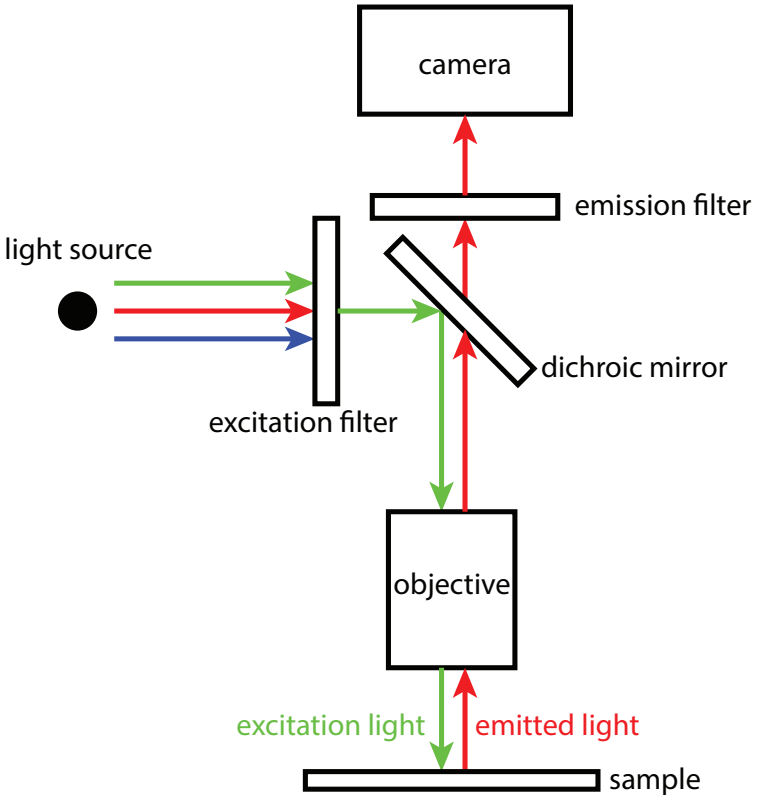

Figure 2.11: Schematic illustrating the essential components of a fluorescence microscope. For the rhodamine dye used in our experiments, $\lambda_{ex} = 554$ nm and $\lambda_{em} = 584$ nm.

dye is incredibly photostable and intense on flagellar filaments. Exposures lasting multiple hours are achievable with an oxygen harvesting system, but even without antioxidants, exposures on the scale of 10 minutes are possible in standard conditions. Another possible concern with fluorescence is that by modifying the flagellar filaments, the behavior will be different than unmodified filaments. This concern has led us to make sure to always check for this problem by heavily utilizing both darkfield and fluorescence for each set of experiments where possible. To date, there has been no observable, repeatable difference in behavior between fluorescently modified flagella and unmodified flagella with the one exception of crosslinking. The crosslinking problem arose in a set of experiments using optical tweezers and a depletant molecule (polyethylene glycol) in order to construct bundles of flagella via the depletion interaction [13]. We found that fluorescently labeled filaments will crosslink (both reversibly and irreversibly) as they are exposed to excitation light. We believe this to be caused by dye molecules on the bundled filaments photobleaching and crosslinking with one another. Unmodified filaments observed under darkfield do not exhibit this same kind of crosslinking behavior.

A final flagella visualization method that can be used is transmission electron microscopy. To clearly see flagella with electron microscopy, a negative stain is used to provide contrast (Figure 2.12). Uranyl acetate (UA) at a concentration of 0.5% is a commonly used stain for this purpose. This stain provided excellent results for 1655 and 1660 strains of flagella, but the low pH of UA cause the 1103 strain to undergo a polymorphic transition to a straight state. To image 1103 filaments without this polymorphic transition, filaments can be stained with 2% phosphotungstic acid (PTA) with a pH of 7.0. The contrast may not be as good with PTA as with UA, but the neutral pH allows for a wider range of structures to be observed including the hook and capping proteins on the proximal and distal ends of the filament respectively.

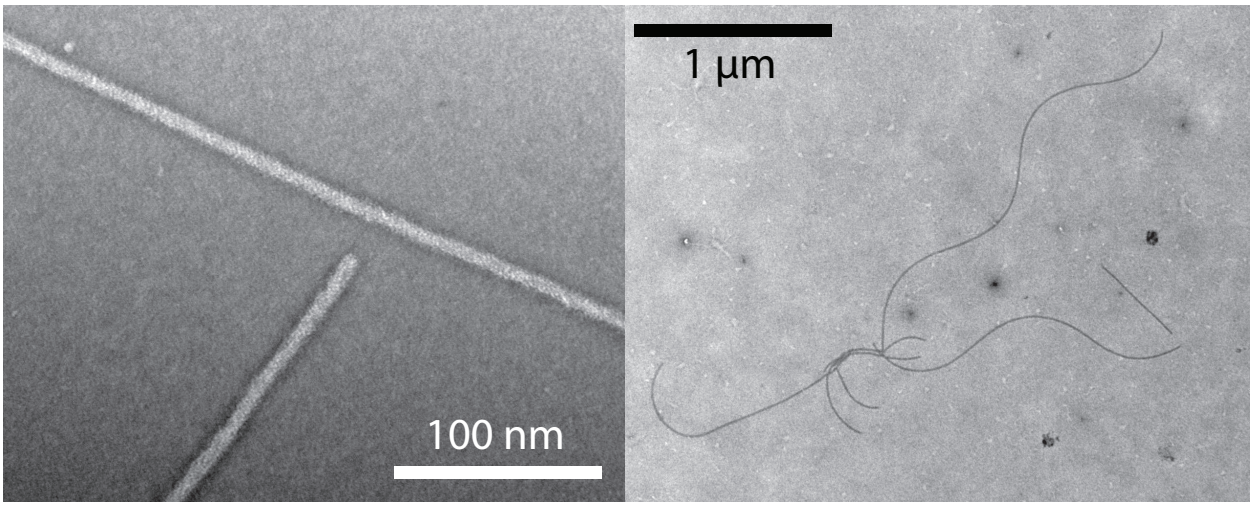

Figure 2.12: EM images of flagella. Left shows R-type straight filaments from SJW 1655 stained with 0.5% uranyl acetate. Right shows some fragments of SJW 1103 in the normal form stained with 2% phosphotungstic acid. Staining 1103 filaments with uranyl acetate causes them to transition into a straight state due to the low pH of the stain.

2.8 Conclusion

The unique properties of bacterial flagella provide an excellent model colloidal system with which to study the effect of particle geometry on colloidal suspensions. By being able to prepare flagella in a straight conformation as well as helical and block copolymer forms, the effect of colloid geometry can directly be measured without confounding external effects. Any kind of intrinsic interactions between colloids will be the same in both straight and non-straight cases, meaning the only contributing effect on samples with different types of flagella would be geometric. Experimentally being able to control the average length of particles as well as making a wide array of modifications to filaments make this system applicable to a wide range of visualization techniques as well as experimental systems. Also, the ability to dynamically switch shape in response to a wide range of stimuli make flagella an ideal colloid with which to study a dynamically changing colloidal suspension.

Chapter 3

Polymorphic Transitions of Bacterial Flagella

3.1 Introduction

The helical shape of bacterial flagella is a defining characteristic and provides the ability for bacterial motility in a low Reynolds number environment. Just as important as the shape is the ability for bacterial flagella to change the helical shape in response to various stimuli. Previous studies have identified various environmental factors that can trigger these changes including pH, ionic strength [47, 83], temperature [84], alcohols [85], sugars [86], and applied force [81, 82]. The ability to change helical shape in response to environmental factors is a trait which could be used in colloidal particle studies to reversibly change many characteristics of the colloidal suspension without resorting to synthesizing new particles and creating another sample.

A goal of studying bacterial flagella polymorphism is to become better able to engineer conditions or flagella in which the filaments will easily transition between different,

well-defined morphologies reversibly. Ideally, the environmental conditions driving the transitions should be an easily controlled stimulus that is non-invasive such as temperature. The approach we have taken in this thesis is to first investigate the phase behavior of the different strains of flagella in response to different environmental stimuli. With better knowledge of the transitions that can be induced environmentally, we then build a system in which transitions can be induced reversibly between two or more states using an easily controlled parameter. This then allows for future measurements of material properties of flagellar suspensions that are tunable by changing the shape of the constituent flagella by way of environmental control.

In this chapter, we detail polymorphic transitions observed in several different strains of flagella through changing solvent conditions. First, we report the changes that dimethyl sulfoxide (DMSO) concentration has on flagellar shape. Then, we will discuss the many different shape changes that can be induced with ethylene glycol in flagella and some of the anomalous behavior in block copolymer filaments specifically. Finally, we will cover a method through which temperature can be used to change the ionic strength of the flagella solution. This can induce polymorphic transitions because of temperature variations and is used to capture the transition process in action.

3.2 Polymorphic Transitions in DMSO

Dimethyl sulfoxide is a commonly used organic solvent with a wide variety of industrial and biological applications. One of the most common applications for DMSO in biology is to suppress secondary structure in PCR reactions [95]. Similarly, proteins in DMSO solutions of a high enough concentration begin to suffer denaturation in higher order structure. DMSO in solution will cause proteins to partially unfold, disruptions of intramolecular peptide group

interactions, and form β-sheets with nearby proteins leading to aggregation and denaturation [96]. This denaturation can lead to hydrophobic amino acids binding with DMSO as unfolding occurs while other polar amino acids have unfavorable interaction with DMSO [97]. These complicated interactions between DMSO and proteins can be used to induce conformational changes in flagellin and therefore the helical supercoiled state of flagella.

When wild type SJW 1103 filaments are exposed to increasing DMSO concentrations, they transition from a normal (9L/2R protofilaments) state into a curly (7L/4R) and normal coexistence region followed by an entirely curly region as shown by the phase diagram in Figure 3.1. The transition from normal to curly changes very little with changing NaCl concentration and the coexistence region spans roughly the same DMSO ranges across the phase diagram. This is an indication that the mechanism driving the transition is primarily caused by the presence of DMSO rather than changing ionic strength. As DMSO concentration is increased further, the curly filaments transition into a straight conformation. This transition occurs in a very narrow region of DMSO concentration, meaning that there doesnt appear to be any coexistence region where both states are relatively stable. Instead, as DMSO Is increased, the curly filaments very rapidly become an unstable protofilament configuration and a straight phase becomes favorable. It is impossible to tell with our methods which of the two straight phases the flagella assume in this phase diagram.

The amount of DMSO needed to induce the curly to straight transition drops measurably between 50 and 100 mM NaCl, but other than this one region, the NaCl concentration seems to make little difference in the transition. As DMSO is increased even more, the flagella will eventually depolymerize as the flagellin is depolymerized. This is an irreversible transition unlike the others which can be reversed by changing the DMSO concentration. Like most the other transitions for these filaments in DMSO, the depolymerization transition is scarcely effected by NaCl concentration.

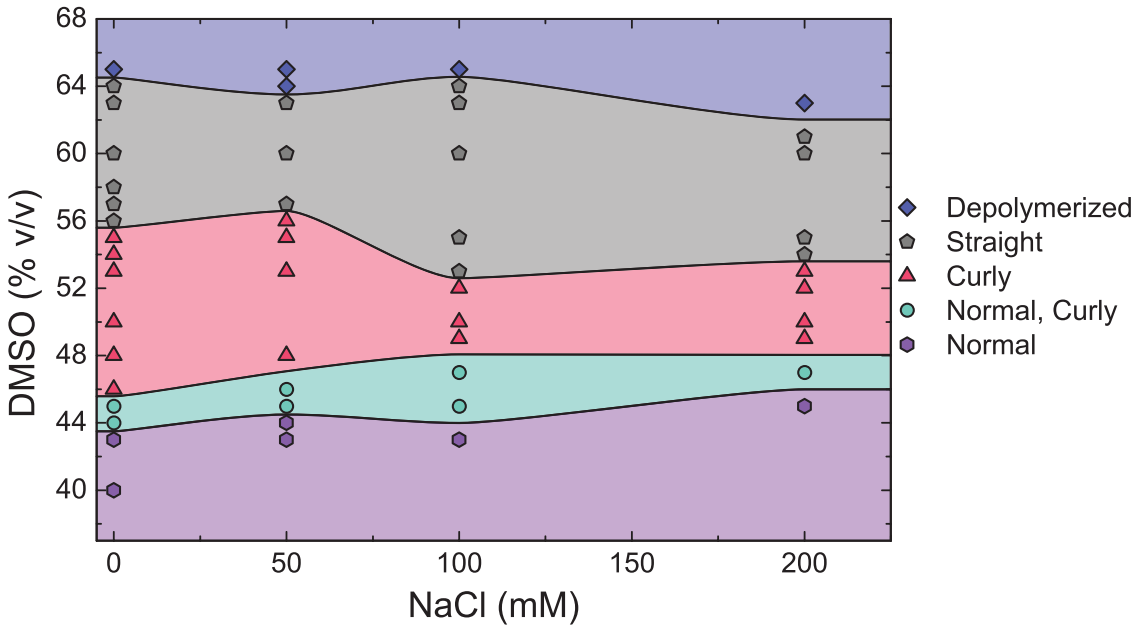

Figure 3.1: Phase diagram for SJW 1103 filaments in DMSO and salt solutions. With increasing DMSO, filaments transition from normal to curly then straight before depolymerization.

SJW 1660 filaments produce a flagellar filament with a straight morphology comprised of 11 L protofilaments and 0 R filaments. When this type of flagella was exposed to DMSO solutions, it transitioned from a straight form into what we have termed a disordered phase as shown in Figure 3.2. A flagellum in this state lacks a specific helical form (Figure 3.3). These flagella often appear to be randomly arranged short segments of flagellar filaments. Some filaments in the disordered state qualitatively appear to become more flexible, while others maintain the rigidity of a filament in one of the standard helical shapes. Quantitatively measuring persistence length of filaments in DMSO solutions is a possible future direction for research. Filaments also seem very prone to crosslinking while in the disordered state, especially with increasing NaCl and DMSO concentrations. With no added NaCl, the filaments can transition out of a disordered state into a normal morphology. The transition to normal signifies a transition of just two of the L protofilaments to the R conformation.

This normal phase only exists in a very narrow region of the phase diagram. Adding more NaCl to the solution causes flagella to exist in the disordered state while adding more DMSO causes the flagellin to denature and the filaments to depolymerize. This seems to be one of the only regions of the phase diagram in which NaCl concentration has a significant effect on the phase of the flagella. The other region of the phase diagram strongly affected by NaCl concentration is at very high concentrations, the flagella will depolymerize at much lower DMSO concentrations. This may be because DMSO has very unfavorable interactions with polar amino acids [97], so as the ionic strength of the solution increases and the charged residues on the protein are screened by ions, the DMSO can more easily interact with the remainder of the proteins.

In general, bacterial flagella in DMSO behaved in much the same way as DMSO-free solutions. Filaments remain rigid as they transition through different helical shapes (the exception being some filaments in the disordered state), transitions are reversible with changing DMSO concentration apart from depolymerization, and fluorescent as well as darkfield imaging is best used to visualize the filaments. Fluorescently labeled filaments do tend to photobleach more quickly in higher DMSO concentrations. The photostability of amine-reactive rhodamine dye, for example, is reduced from an hour or more with no DMSO to on the order of several minutes just before depolymerization levels of DMSO. Temperature seems to play little to no effect on flagellar shape in DMSO solutions. By changing the temperature of samples very close to a transition boundary on the phase diagram we were unable to induce polymorphic transitions. We did observe that in higher temperatures, flagella were more likely to crosslink, especially with increased ionic strength in the solution. This crosslinking was observed with both fluorescently labeled as well as unmodified flagella.

These many issues with DMSO mean that it is most likely not the way forward with engineering reversible transitions in flagella. Filaments crosslink, depolymerize, and assume

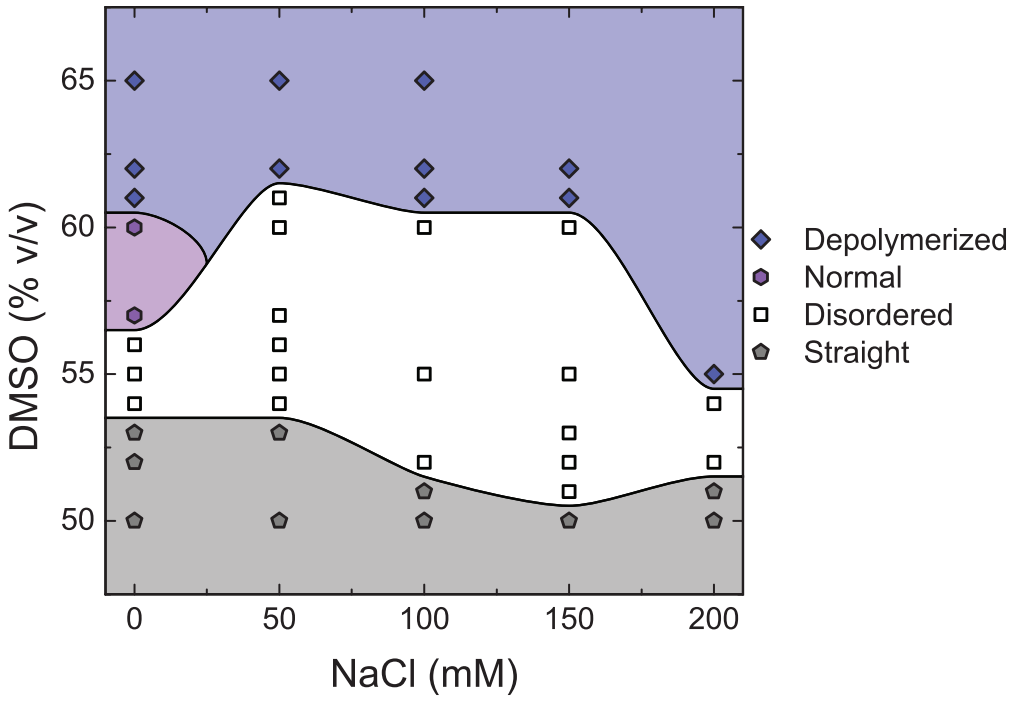

Figure 3.2: Phase diagram for L-type filaments, SJW 1660, in DMSO solutions. There is a small section of the phase diagram in which the filaments assume the normal phase, but for a large portion of the phase space, the filaments assume a disordered shape. A disordered filament is one in which there is no defined helical or straight shape over the length of the filament.

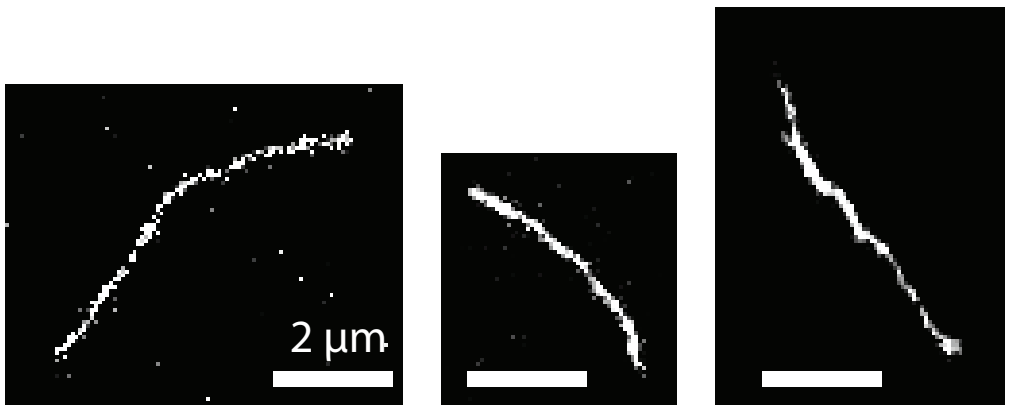

Figure 3.3: Examples of SJW 1660 filaments in a disordered configuration. Sample conditions varied, but are all in the disordered region of the phase diagram.

ill-defined states all too often in DMSO samples. The next section covers another protein denaturant used to induce polymorphic transitions in a different strain of flagella in previous experiments [85].

3.3 Polymorphic Transitions in Ethylene Glycol

Ethylene glycol has a wide array of industrial applications ranging from coolants to antifreeze. This is because ethylene glycol molecules have a short hydrocarbon chain with a hydroxyl group at either end. These hydroxyl groups are prone to forming hydrogen bonds with other ethylene glycol molecules, water molecules, and biological molecules meaning that it can influence any system in which hydrogen bonding is important [98]. For biological applications, ethylene glycol is often used as a denaturant. In high enough concentrations, ethylene glycol will disrupt hydrogen bonds holding a protein in the correctly folded state leading to denaturation. With regards to bacterial flagella, ethylene glycol has been shown capable of inducing polymorphic transitions qualitatively In previous studies with a different strain of flagellin [85].

3.3.1 SJW 1103 Flagella

Wild type flagellar filaments, SJW 1103, show a rich phase behavior in ethylene glycol and NaCl solutions as shown in Figure 3.4. Filaments transition from a normal to a coiled morphology with increasing ethylene glycol indicating a transition from a 9L/2R protofilament arrangement to a 8L/3R state. This transition exhibits a wide coexistence region with increasing ethylene glycol in which both coiled and normal shapes are stable and present in significant quantity. Additionally, we show that the coexistence region of coiled and normal filaments exists down to 30% v/v ethylene glycol. Varying NaCl concentration in the sample

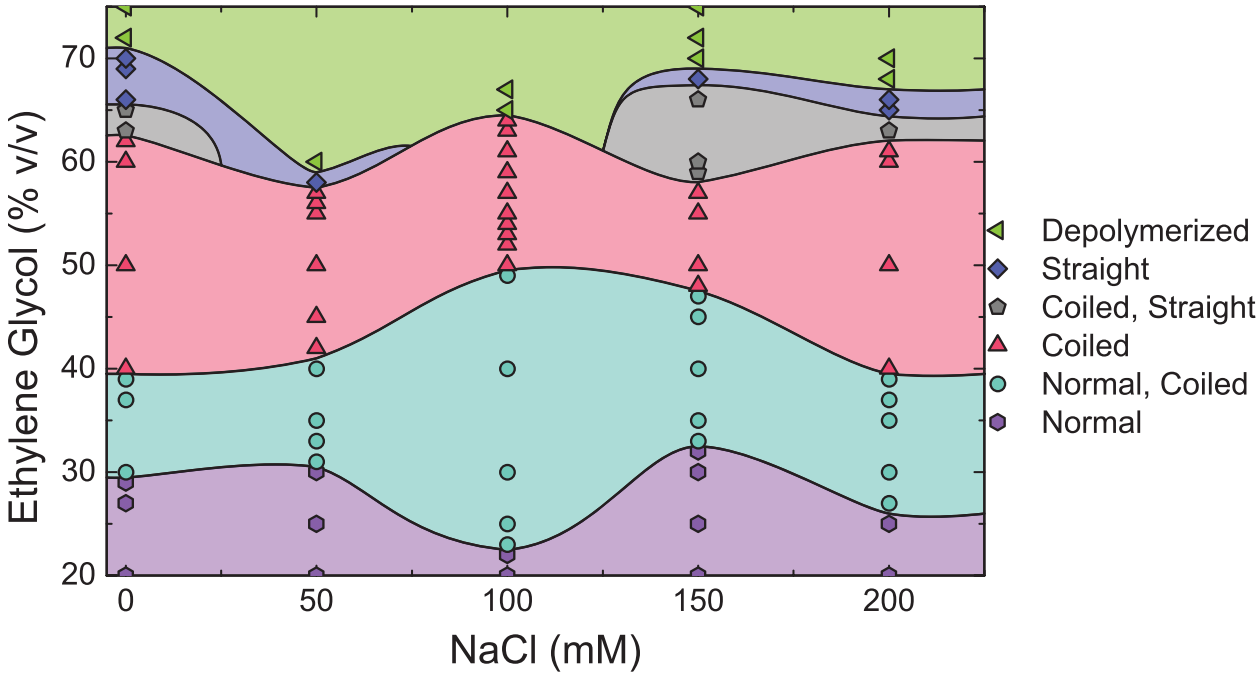

Figure 3.4: Phase diagram for wild type SJW 1103 filaments in ethylene glycol and NaCl solutions. At 0 mM NaCl, we reproduce the results from SJ 25 filaments that show coiled at 40% and straight at 70% ethylene glycol [85]. The normal to coiled transition takes place over a broad region of coexistence whereas the coiled to straight transition has little to no coexistence depending on the salt concentration.

can significantly change the size of this coexistence region, peaking in size around 100 mM NaCl.

As the ethylene glycol concentration is increased, SJW 1103 filaments transition from a coiled state into a straight phase with the exception around 100 mM NaCl in which there is no straight phase, filaments will instead depolymerize directly. It is unclear using optical techniques whether this is a transition from an 8L/3R state to a 0L/11R or an 11L/0R state. The phase behavior for this transition is highly dependent on the NaCl concentration of the sample. With small amounts of salt, there is a narrow coexistence region in which both coiled and straight are present. However, higher salt concentrations lead to a broadening of this coexistence region.

These results for SJW 1103 filaments are consistent with a previous study of SJ 25 filaments in ethylene glycol solutions [85]. In the previous work, SJ 25 filaments were fixed to a glass slide and had different ethylene glycol solutions flowed over them while the shape was observed. With no added ethylene glycol, the filaments were in the normal conformation. At 40% ethylene glycol, the filaments exhibited a coiled morphology. And finally, at 70% ethylene glycol, the flagella were in a straight conformation. These three data points are in agreement with the more expansive phase diagram we measured for SJW 1103 filaments in Figure 3.4.

3.3.2 SJW 1660 Flagella

Polymorphic transitions are also observed in the all L straight strain of flagella, SJW 1660, when exposed to ethylene glycol and salt solutions (Figure 3.5). In the absence of added NaCl, the only transition is when the straight filaments depolymerize. However, as salt is added to the solution, the filaments can assume a normal morphology. This transition is caused by two protofilaments changing conformation so that the configuration changes from an 11L/0R to a 9L/2R state. Interestingly, the normal phase in the phase diagram widens with increased salt, but overall can go to higher ethylene glycol concentrations before depolymerization occurs. This trend suggests that the transition to a normal phase makes the filaments more stable and resistant to denaturation and depolymerization than staying in the, under normal conditions, preferred all L straight state.

The straight to normal transition in 1660 filaments does not exhibit any kind of coexistence region where both phases are stable for long periods of time. This stands in contrast to most of the transitions exhibited in 1103 filaments where coexistence regions were present to some extent for all observed transitions. The lack of a coexistence region for this transition

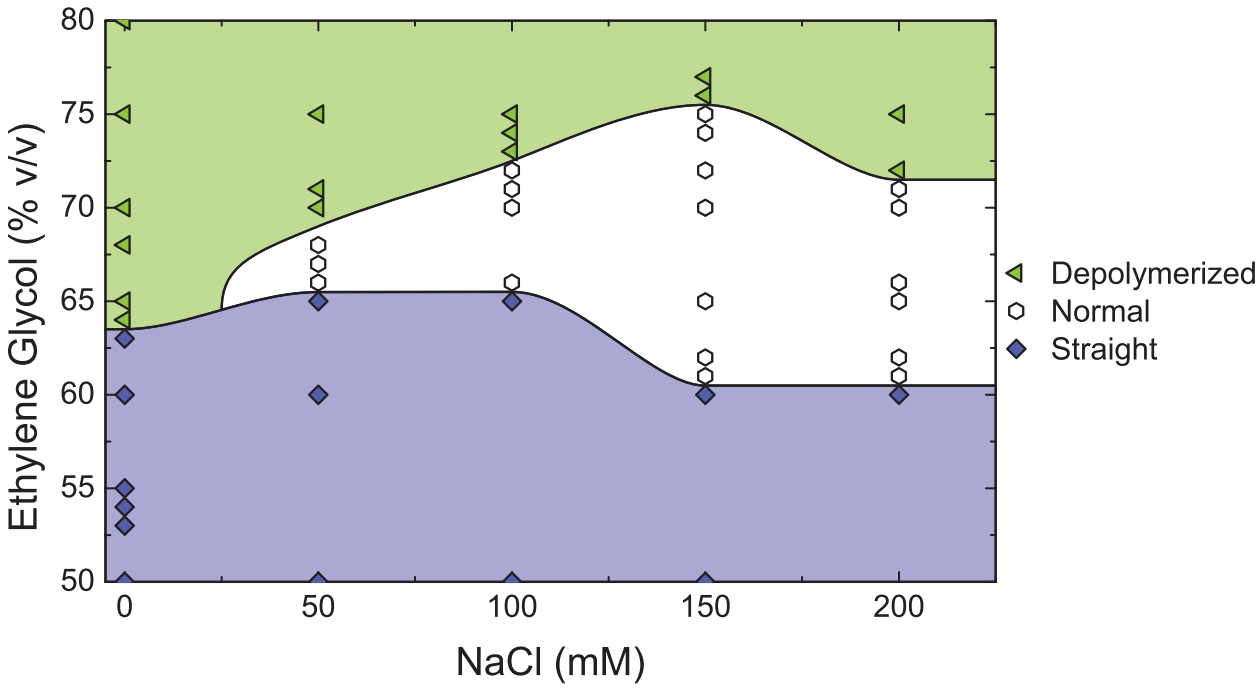

Figure 3.5: Phase diagram for SJW 1660 filaments in ethylene glycol and salt solutions. Adding salt to the solution enables the filaments to transition into a normal morphology with increasing ethylene glycol. Once in the normal form, the filaments are generally able to withstand higher ethylene glycol concentrations than in the straight form.

is a good indication for being able to induce this transition in bulk samples reliably. This is because the vast majority of filament all transition in a very narrow region rather than the wide disparity exhibited in other transitions through a large coexistence region of two helical forms.

Another feature of the 1660 phase diagram that is absent is the existence of a disordered phase such as found over a broad region of the phase diagram for 1660 filaments in DMSO. This means that DMSO and ethylene glycol are changing the conformations of flagellin through different means at a molecular level. This is further evidenced by the fact that added salt facilitates the transition to a normal conformation in ethylene glycol solutions as opposed to DMSO solutions where an increasing salt concentration causes the normal phase to disappear. The fact that 1660 filaments can transition to a normal conformation in both ethylene glycol and DMSO and 1103 filaments can transition to straight filaments in both ethylene glycol and DMSO means that the same type of filament can be used to study either shape in different conditions.

3.3.3 SJW 1655 Flagella

The all R straight strain of SJW 1655, different from both the wild type 1103 and all L straight strain of 1660, showed no polymorphic transitions in ethylene glycol and salt solutions as shown in Figure 3.6. The only transition for 1655 filaments is the depolymerization transition. The ethylene glycol concentration at which this transition occurs varies with the salt content. Small amounts of added salt enable the ethylene glycol to reach higher concentrations before depolymerization occurs. However, past 50 mM NaCl, more salt leads to lower ethylene glycol concentrations required for depolymerization. The fact that there are no polymorphic transitions in 1655 filaments may indicate that the all R configuration

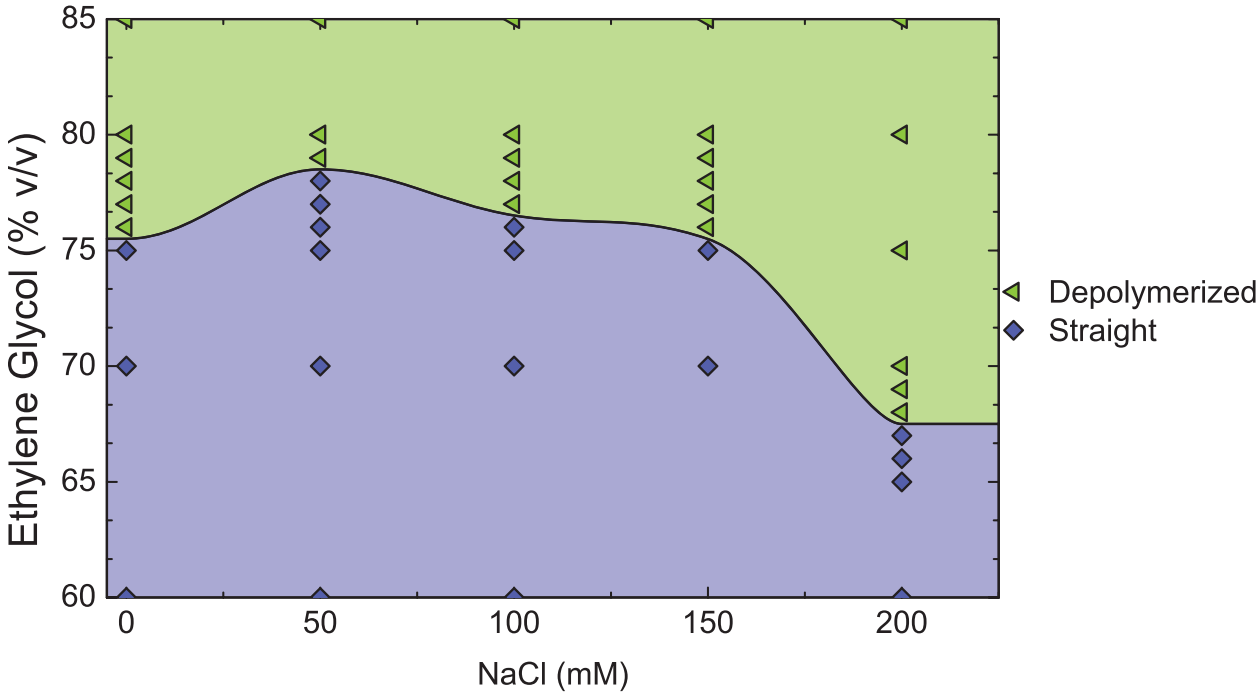

Figure 3.6: Phase diagram for SJW 1655 filaments in ethylene glycol and salt solutions. Unlike the other straight mutant, 1660, the all R filaments are unable to transition into a normal phase with added salt. However, even though they are unable to transition, they are able to go to higher ethylene glycol concentrations before depolymerizing compared to the 1660 filaments.

is the most stable configuration in the presence of ethylene glycol or that the energy cost of transitioning out of the all R state is too large and therefore will only happen extremely rarely or not at all.

3.3.4 Block Copolymer Flagella

The question of how a block copolymer, comprised of two of the previous sections flagella types, responds to ethylene glycol solutions could have two different responses. Perhaps the most logical hypothesis for how the block copolymers respond to ethylene glycol is that each side of the block copolymer will respond with the same phase behavior as an isolated filament

of that strain. In other words, the block copolymer is comprised of two isolated filaments that each respond to the ethylene glycol according to the phase diagrams from above, but have no direct effect on the other side of the block copolymers phase response.

Another hypothesis for how block copolymer might respond to ethylene glycol is that the phase behavior will be completely new and different from the phase diagrams of each individual strain. This would occur because the point where the two sides of the block copolymer are joined necessarily has flagellin monomer arranged in a geometrically frustrated way because at least two protofilaments are broken across the joint for the two sides to be in different conformations. As the ethylene glycol concentration increases, conformational changes in the monomers at the joint could propagate down the length of either side of the filament. It is plausible that a change at one end of a filament can propagate the entire length because that is exactly what occurs regularly in *in vivo* systems. Changes in conformation occur at flagellin monomers near the rotary motor as the motor changes and propagate the length of the filament in order to facilitate the polymorphic transitions used for run and tumble behavior.

Experimental results of the first type of block copolymer investigated, 1103/1655 normal/straight filaments, are presented in Figure 3.7. When exposed to ethylene glycol solutions, these block copolymer filaments transition from a normal/straight shape to a coiled/straight shape. This transition shows a very broad coexistence region in which both normal/straight and coiled/straight are present in samples. The fact that the 1103 side of the filament transitions from normal to coiled is perhaps expected since this is the same transition that 1103 filaments undergo when not assembled into a block copolymer filament. The concentration of ethylene glycol necessary to induce this transition is similar to the concentration required to induce the normal to coiled transition in isolated 1103 filaments. The primary difference in these transitions is that by increasing NaCl concentration, it is possible

to induce a coiled/straight state without having any ethylene glycol in solution. As ethylene glycol concentration is increased further, the coiled/straight filaments transition into fully straight filaments. The fully straight filaments may or may not have a residual bend at the joint between the two types of monomers. For more discussion about this residual bend, see the next section.

For very low and high salt content, there are coiled/straight and straight coexistence regions in the phase diagram where both states stably exist. However, for salt concentrations around 50 mM, the coexistence region disappears and the filaments will transition very rapidly with increasing ethylene glycol to a fully straight phase. Increasing the ethylene glycol concentration past the straight phase leads to depolymerization of the flagellar filaments. Overall, each side of the 1103/1655 block copolymer filaments exhibit the same phases as isolated 1103 or 1655 filaments with the 1655 side staying straight until depolymerization while the 1103 side of the filament transitions from normal to coiled to straight before it depolymerizes with increasing ethylene glycol.

In addition to the 1103/1655 block copolymers, we also synthesized 1103/1660 block copolymers using the same *in vitro* polymerization technique. The filaments morphologies are the same, showing a normal helix on one side of the block copolymer and a straight segment on the other. However, the difference is that the straight segment of these block copolymers, being made from 1660 monomers, has an 11L/0R protofilament configuration as opposed to the previous block copolymers 0L/11R. If each side of these block copolymers were to exhibit the same phases as the individual filaments, then from a normal/straight morphology with no added ethylene glycol, the normal side would transition to coiled and then straight before depolymerizing; the straight side would transition to a normal state before depolymerizing. This could possibly lead to a scenario in which a normal/straight filament could, with increasing ethylene glycol, transition to a straight/normal state in which

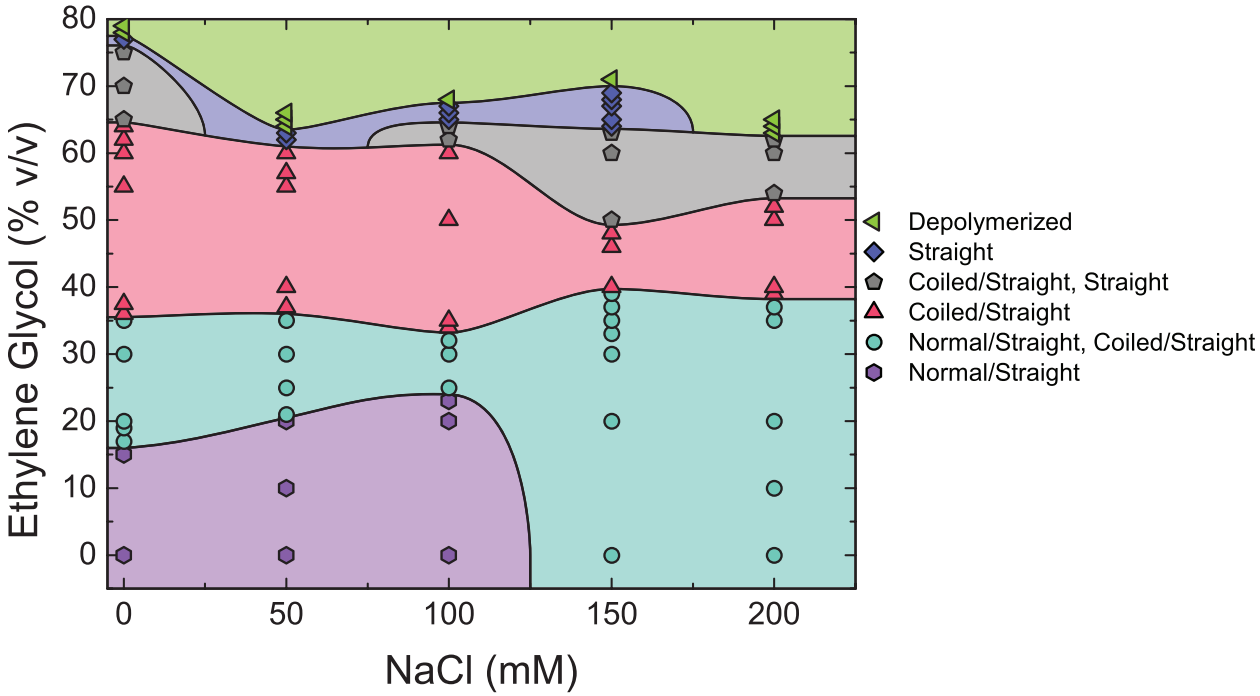

Figure 3.7: Phase diagram for 1103/1655 block copolymers in ethylene glycol and salt solutions. These block copolymer filaments exhibit phase transitions consistent with the 1103 and 1655 filaments individually. Namely, the 1655 side of the filament is straight for all phases and the 1103 side of the filament will transition from normal to coiled to straight with increasing ethylene glycol.

the two sides of the filament exhibit the others initial morphology.

However, 1103/1660 block copolymers, by way of being joined in a block copolymer do not exhibit the same phase behavior as isolated filaments (Figure 3.8). As ethylene glycol is increased, 1103/1660 block copolymers will transition to a curly state as shown in Figure 3.9. This consists of the entire length of the filament assuming a curly morphology, 1103 and 1660 monomers alike. For the 1103 side of the block copolymer, this represents a transition from a 9L/2R protofilament configuration to a 6L/5R arrangement. Meanwhile the 1660 portion of the filament undergoes a transition from an 11L/0R configuration to a 6L/5R arrangement of protofilaments. Increasing the ethylene glycol further causes a transition in a single protofilament leading to a semicoiled state along the entire filament. This means that the filament transitioned to a 7L/4R protofilament configuration. Increasing the ethylene glycol further introduces a fully straight morphology. This is the expected phase response of isolated 1103 filaments and for 1660 filaments in low salt conditions. The only transition at a higher ethylene glycol concentration from the straight phase is the depolymerization boundary.

The 1103/1660 block copolymers exhibit phases in the block copolymer phase diagram that neither filament show as isolated filaments in ethylene glycol. The act of joining the two filaments together as a block copolymer somehow changes the phase response of the filament. The cause of these changes are likely to be localized to the point at which the monomers from the two sides of the block copolymer join together. This is because any conformational change at any point in a protofilament propagates along the protofilament. This is why conformational changes are observed *in vivo* to occur at the proximal end of the filament where it is joined to the flagellar motor and then propagate outward to the distal end. In this case, the two sides are initially different conformations, the monomers at the joint cannot be regularly arranged into protofilaments like the rest of either side of the filament. Otherwise,

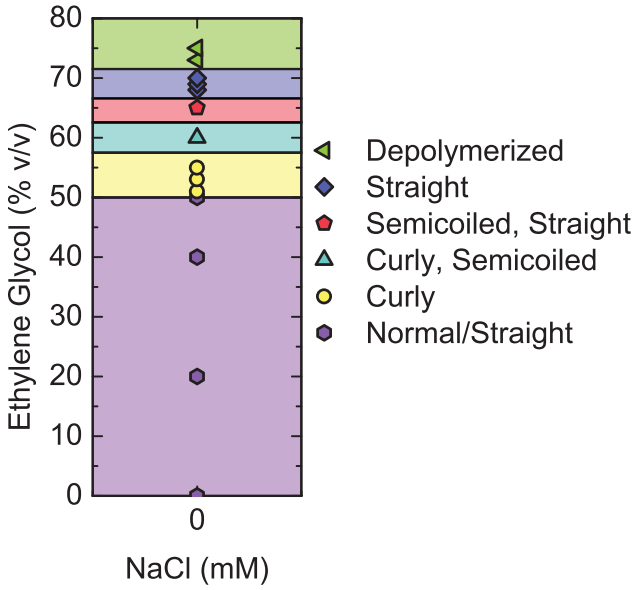

Figure 3.8: Phase diagram with no added salt for 1103/1660 block copolymers in ethylene glycol solutions. Unlike the 1103/1655 block copolymers, new phases that are not in either individual filaments phase diagrams appear. The curly and semicoiled phases propagate through the entire filament. The arrangement of monomers at the joint between the two types of flagellin must interact with the protofilaments of either side to cause these anomalous transitions to occur.

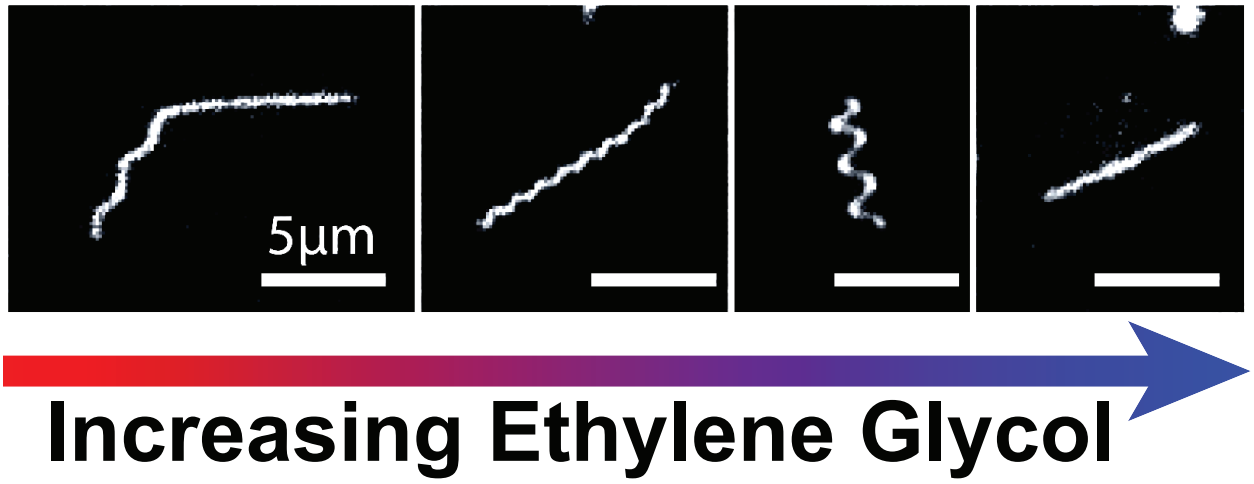

Figure 3.9: The different phases that 1103/1660 block copolymers exhibit as ethylene glycol is increased. The 1660 part of the block copolymer exhibits phase transitions along with the 1103 side of the filament. The transitions are reversible if the ethylene glycol concentration is reduced. The curly and semicoiled phases are not present in either 1103 or 1660 filament phase diagrams and only appear when the two types of flagellin are present in a block copolymer filament.

protofilaments would have to assume more than one conformation simultaneously and they would therefore not be in a stable configuration. Instead, the monomers located at the joint must experience some sort of packing frustration. It may be that some of the protofilaments are able to continue unabated across the joint into the other side of the filament, but it is necessary that at least the two R protofilaments of the 1103 side of the filament terminate at the joint.

The monomer packing at this joint and the discontinuous protofilaments somehow is able to have a great effect on the conformation of monomers in the protofilaments as ethylene glycol concentration is increased. Exactly how this is accomplished is unclear, but it exhibits consistency across all 1103/1660 block copolymers. If the monomers were arranged in a disordered fashion at this joint, it would be reasonable to suspect that different filaments would behave in different ways depending on the precise arrangement of monomers. However,

because the transitions are so consistent across all the filaments, it is reasonable to assume that the monomeric arrangement must at least be very similar for all the filaments.

The fact that 1103/1660 block copolymers can share up to 9 protofilaments in common may explain why it assumes the same morphology along the entire filament while 1103/1655 filaments, which can only share up to 2 protofilaments in common, have each side of the filament seem to behave independent of one another. Having more protofilaments that are able to be joined continuously along the joint between the two types of monomer may enable the 1103/1660 filaments to more cooperatively transition one or more of those protofilaments in order to ease any deformations caused by the irregular packing of monomers at the joint. If multiple protofilaments are unbroken across the joint, then it would also help explain why there is such consistency between different filaments in the phase behavior. The more protofilaments that are unbroken across the joint, the less space for monomers to disorderly arrange themselves to try to bridge the gap between protofilaments that do not continue unbroken across the gap. This means that there would be fewer possible arrangements that these irregularly packed monomers could assume, leading to more consistent phase behavior across the population of 1103/1660 block copolymers.

Overall, polymorphic transitions of bacterial flagella in ethylene glycol and salt solutions exhibit several things in common. There was never any observed difference in phase behavior between purified and polymerized filaments. Not every sample condition was checked, but each phase diagram was spot checked and the observed phase behavior was the same for both types of filament. Similarly, whether a filament was fluorescently labeled or unmodified and observed via darkfield had no effect on the observed phase behavior. This was again determined by spot checking different phase diagrams, but no differences were observed. All the transitions, with the exception of depolymerization, are fully reversible if the solvent conditions change. This includes the 1103/1660 block copolymers in which they appear to

no longer be block copolymers after they transition into a curly phase. If they are exposed to a solution with little or no ethylene glycol, they will once again assume a block copolymer shape of normal/straight.

3.4 Temperature Mediated Polymorphic Transitions

3.4.1 Methods

Phase diagrams showing the polymorphic shapes that flagella assume in differing sample conditions only show steady state polymorphic states. One of the key biological functions for flagella is to be able to dynamically change helical shape in response to a changing environment. Previous studies have studied polymorphic transitions in changing environments through a range of different experimental techniques including flowing solution over tethered filaments [82, 85], exerting force via optical tweezers [81, 99], applying torque [59, 81], and changing temperature [84]. It is this last strategy that we pursue in the results presented here. Previous studies were conducted with acidic (pH 4-6) solutions, where our results are in a basic (pH 7.5-8.5) range. With the sample conditions presented in the phase diagrams of the previous section, changing the temperature of the sample is unable to cause a change in filament morphology.

To make samples more temperature sensitive, we added a considerable concentration of Tris buffer rather than just the potassium phosphate buffer used normally. Tris has a very temperature sensitive pK_a and therefore the pH will change considerably with the temperature of the solution [100–104]. With an increase in temperature of 1°C, the pH of the Tris solution changes by -0.028. This means that a sample prepared at room temperature with a pH of 8.0, when heated to 40°C, will have a pH of approximately 7.7 and when cooled

to 10°C the pH will be approximately 8.4. However, changing the pH of the solution is not sufficient to induce the transitions described in this section. This is checked by preparing Tris buffers at different pH values and checking the morphologies of the filaments in a range of conditions. In all of the following results, both the pH value and the temperature are necessary components to trigger a polymorphic transition.

Not every polymorphic transition observed in ethylene glycol solutions lends itself well to being triggered using a Tris solution. One characteristic that transitions need to have to behave predictably and repeatedly with Tris-mediated temperature induced polymorphic transitions are that the transition should have a small or non-existent coexistence region with the two morphologies of the transition. Coexistence regions indicate that either morphology in those regions is relatively stable. Trying to use temperature to induce these transitions leads to either filaments that show no transition or only a very small number of the filaments will undergo a shape transition. Another factor we have found to be a good indicator that a transition will occur via pH changes in Tris solutions is that the filaments are sensitive to salt concentration. Only transitions for which the ethylene glycol concentration can change significantly depending on the salt concentration are easily triggered by the changes in pH. Experimentally, samples were prepared with refrigerated flagella in storage buffer. The non-flagella components of the final sample were combined and mixed well before adding flagella to the sample. Tris buffers were prepared with a pH of 8.0 and the resulting samples with ethylene glycol, salt, potassium phosphate buffer and Tris combined had a pH very near 8.0 due to the high concentrations of Tris used.

The sample temperature was controlled via a Peltier module that was used to heat and/or cool the oil-immersion objective of the microscope. The objective would then, by way of direct contact, heat or cool the slide containing the sample. The temperature is measured by way of a thermistor embedded between the Peltier device and the objective. Reported

temperatures reflect this value rather than the true value of the temperature of the sample, which is exposed to room temperature air on the side opposite the objective. This means that the true sample temperature is closer to room temperature (approx. 23°C) than the reported value. In all of the temperature based experiments, flagella that was purified had the same phase response as that of polymerized filaments. Similarly, fluorescently labeled filaments imaged via fluorescence as well as unmodified filaments imaged via darkfield showed the same behavior. The main difference for these experiments is that fluorescent filaments in ethylene glycol solutions photobleach must faster than without ethylene glycol present.

Overall, temperature induced polymorphic transitions have several things in common. Apart from 1660 filaments transitioning from straight to normal, all the transitions were reversible to some degree by changing the temperature in the opposite direction. Purified and polymerized filaments behaved the same in all experiments and showed the same transitions. The same is true for fluorescently labeled and unmodified filaments; the method of visualization made no difference to the transitions between phases. Flagella concentration does affect the phase behavior in that either a higher temperature of the Tris solution is required or additional salt needs to be added to the solution to keep the transition temperature the same. For each 1 mg/mL increase in the concentration of flagella, 5 mM of NaCl must be added in order to keep the same transition temperature.

3.4.2 SJW 1103 Flagella

With these limitations in mind, one transition that works well in practice is the coiled to straight transition in 1103 filaments. By preparing samples with a high Tris concentration, it is possible to induce 1103 filaments to transition into a straight form from a coiled state by increasing temperature (Figure 3.10). Under ideal conditions, the lowest temperature with

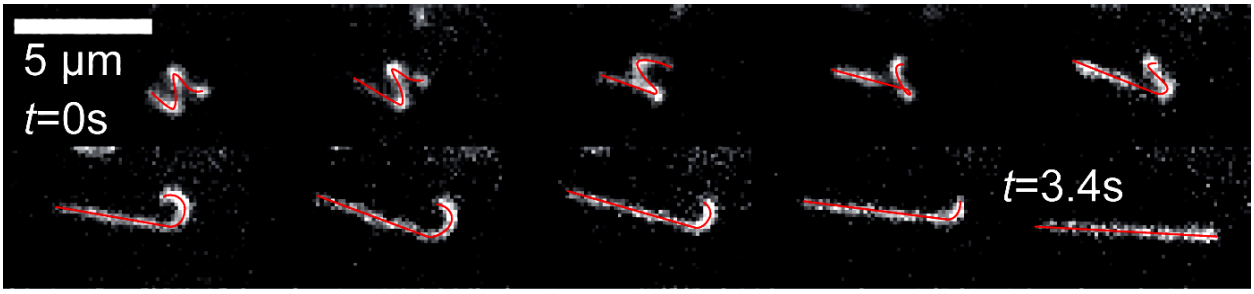

Figure 3.10: Timelapse of an SJW 1103 filament transitioning from a coiled state to a straight state with increasing temperature. This video was recorded with sample conditions of 60% v/v ethylene glycol, 400 mM Tris pH 8.0, 10 mM potassium phosphate and the temperature was being raised from room temperature ($\approx 23°C$) to 40°C.

which we could induce this transition is 34°C. At these temperatures, the filaments are stable. If the temperature of the system is increased beyond the transition point, flagella will begin to bind together and cross-link with one another. With a further increase in temperature, the cross-linked flagella will begin to depolymerize. We have shown the transition to be mostly reversible through lowering the temperature with a small population of filaments that will fall back into a normal state instead of coiled and another small population that stay in the straight state indefinitely as shown in Figure 3.11. The relative time scales of the two transitions are different as well. The transition from coiled to straight as the sample is heated happens over the course of roughly a minute for the entire sample to undergo the transition. Meanwhile, when the sample is cooled below room temperature, it can take 30 or more minutes for the flagella to transition back into either coiled or normal.

Another sample parameter that was found to change the transition behavior was flagella concentration. Higher concentrations of flagella required higher ionic strengths or higher temperatures to induce the transition. To avoid depolymerization and aggregation problems that arise with a high temperature, adding NaCl is the preferred method. We found that an increase in concentration of 1 mg/ml flagella requires approximately a 5 mM increase in

NaCl concentration to keep the transition temperature the same as before the increase in concentration. It is not clear what causes the concentration of flagella to affect the phase behavior in this way, but it is likely related to electrostatic interations. This is because changing the temperature of the tris solution (and therefore the pH) and changing the salt concentration of the solution influences the electrostatic interactions of the flagellin monomers.

The 1103 filament, as it transitions from coiled to straight exhibits two morphologies simultaneously for a period of time, similar to a block copolymer filament. Normally, block copolymer filaments in a dense suspension are in a jammed system and cannot reptate through the network (see chapter 4). So, it might be surmised that in a dense suspension of flagella in a coiled state, as the transition occurs, the flagella may get jammed partway through the transition while in a block copolymer state. However, in practice, this doesnt occur. In a dense suspension, both helical filaments and straight filaments are still able to reptate longitudinally through corkscrew motions and diffusion respectively. So, as a coiled filament transitions to straight, the coiled segment of the flagellum can rotate freely in the suspension at the same rate at which the straight segment can diffuse longitudinally. This essentially acts as the helical portion is rotating in order to feed the straight segment of the flagella. This same behavior takes place in reverse when a straight filament transitions to a helical shape. This enables filaments to freely transform between helical and straight states without the problems of getting into a jammed state and stuck partway through a transition.

3.4.3 SJW 1660 Flagella

Another transition that lends itself well to be induced via temperature control is that of the straight to normal transition in 1660 filaments. In the right conditions, an increase in

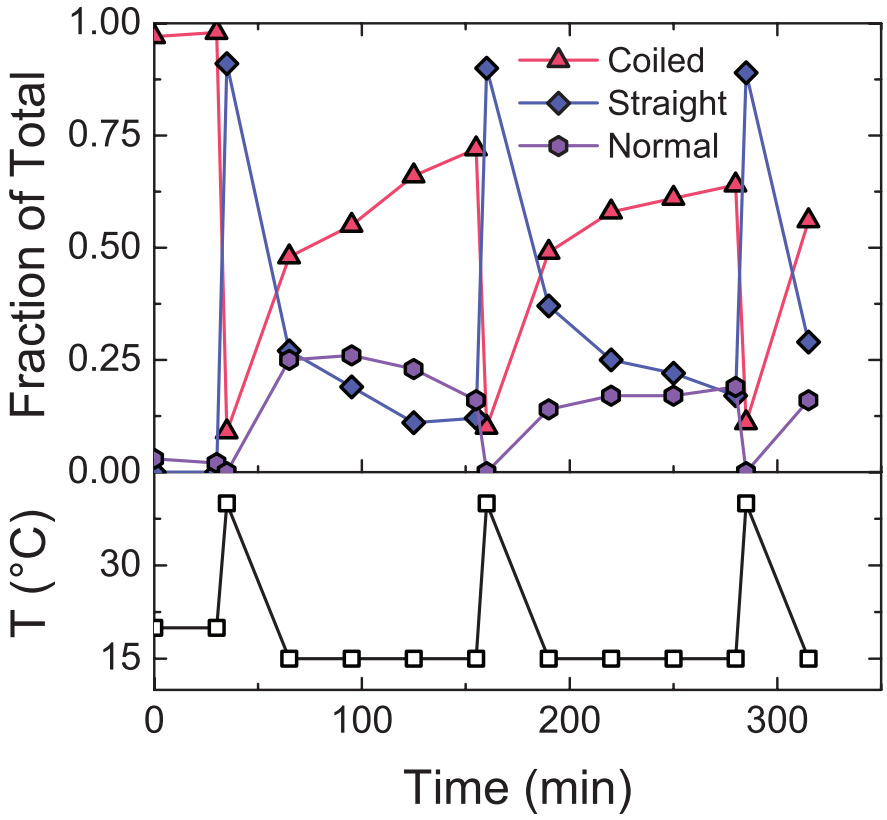

Figure 3.11: A single sample undergoing multiple temperature induced polymorphic transitions. Initially, the temperature of the sample is room temperature and the flagella are almost entirely in the coiled form. When the temperature is briefly raised, the filaments transition to a straight shape. When the sample is cooled again, the filaments assume a variety of shapes: straight, coiled, and normal. The fraction of coiled filaments slowly increases as the sample is kept cold and the fraction of straight filaments correspondingly lowers over this same time frame. Three total hot cycles are shown.

temperature can trigger a polymorphic transition so that the straight (11L/0R) filaments transition into a normal (9L/2R) morphology as shown in Figure 3.12. This transition happens on a much longer timescale than the coiled to straight transition in 1103 filaments. In sample conditions of 63% v/v ethylene glycol, 400 mM Tris, and 10 mM phosphate buffer, 1660 filaments can take an hour or more at 37°C before the transition to a normal state occurs. Increasing the concentration of filaments also increases the timescale at which the transition occurs. A sample at 10 mg/ml or greater can take four hours or more to transition to a normal morphology.

Another difference between this transition and the coiled to straight transition in 1103 filaments is that the 1660 filaments, once in the normal state, will not transition back to a straight filament when the temperature is reduced. This lack of reversibility suggests that a normal state may be the more stable configuration for filaments even at lower temperature, there is just an energy barrier that is too large to overcome with the smaller amount of thermal energy. This is corroborated by the phase diagram of 1660 filaments in ethylene glycol in which it can be seen that 1660 filaments that have transitioned into a normal state are more stable than those that remain straight. This is evident by the fact that the normal phase filaments can go to higher ethylene glycol concentrations before depolymerization than the straight filaments. Taken together, both of these experimental results suggest that, for 1660 filaments, the straight conformation is merely a long lived metastable state just below the transition point at which the flagella assume a normal morphology.

3.4.4 Block Copolymer Filaments

Another polymorphic transition that we observe by changing the temperature of a Tris solution is the coiled/straight to straight transition in 1103/1655 block copolymer filaments.

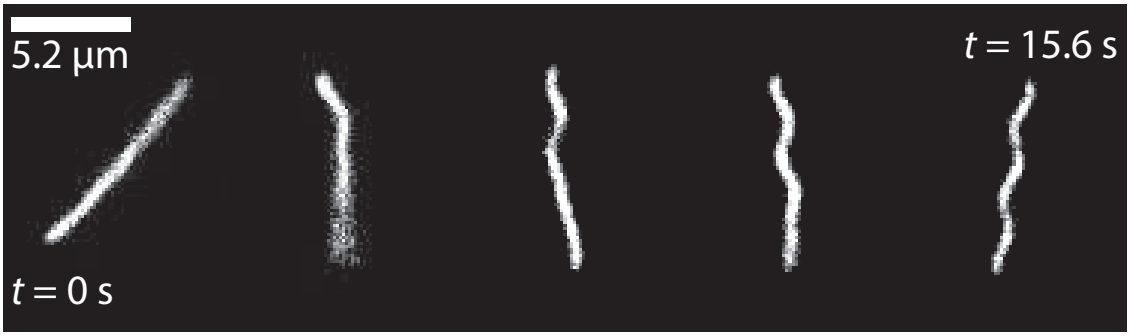

Figure 3.12: A straight SJW 1660 filament undergoing a temperature induced transition to a normal state. The sample conditions are 63% v/v ethylene glycol, 400 mM Tris pH 8.0, 10 mM potassium phosphate and the temperature was raised from room temperature to 40°C. This transition signals that two of the 11 protofilaments transitioned from an L state to an R state. Also, this transition is irreversible through temperature.

Surprisingly, we observe two different pathways by which this transition occurs. The first type of transition is that the coiled side of the filament will transition directly to a straight morphology. This typically leaves the filament with a residual bend located at the point where the two types of flagellin monomers are joined (Figure 3.13). This residual bend at the joint maintains a fixed angle and remains stable for long periods of time. This means that the transition occurs on the 1103 side of the filament in isolation, not propagating through the junction to the 1655 side of the filament. The disordered arrangement of flagellin monomers at the joint are arranged in such a way so as to stop this kind of morphological propagation. This type of transition is essentially no different than the coiled to straight transition in isolated 1103 filaments.

The other method that 1103/1660 block copolymers transition into a straight state is that as the temperature increases, the filaments will first transition from coiled/straight to a curly/straight state (Figure 3.14) which then transitions to a fully straight state that lacks any residual bend left in the filament (Figure 3.15). This fundamentally differs from the other transition method in that a new phase, curly, appears that is not a phase assumed

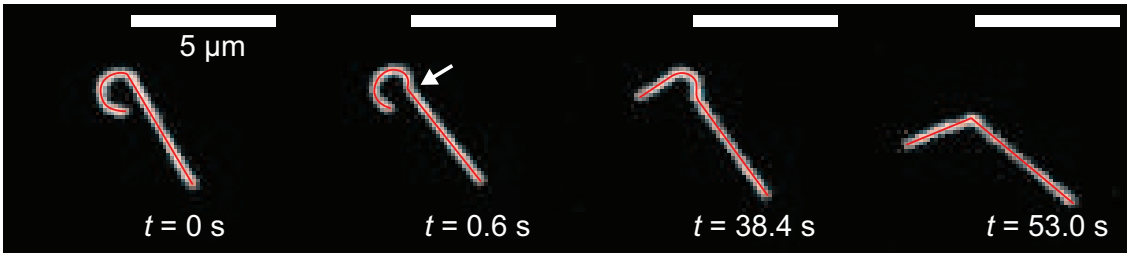

Figure 3.13: A 1103/1655 block copolymer undergoing a transition from coiled/straight to straight with a leftover bend at the joint. The sample conditions were 60% v/v ethylene glycol, 400 mM tris pH 8.0, 100 mM NaCl, 10 mM potassium phosphate and the temperature was raised from room temperature to 37°C. The transition begins with a pronounced bend at the location that the two flagellins are joined (marked with arrow) but then the far end transitions to straight and the transition propagates to the joint but no farther.

by either type of filament in isolation. In all other observed polymorphic transitions of 1103/1655 block copolymer filaments, either side of the block copolymer exhibits the same phases as the respective types of filaments in isolation. The time scales of each of the two steps of this transition are both on the order of minutes with the coiled to curly transition happening faster than the curly to straight transition. For similar reasons as presented for the 1103/1660 block copolymers, the difference between filaments that go through the curly phase before straight and filaments that go directly to straight must lie in the monomer packing at the joint. Looking at the phase behavior of 1103/1655 block copolymers that follow this transition pathway shows a trend in the 1103 side of the filament with regards to protofilament conformation.

The first transition with increasing ethylene glycol is a transition from normal, 9L/2R, to coiled, 8L/3R. With more ethylene glycol, the next transition is from coiled, 8L/3R, to curly, 6L/5R. Each transition sees more protofilaments change from the L to R state. The 1655 side of the filament is in a 0L/11R state for each of these transitions. After the curly phase transitions to straight, there is no remaining bend left in the filament, indicating that the protofilaments are likely able to anneal any defects at the joint by going through

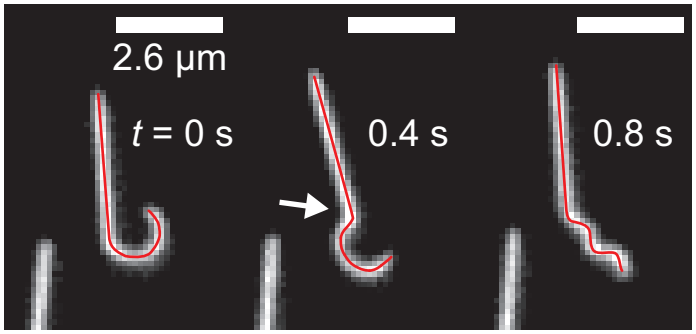

Figure 3.14: An 1103/1655 block copolymer filament undergoing a temperature induced transition from a coiled/straight shape to a curly/straight form. The sample conditions were 60% v/v ethylene glycol, 400 mM tris pH 8.0, 100 mM NaCl, 10 mM potassium phosphate and the temperature was raised from room temperature to 37°C. Like the transition to straight that leaves a residual bend at the joint, this transition pathway begins with a pronounced bend at the joint between the two types of flagellin monomers. The curly shape is not present in the 1103 filament phase diagram and only appears when the filament is assembled in a block copolymer.

the curly phase and are likely in the 0L/11R state just like the 1655 side of the filament. It is unclear why some filaments transition to curly before becoming straight while others transition directly to a straight phase but with a residual bend. The difference must be related to the monomer packing at the joint of the two types of monomers. The filaments that transition directly to straight have a discontinuity in their protofilaments while the flagella that go through the curly phase can anneal the protofilaments together to eliminate the residual bend at the joint.

In general, block copolymer filaments appear to be a great model system in that reversibly inducing a transition from a block copolymer to a non-block copolymer would have a dramatic effect on the material properties (Chapter 4 for more discussion). The transitions in block copolymer are the least efficient of any measured. While isolated filaments in the sample undergo the transitions presented in this section, there is a sizable portion of block copolymers (roughly half) that do not undergo the transition at all in these samples. So,

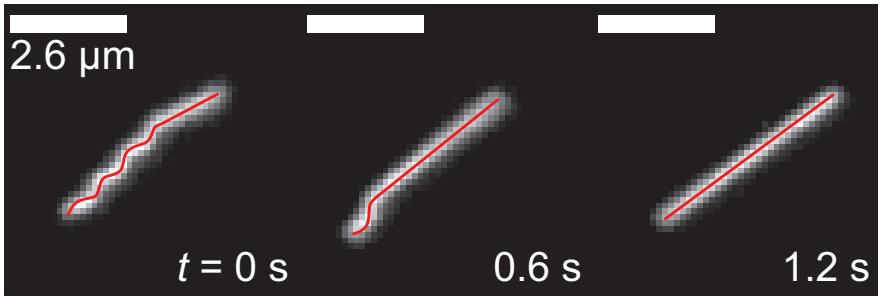

Figure 3.15: An 1103/1655 block copolymer filament undergoing a temperature induced transition from a curly/straight to a straight form. The sample conditions were 60% v/v ethylene glycol, 400 mM tris pH 8.0, 100 mM NaCl, 10 mM potassium phosphate and the temperature was raised from room temperature to 37°C. This transition occurs at the same conditions and sequentially after the coiled/straight to curly/straight transition. Typical filaments will transition from coiled/straight to curly/straight and then, after several minutes will transition again to a completely straight form. Filaments undergoing this transition pathway are left as straight filaments without a residual bend at the joint.

while the block copolymer results are interesting and could inspire further research to locate conditions in which a transition is reliable, scaling up block copolymer transitions to bulk samples is not feasible for this study.

3.5 Conclusion

Polymorphic transitions in bacterial flagella, in addition to aiding bacteria switch from a run phase to tumble and back [59, 81, 105], offer the opportunity for dynamic behavior of the colloidal particles. Helical colloidal particles have been synthesized and studied before [65–67, 72, 106–108], but no synthetic helical particles can undergo polymorphic transitions. While synthetic helical particles do have the advantage that parameters such as pitch and radius can be adjusted experimentally, changing these parameters involves synthesizing new particles.

Bacterial flagella are able to be prepared with a range of helical properties based purely

on the conditions they are in. For instance, a purification of 1103 filaments can assume any of the following shapes just from the results presented in this work: straight, normal, coiled, and curly. The ability to change the filament shape with temperature also allows for investigation of dynamic colloidal systems that are undergoing a morphological change. This is typically a behavior exhibited by active systems such as self-propelling particles [109] or motor proteins [110, 111]. In the case of flagella, thermal energy is used to dynamically change shape, completely changing the properties of the colloidal suspension. A more detailed discussion of bacterial flagella suspensions and the effects of filament geometry is presented in the next chapter.

Chapter 4

Properties of Bacterial Flagella Suspensions

4.1 Introduction

Chapter 3 presented results illustrating the rich phase response of different bacterial flagella strains to changing environmental conditions. However, the phase behavior and induced transitions are all single filament properties. In this chapter, we present results of experiments conducted on dense suspensions of many flagella. In dense concentrations, bulk material properties of the suspensions emerge as the result of the many particles becoming entangled with one another within the sample. The way in which the individual filaments entangle depends on the geometry of the filaments. This, in turn, depends on the environmental conditions and the strain of flagellin being used and is the way in which the results from chapter three segue into the following chapter. Better understanding the individual flagellar filaments response to environmental conditions enables better insights into the bulk material properties of dense suspensions.

In this chapter, we discuss how individual colloidal particles behave in a suspension and how the shape of bacterial flagella can change this behavior. Additionally, we discuss bulk rheology measurements of complex materials and present rheological results for bacterial flagella suspensions of differing concentration and shape. Finally, we discuss microrheology results for concentrated bacterial flagella solutions.

4.2 Flagella Dynamics

4.2.1 Theory of Reptation

Understanding the dynamics of bacterial flagella, a biopolymer, in dense suspensions, first requires understanding of dynamics in polymeric solutions in general. The theory describing polymer solution behavior was first proposed by de Gennes and later refined by Doi and Edwards [21, 22]. These theories describe model systems in which polymers are in the flexible regime and can easily become entangled through bending. More relevant to the system in this study, Doi and Edwards later went on to describe the reptation of rigid, rod-like particles in suspension [112]. The reptation model essentially states that polymers are undergoing Brownian motion, but are constrained by the neighboring particles in how far they can diffuse in any given direction. The neighboring particles are essentially acting as a cage around the particle of interest (Figure 4.1). Diffusion is freely allowed within the tube around the polymer bound by the nearest neighbors.

Reptation of rigid rod-like particles is similar to the theory for flexible filaments except that the particles are no longer isotropic in all directions. Rod-like particles have a long axis and a transverse axis that need to be treated separately [113]. Flexible polymers undergoing reptation can be approximated by a random walk [22, 24], equally likely to diffuse in any

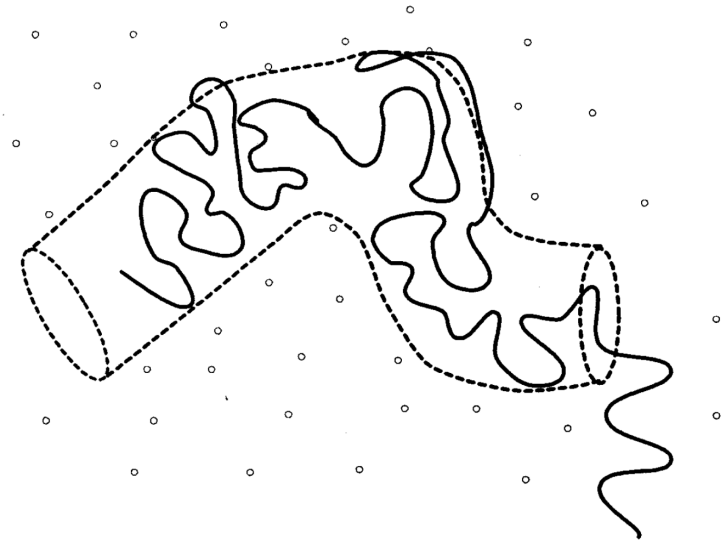

Figure 4.1: Schematic representation of a flexible polymer (solid line) confined inside a tube (dashed line) defined by the nearest neighbors of the polymer (small circles). Figure reprinted from [25].

direction because it can easily bend around obstacles at very sharp angles. However, this is not true for rigid rods. If the rotational diffusion is in any way inhibited, the rigid rod-like particles will preferentially diffuse in a direction parallel to the long axis [113]. In general for rod-like particles, the diffusion coefficient for the long axis and the transverse axis is given by

$$D_\alpha = \frac{k_\mathrm{B}T}{\gamma_\alpha} \tag{4.1}$$

where γ is the translational hydrodynamic friction coefficient and α can either be $\parallel$ or $\perp$ denoting the long axis and the transverse axis respectively. The value of $\gamma_\parallel$ is typically much less than $\gamma_\perp$ (a factor of 2 in the dilute limit, a larger difference in semi-dilute and concentrated solutions) meaning that diffusion in the long axis direction occurs much faster than in the transverse direction [16, 113].

The diffusion of rigid rods in dilute suspensions exhibit timescale-dependent behavior.

Because diffusion occurs faster along the long axis of the rod-like particle, the rotational motion of the particle appears diffusive only at longer timescales. Above timescales given by τ_r, the motion of rod-like particles appear diffusive where τ_r is given by

$$\tau_r = \frac{1}{2D_r} \tag{4.2}$$

where D_r is the rotational diffusion coefficient of the particle. In the semidilute regime D_r can be approximated by

$$D_r \simeq \beta D_{r0}(vL^3)^{-2} \tag{4.3}$$

where D_{r0} is the rotational diffusion coefficient in dilute suspensions, v is the number density of rods, L is the length of the rods, and β is a numerical factor (typically on the order of 10^3) [16]. This means that the rotational relaxation timescale, τ_r, increases accordingly.

$$\frac{\tau_r}{\tau_{r0}} = \frac{(vL^3)^2}{\beta} \tag{4.4}$$

where τ_{r0} is the rotational relaxation time given by Equation 4.2 using $D_r = D_{r0}$ [16]. The strong concentration and especially strong length dependence exhibited in semidilute solutions of rods means that investigating bacterial flagella dynamics over a wide range of timescales is necessary.

In this section, we present results of imaging and tracking individual flagellar filaments diffusing through concentrated suspensions. Data was obtained through fluorescently imaging individual flagellar filaments in a suspension of non-fluorescently labeled filaments. The long axis, transverse axis, and rotational motion were each tracked and mean squared displacement calculated. This enables for the calculation of the diffusion coefficient for each type of diffusive motion and helps to identify anomalous diffusive behavior. Normal diffusive

behavior is seen when the mean squared displacement is proportional to the lag time.

$$\left\langle r^2(t) \right\rangle = 2nDt \tag{4.5}$$

where n is the dimensionality, and D is the diffusion coefficient. More generally, anomalous diffusion is accounted for by introducing an exponent, α.

$$\left\langle r^2(t) \right\rangle = 2nDt^{\alpha} \tag{4.6}$$

Systems with a value of α greater than 1 are called superdiffusive, meaning that the motion is greater than that of diffusion alone, while systems with a value less than 1 are referred to as subdiffusive. This means there is something that is inhibiting the diffusive motion of the particles.

4.2.2 Previous Results

From previous studies looking at the motion of straight bacterial flagellar filaments as they diffuse, it is clear that the diffusion along the long axis of the filaments is much greater than that of the transverse or angular directions [114]. This is consistent with reptation theory for rigid rods because the tube in which diffusion is allowed would be much less constrained in a longitudinal direction than transverse (Figure 4.2). This is also apparent in the mean squared displacement curves for straight filaments. As can be seen in Figure 4.3, in the direction of the long axis, motion is shown to be purely diffusive while for the transverse direction the motion is subdiffusive over intermediate time scales, smaller than the reputation time but larger than the time to diffuse within the cage defined by its nearest neighbors.

Filaments in a normal conformation also show diffusive behavior in the long axis direction as well as can be seen in Figure 4.5 [114]. However, the means by which this diffusion occurs

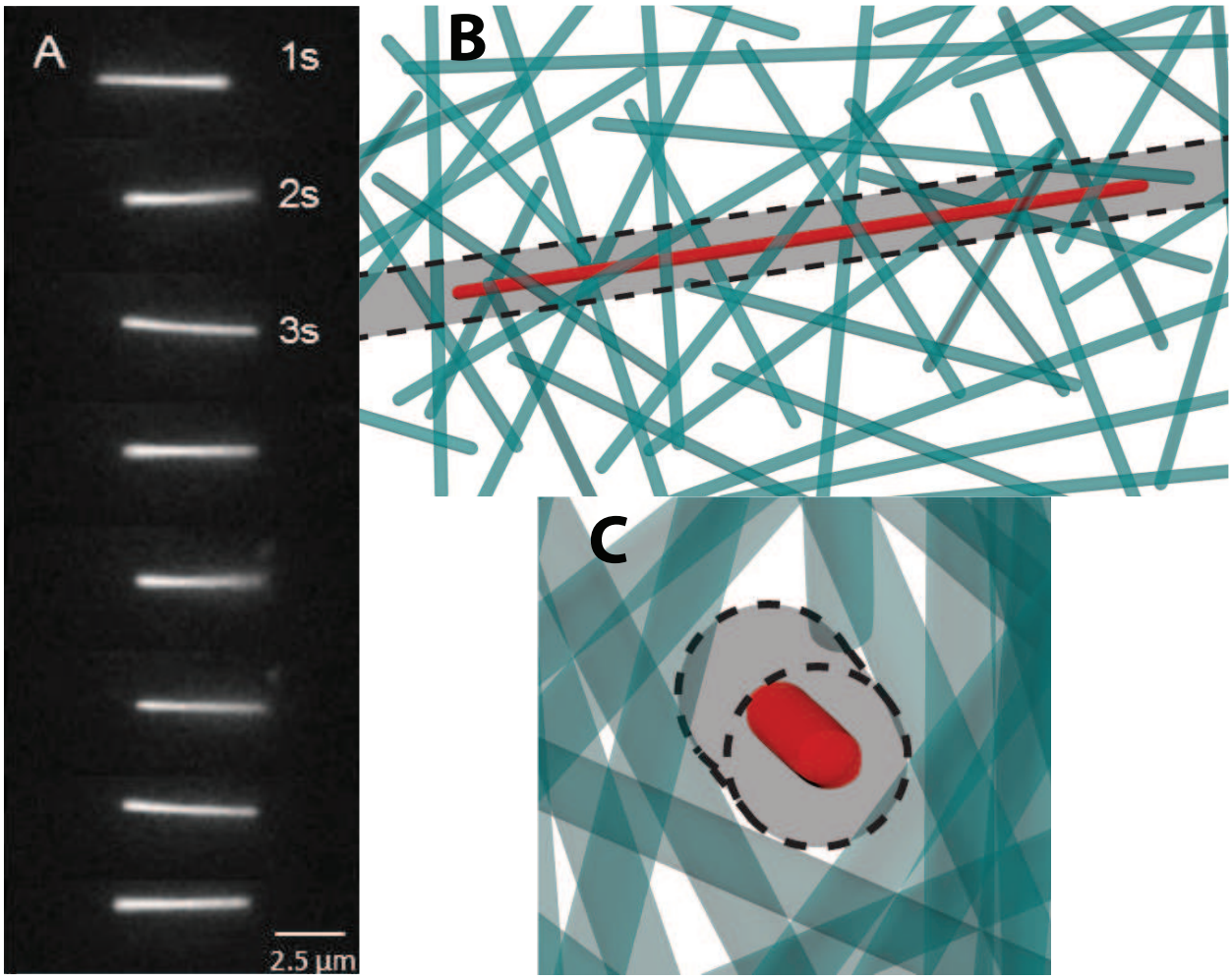

Figure 4.2: A) Time series of a straight flagellum that is fluorescently labeled undergoing diffusion in an unlabeled background of straight filaments. Diffusion primarily takes place in the direction of the long axis. B) Top down schematic of a labeled (red) straight flagella undergoing diffusion in a crowded environment of straight flagella. C) Same configuration as B, but with the point of view rotated to look down the long axis of the marked filament. This enables visualization of the tube around the straight filament in which it is free to diffuse unimpeded.

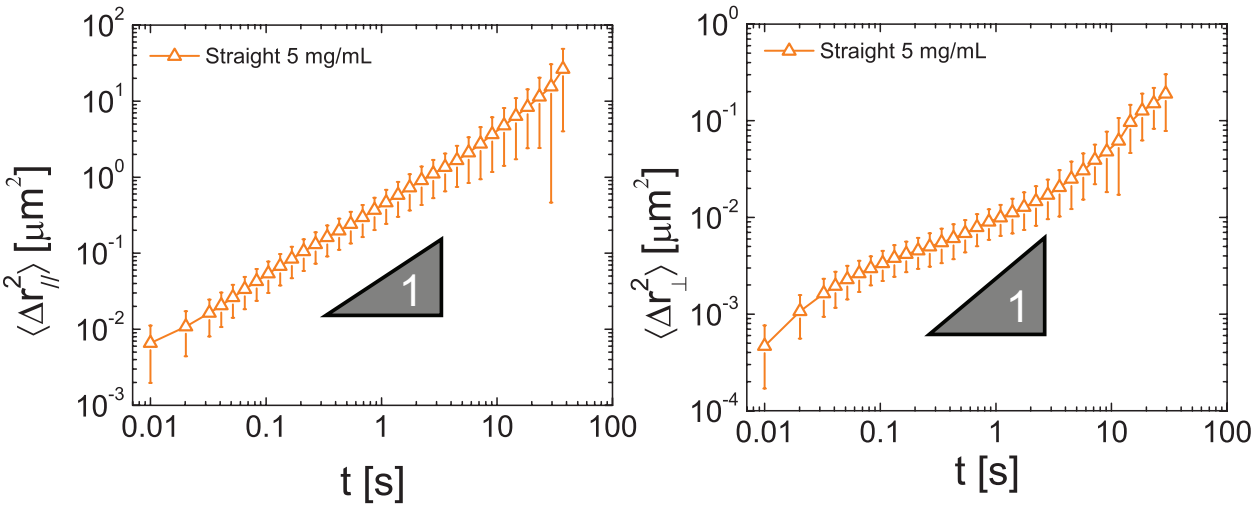

Figure 4.3: Left shows the MSD of a straight filament along the long axis in a 5 mg/ml sample. A slope of 1 is indicated meaning that the filament is purely diffusive in this direction. Right shows the MSD of a straight filament along the transverse axis, perpendicular to the long axis. Intermediate times show subdiffusive behavior as the filament is caged at these time scales.

is different than that of straight filaments. Simply translating along the long axis of the filament is not possible for normal filaments due to its helical nature. The geometry of the filament would impede this translation through collisions with other nearby helical filaments that are intercalated with one another. Instead, as can be seen in Figure 4.4, the helical filaments reptate through rotation around the long axis of the filament. This essentially acts like a screw in that rotation in this axis causes translation along the axis of rotation. Because the filaments are in the semi-dilute regime, this form of motion remains largely clear of obstruction and diffusion along the long axis can take place. A previous study of the diffusion of normal filaments shows that the diffusion coefficient in the longitudinal axis for both straight and helical filaments is independent of the filament concentration in the semi-dilute regime ($\sim 0.6\mu m^2/s$) [114]. This corroborates the assertion that the longitudinal axis is mostly clear of obstructions. Similar to straight filaments, motion along the transverse

axis is subdiffusive for intermediate time scales. This is also consistent with reptation theory which asserts that $D_{\parallel} \simeq D_{\parallel 0}$ in the semidilute regime [16].

Averaged across many filaments, the longitudinal diffusion coefficient remains constant over concentrations in the semi-dilute regime. However, by analyzing straight filaments and binning according to length, we have identified that filament length does change the diffusion coefficient (Figure 4.6). Longer filaments unsurprisingly diffuse slower than shorter filaments in the longitudinal direction. The length dependence of this diffusion is predicted to scale with L as $\ln(L)/L$ [16]. More length dependent results would need to be collected to show if the data supports this theory.

4.2.3 Dynamics of Block Copolymer Flagella

So far, in this section, we have shown that bacterial flagella in bulk suspensions exhibit different types of motion depending on the geometry of the filament. Straight filaments behave according to reptation of rigid rods and are diffusive in the longitudinal direction while being subdiffusive and caged in the transverse and angular directions. Also, though the diffusion coefficient is constant with respect to concentration of filaments, the diffusion coefficient for an individual filament is dependent upon the length of the filament where longer filaments will have a lower diffusion coefficient than shorter filaments. Helical filaments also exhibit diffusion along the long axis of the filament and subdiffusive motion in the transverse and angular directions similar to straight filaments. However, helices cannot translate along the long axis without a corresponding rotation of the filament around the long axis. This screw-like diffusion is effective enough at enabling diffusive motion helical filaments show no signs of being caged by neighboring filaments in the longitudinal direction and exhibit a concentration independent diffusion coefficient in the semi-dilute regime.

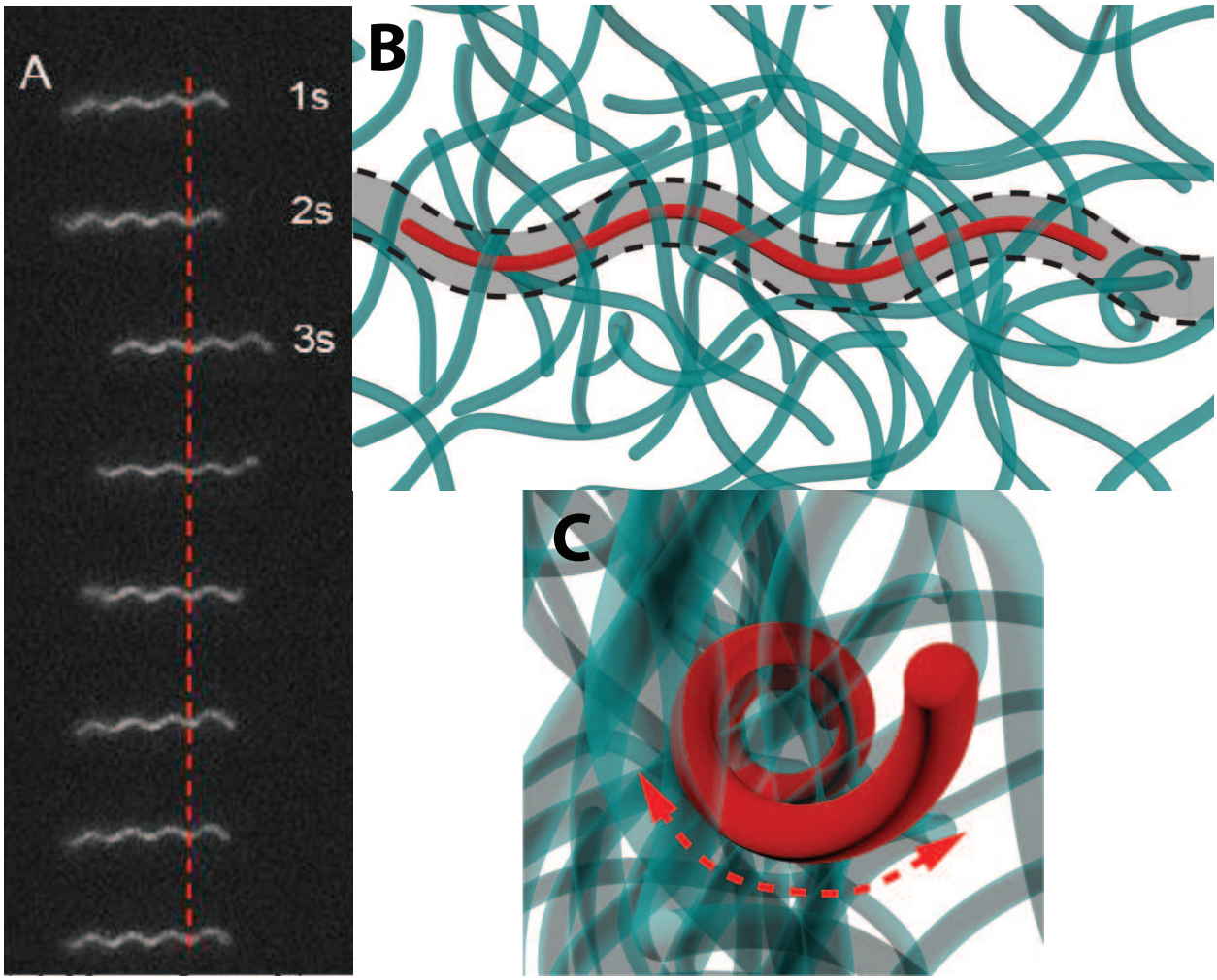

Figure 4.4: A fluorescently labeled normal filament in a background of unlabeled normal filaments undergoing reptation through the network. Note that the red line illustrates that the filament does not translate by direct movement, but instead translates through a rotation around the long axis of the filament. B) Top down schematic of a normal filament entangled in other normal filaments. C) Same view as B but rotated to look down the long axis of the marked filament. This shows why a helical filament cannot simply translate as the straight filament does and instead has to rotate around the long axis.

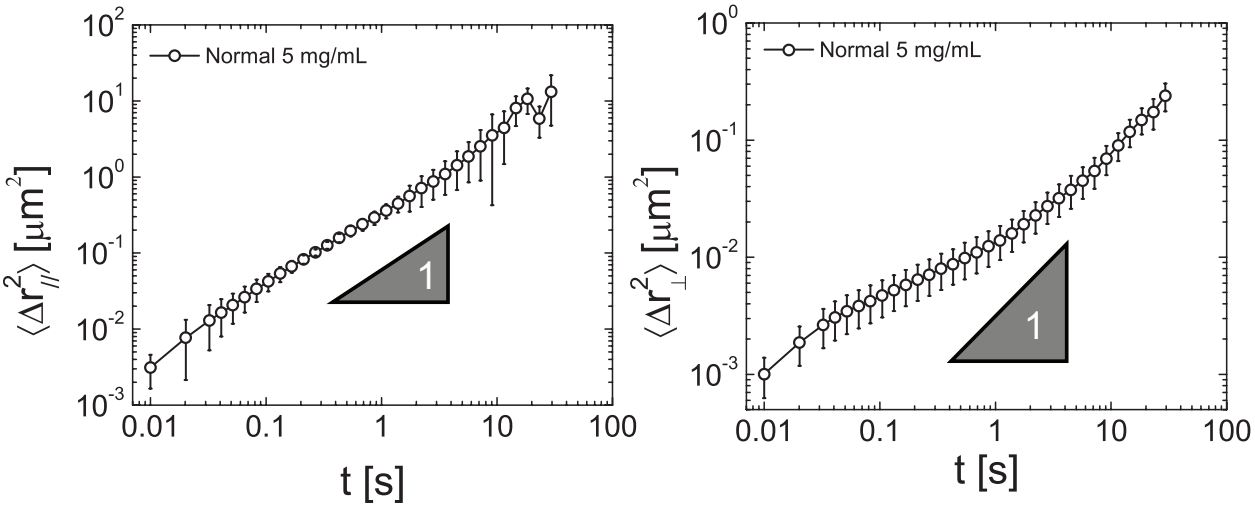

Figure 4.5: Left shows the MSD of a normal filament along the long axis in a 5 mg/ml sample. A slope of 1 is indicated meaning that the filament is purely diffusive in this direction. Right shows the MSD of a normal filament along the transverse axis, perpendicular to the long axis. Intermediate times show subdiffusive behavior as the filament is caged at these time scales.

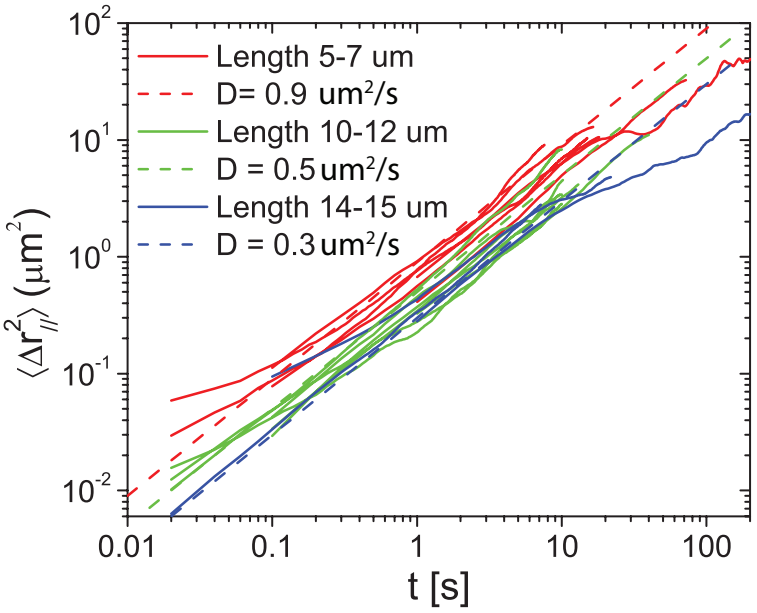

Figure 4.6: MSD curves of individual straight filaments along the long axis are plotted and colored by filament length. Three different diffusion coefficients are plotted (dashed lines) showing that longer filaments diffuse at a slower rate than shorter filaments.

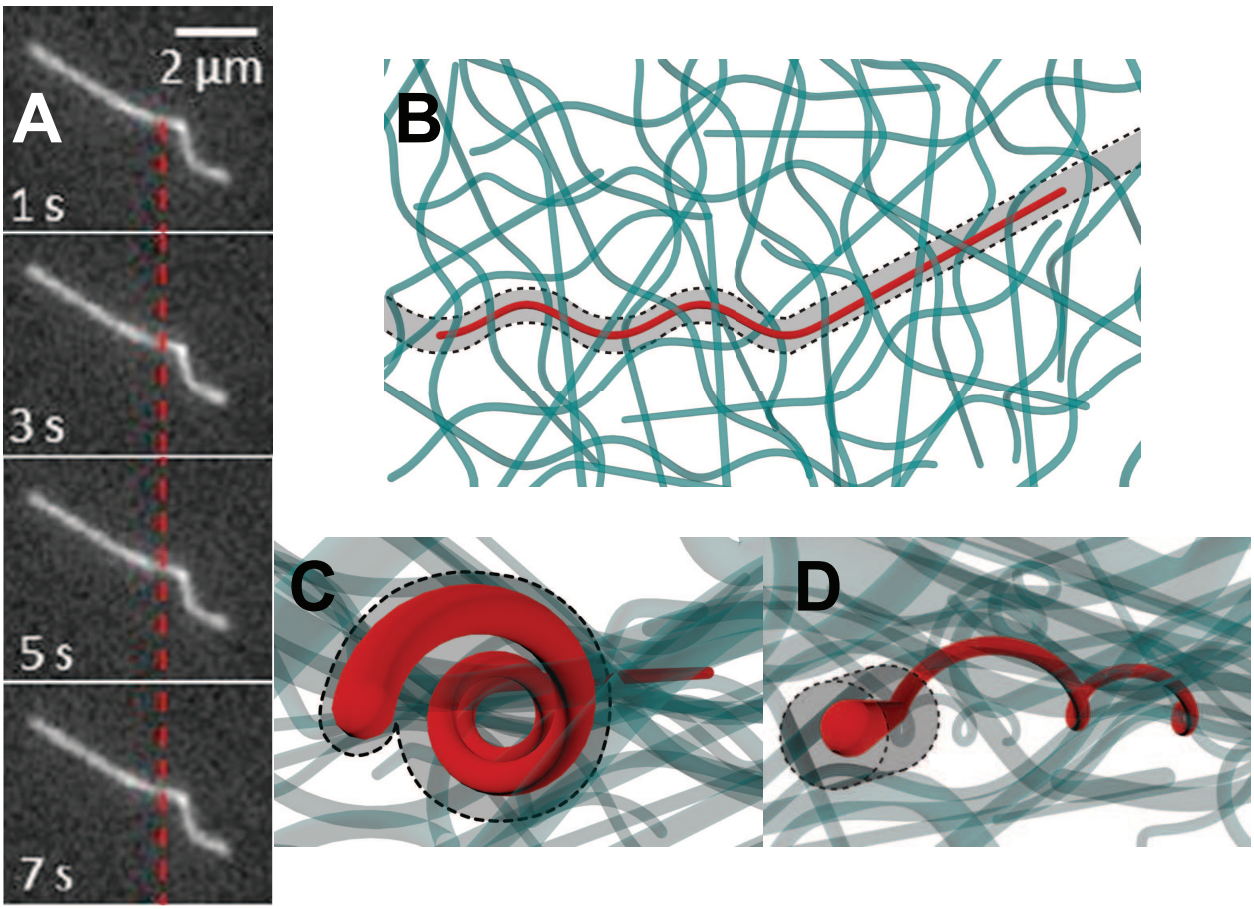

Figure 4.7: A) Time series showing a fluorescently labeled block copolymer filament undergoing diffusion in a sample of unlabeled block copolymer filaments. The red line indicates that the position of the block copolymer is mostly unchanged over this entire time frame. B) A top down schematic of a block copolymer in suspension with the tube defined by its nearest neighbors indicated. C) The same view as B, but rotated to look down the long axis of the helical side of the filament. Note that the straight filament in the background would need to move in a transverse direction to allow the helix to rotate around its long axis. D) The same view as B, but rotated to look down the long axis of the straight side of the filament. Due to the attached helix, the straight side of the filament is unable to translate along its long axis.

Block copolymer filaments, consisting of both a helical and straight portion of the filament, are prevented from reptation in either of the ways described above for straight and helical filaments. This is due to the unique geometry of the filaments as shown in Figure 4.7. The straight side of the filament has a fairly unobstructed tube through which it can diffuse, except that the helical side of the filament is attached and would need to be moved with the straight portion. Because the straight portion of a filament is tangent to the helix, the long axis of the straight filament will always be at an angle to the long axis of the helical portion of the filament. This means that, as long as the concentration of flagella is high enough so that there are neighboring filaments intercalated with the helical portion, the flagella will be mostly obstructed from diffusing along the long axis of the straight portion of the filament. The helical part of the filament has a tube around it in which it could reptate via a rotation around the long axis of the helix, like a screw. However, doing so would mean that the straight portion of the filament would need to move in a transverse direction to its long axis and likely be obstructed by neighboring filaments. The combination of these two effects means that the block copolymer filaments are essentially unable to diffuse in any direction except on very small length scales.

To experimentally determine if this geometrically driven jamming occurs, block copolymers were prepared as described in Chapter 2 and a small portion fluorescently labeled. The labeled filaments were tracked via fluorescence microscopy in suspensions of varying concentrations of unlabeled filaments. From the results in Figure 4.8, block copolymers show clearly subdiffusive behavior even along the long axis of the filament with a slower diffusion as the concentration increases. Subdiffusive motion is present in the transverse and the angular directions as well (Figure 4.9). The motion of block copolymer filaments shows a clear dependence on the flagella concentration that is not present in helical or straight filaments. As the concentration of filaments increases, the distance that the flagella can diffuse decreases in

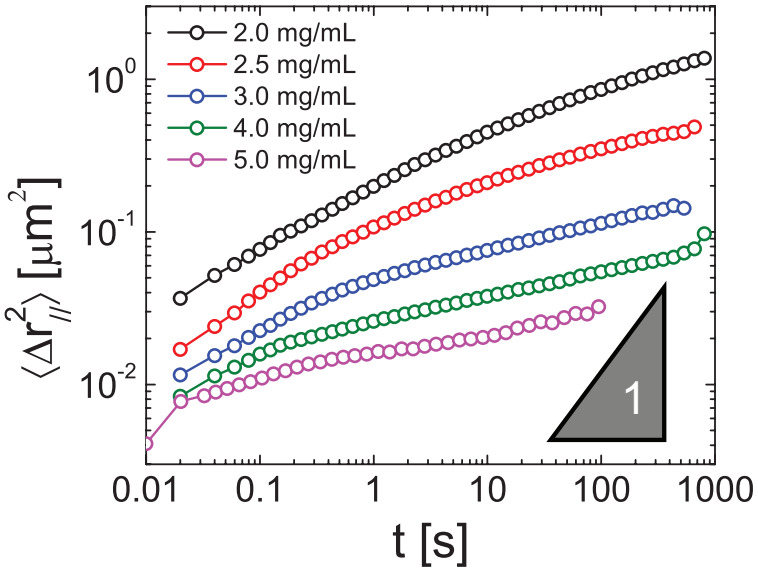

Figure 4.8: MSD curves of block copolymer filaments in the direction of the filaments long axis at different concentrations. As the concentration is increased, the motion is more subdiffusive. All the concentrations observed showed subdiffusive behavior even at very long time scales.

all directions. Because the longitudinal direction is subdiffusive, block copolymers must be caged by neighbors in the long axis direction as well as the transverse and angular directions. In fact, block copolymer filaments remain subdiffusive in the longitudinal direction down to concentrations at least as low as 2 mg/mL. This is still firmly in the semidilute regime as the overlap concentration is approximately 0.03 mg/ml.

These results confirm that block copolymers become jammed in dense suspension and are unable to diffuse even for very long time scales. Block copolymers essentially represent a system in which the constituent particles are prevented from diffusing simply through the geometry of the particles. This is similar in principle to a crosslinked network where binding prevents diffusion of constituent particles from diffusing. However, in the block copolymer suspension, there are no crosslinks or inter-molecular interactions required to achieve the same result.

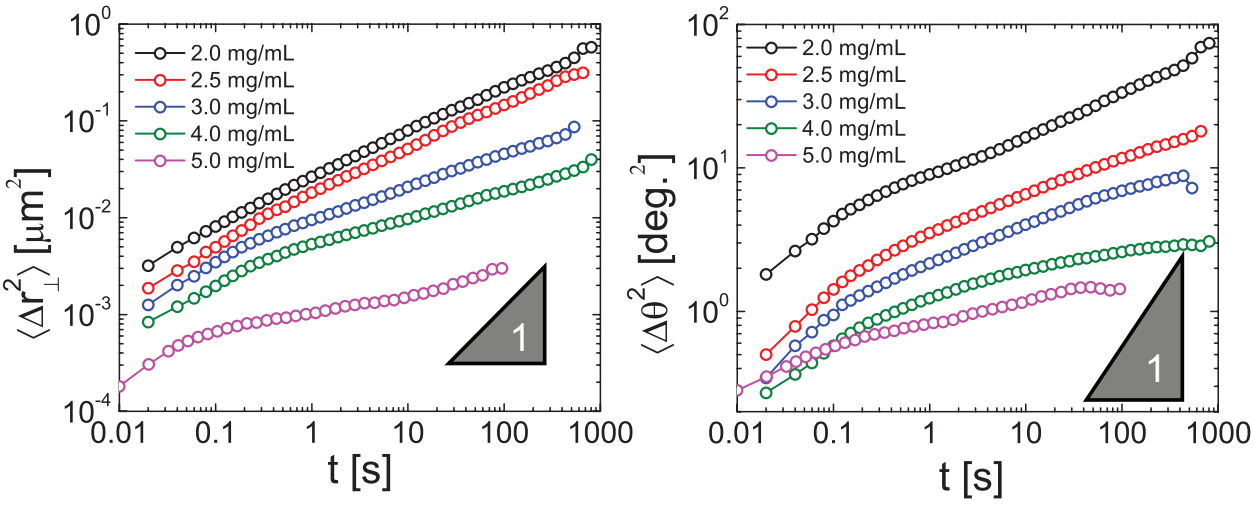

Figure 4.9: MSD curves of block copolymer filaments at different concentrations in the transverse (left) and angular (right) directions. For all concentrations measured, the samples were less diffusive as the concentration increased. Also, similar to the long axis direction, the motion was subdiffusive for all measured concentrations.

4.3 Bulk Rheology

4.3.1 Rheology Theory

An important experimental technique for characterizing the material properties of complex fluids such as colloidal suspensions is bulk rheology [28]. In general, rheology is the study of how materials deform and flow and has applications in a wide range of fields and industry. Rheological properties are finely tuned in everyday consumer products such as pharmaceutical and cosmetic creams [115, 116], a wide array of food products [117], as well as cement and concrete [118]. All of these materials are neither perfect solids or perfect fluids, meaning that they are considered a complex fluid.

To better understand the non-trivial nature of complex fluids, it is helpful to first understand elastic solids and Newtonian fluids. An elastic solid behaves like a spring in that if a deformation were imposed on the solid, the work required to cause the deformation would

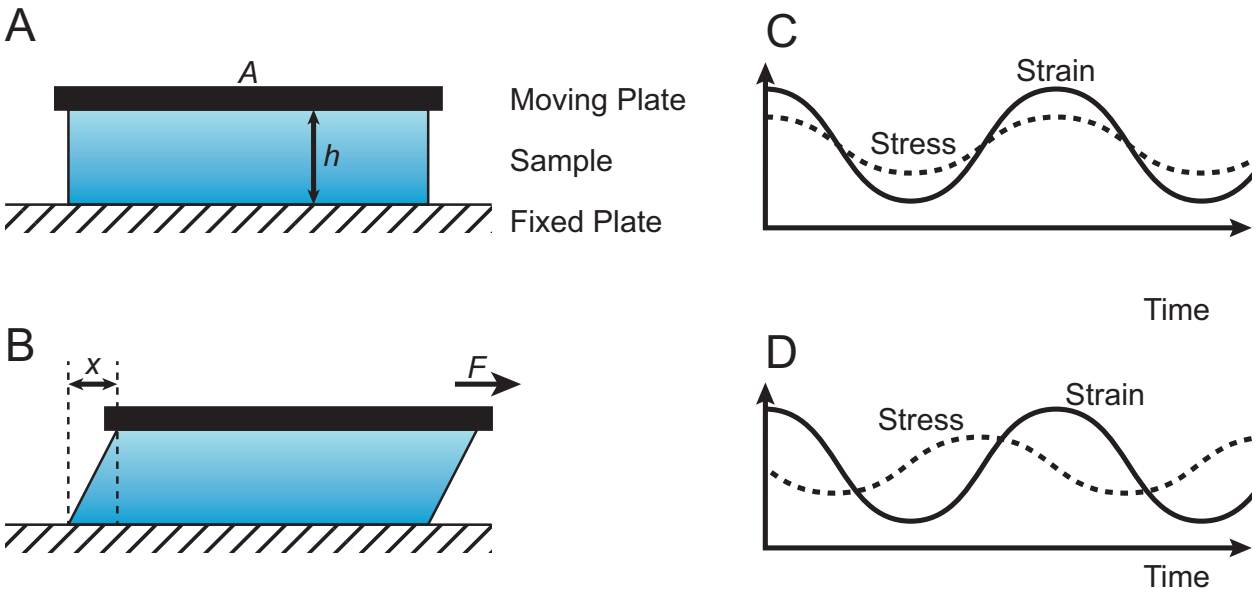

Figure 4.10: A) Parallel plates with a sample between them. The area of contact with the moving plate is given by A and the gap between the two plates is given by h. B) The top plate is moved by a distance x with a force of F. The applied strain on the sample is given by $\gamma = x/h$ and the resulting stress is given by $\sigma = F/A$. C) Strain and stress as a function of time for a perfectly elastic solid. In this ideal, an oscillating strain results in a stress that is exactly in phase with the strain. D) Strain and stress as a function of time for a Newtonian fluid. Unlike the elastic solid, for a sinusoidal applied strain, the resulting stress is $\pi/2$ radians out of phase, proportional to the time derivative of the strain.

be stored in the solid as a potential energy. As an example, consider an elastic solid placed between two plates (Figure 4.10). If the top plate were to be moved in a direction parallel to the other plate by some applied force, F, assuming a no-slip boundary condition with the solid, the solid material will deform. In this case, we have applied a strain, γ, to the solid. The strain is defined as the ratio of the horizontal motion to the gap height between the plates, making it a unitless quantity. By measuring the amount of force required to impose the strain on the solid material, we can measure the resulting stress on the material from the deformation. The stress, σ, is defined to be the force applied to the sample divided by the area of the plate over which the force is applied to the material.

In real world applications, strain and stress are going to change depending upon frequency with which a deforming force is applied. Oscillatory measurements are often taken in order to understand a materials response over a range of frequencies. A perfectly elastic solid has a trivial dependence on frequency. Namely, if the strain is applied in a sinusoidal fashion, then the resulting stress will also be sinusoidal and in phase with the applied strain. This is equivalent to saying that the elastic solid will instantly respond to any applied strain with the appropriate stress.

Newtonian fluids differ from elastic solids in that applying a strain does not store potential energy in deformation, but instead the energy is dissipated by viscous flow. In the parallel plate configuration shown in Figure 4.10, applying a strain with the top plate leads to a resulting stress while in motion, but once the deformation is applied and the plate stops, the stress drops to zero. This is because, unlike elastic solids in which stress was proportional to strain, stress in Newtonian fluids is proportional to the rate of change in strain. This means that for sinusoidal, frequency dependent strains, the resulting stress will be exactly out of phase with the applied strain. This is equivalent to saying that the fluid will instantly oppose any motion, but after a strain is applied and the strain is no longer changing, the stress will go to zero.

Most real-world materials are neither a perfectly elastic solid or Newtonian fluid, but somewhere between these two extremes. Oscillatory rheology is able to measure which frequency ranges a complex material may be more fluid-like or solid-like. This is done by applying a sinusoidal strain to the complex fluid sample and measuring the resulting sinusoidal stress. The stress most likely is not perfectly in or out of phase with the applied strain, so it is broken into components; one that is in-phase and one that is out of phase with strain. The amplitude of the in-phase component of the stress is essentially how solid-like the material behaves when deformed. This value is often referred to as the storage modulus,

G', after the ability for the material to store potential energy when deformed. Likewise, the amplitude of the out of phase component of the stress is a measure of how fluid-like the material responds to deformation. This value is referred to as the loss modulus, G'', after the fact that any work done to the system is lost to the viscous fluid.

In typical materials, both G' and G'' are dependent upon the frequency with which the strain is applied. It is entirely possible for a material to exhibit a solid-like response for a specific frequency range but then, given a frequency outside that range, respond more like a fluid. Materials that exhibit both elastic and viscous responses to deformation are referred to as viscoelastic [119]. An example of a viscoelastic material would be the childrens toy of Silly Putty. Allowed to sit undisturbed for a long time, Silly Putty will flow as if it were a very viscous fluid. However, if thrown against the ground, it will recoil and bounce as if it were a solid. For this example, deformations that happen at a very low frequency would see G'' be larger than G' and the material would be liquid-like. Deformations that occur at high frequency would exhibit G' dominance and would be solid-like. The frequency at which $G' = G''$ is called the crossover frequency and is the inverse of the relaxation time. This is the time that the material takes in order to relax applied deformations through viscous flow.

A material like Silly Putty derives its viscoelasticity from the flexible polydimethylsiloxane (PDMS) polymers it contains that entangle with one another. In bacterial flagella systems, we also see viscoelasticity due to the flagellar filaments becoming entangled with one another. In order to quantify this viscoelasticity, we measured the rheological properties of flagella suspensions over a range of frequencies using a strain controlled rheometer (Anton Paar MCR 702). This rheometer functions by applying a strain to a sample and measuring the resulting stress, as described earlier. Instead of shearing the sample linearly with parallel plates, modern rheometers function with circular geometries and apply a strain by rotating tools that the sample is sandwiched between (Figure 4.11).

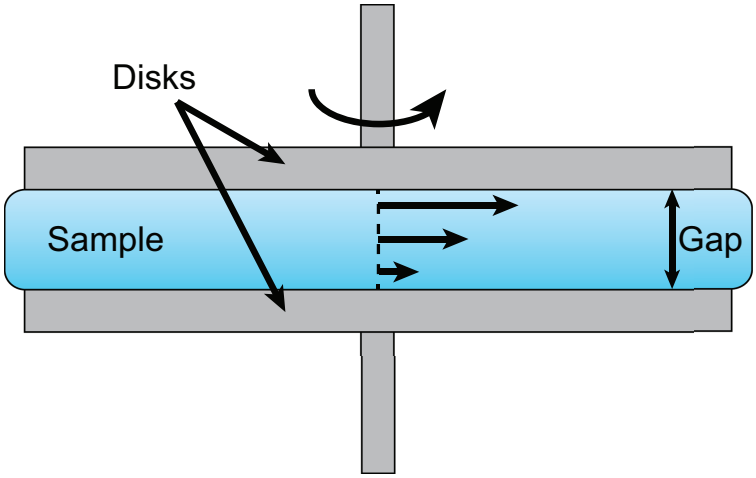

Figure 4.11: Schematic of a parallel plate oscillatory rheometer. In this device, the top plate is rotated either a specified angle (strain controlled) or with a specific torque (stress controlled) and the resulting torque or deflection angle is measured respectively. This rotation induces shear in the sample, allowing for an elastic or viscous response to be measured.

The two most common rheometer tool geometries used are the parallel plate and the cone plate configurations. The parallel plate geometry has the advantage that the gap height can be adjusted arbitrarily and can be adjusted to accommodate large and small sample volumes. The disadvantage with the parallel plate configuration is that the applied strain is a function of the distance from the center of the tool. This means that different parts of the sample will undergo different amounts of strain, possibly leading to the problem that one region of the sample will dominate the measured signal due to the difference in strain. This problem is compounded for complex fluids in which part of the sample may be in a solid-like regime while another may be in a liquid-like regime or even in a nonlinear regime of strain. The cone plate geometry alleviates this problem by making one of the tools be a shallow cone rather than a flat disk. This causes the gap height to vary as a function of radius. The angle of the cone is chosen so that the strain remains constant over as much of the sample as possible. However, this means that the cone plate is only designed to work with a specified

gap height (measured at the center of the tool). If a different gap height is desired, either a different cone plate or a different tool geometry must be used. In the experiments presented in the next section, unless otherwise noted, a cone plate geometry with a diameter of 50 mm and gap height of 0.099 mm was used.

Finally, to avoid evaporation of the sample during data collection, light mineral oil was placed around the outside of the edge of the tool to seal the sample inside. However, confocal microscopy imaging revealed that flagella would adhere to the oil-water interface at the boundary and the local concentration would greatly increase (Figure 4.12). This can be especially problematic in a rheology experiment because the oil-water interface is located at the largest radius from the tool center. This means that any elastic forces at the oil-water interface would have a disproportionally large signal in the resulting measurement. To prevent this adhesion, we added 2% by weight Abel EM 90 surfactant to the mineral oil. Confocal imaging confirmed that the buildup of flagella at the interface in the presence of the surfactant no longer occurred.

4.3.2 Rheology of Straight Filaments

Previous rheological studies of rigid rod-like biopolymers consist purely of rods with a straight geometry [44, 62]. Specifically, for microtubule solutions, interfilament interactions lead to suspensions exhibiting viscoelastic material properties. For comparison, we measured the rheological properties of straight flagellar filaments. The straight filaments of the SJW 1660 mutant strain were measured using a double gap rheometer geometry. This geometry was chosen to maximize the surface area of the interface between the sample and the tool. This increases the rheometer sensitivity for low viscosity solutions. The concentration of straight flagella was kept below 7 mg/ml to avoid the straight filaments forming a nematic liquid

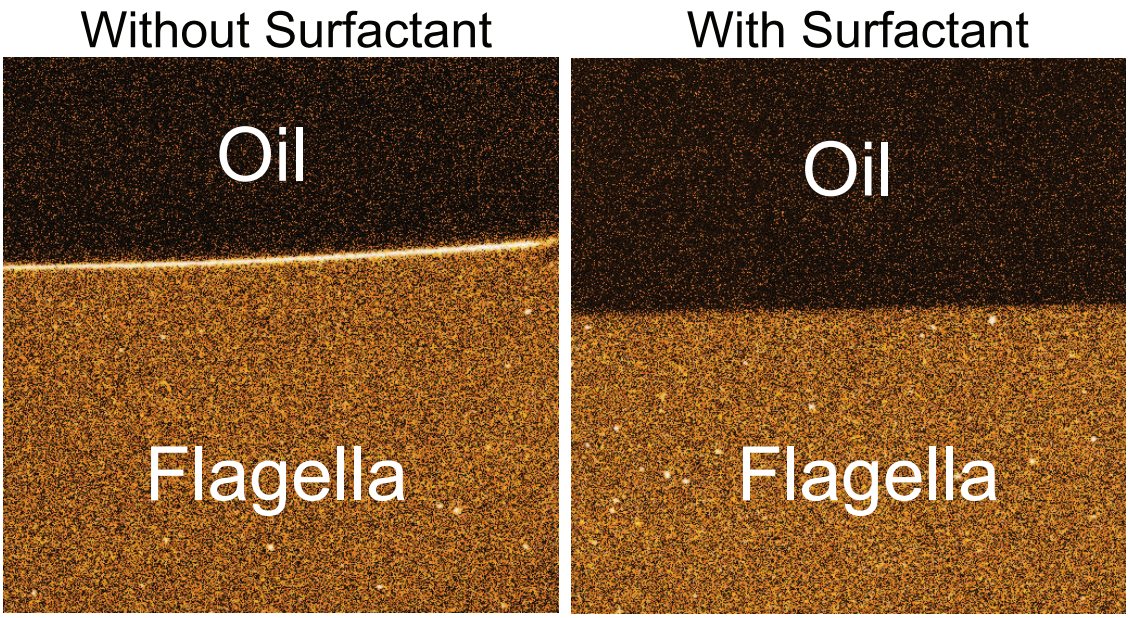

Figure 4.12: Confocal imaging of an oil-water interface which has fluorescently labeled flagella in the aqueous phase. Without a surfactant at the interface (left), there is a buildup of flagella adhered to the oil phase. This can cause problems on a rheometer as the structure built up at the interface can provide false signal and overwhelm the true response of the bulk material. With 2% w/w Abel EM 90 surfactant added to the oil phase (right), the buildup of flagella is no longer present.

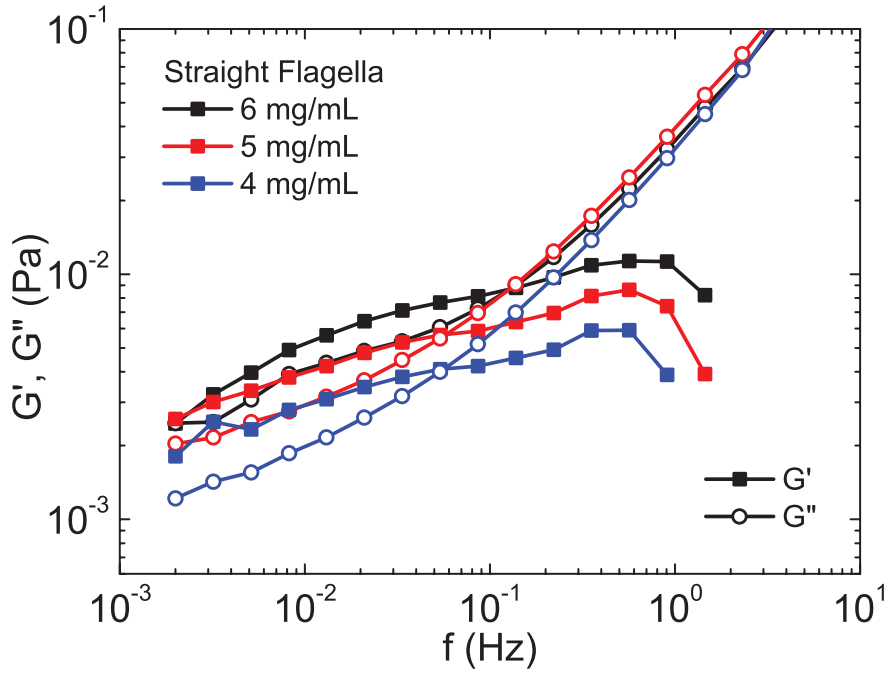

Figure 4.13: Bulk rheology measurements for straight flagella using a double gap tool geometry. These results are very near the noise floor of the instrument and suggest that straight filament suspensions have very weak elastic moduli and a small viscosity.

crystal phase, occurring at approximately 7.5 mg/ml. Viscoelasticity is observed in straight flagella in that for high frequencies the solutions are G'' dominated and liquid-like (Figure 4.13). For lower frequencies, G' dominates and the sample is solid-like. Additionally, as the concentration of flagella increases, the magnitude of the moduli increase as well as the frequency at which G' and G'' crossover.

The fact that moduli and the crossover frequency increases with concentration makes intuitive sense. The high frequency liquid-like behavior represents a regime in which energy is dissipated by the solvent more efficiently than stored in the flagella networks. As the frequency decreases, the flagella network is able to propagate the deformations through the network and deform in response, causing a more solid-like response. Higher concentrations of flagella mean that there is a smaller tube inside which the straight filaments can move

without colliding with a neighboring filament. This means that the timescale at which the solution would be able to respond elastically to deformations would be shorter due to the shorter time to traverse the distance between neighboring filaments.

However, there are several problems with this data to suggest further experiments are necessary to quantitatively investigate straight filament suspensions. First, the magnitude of the moduli, even with the double gap geometry, is at the extreme low end of the instrument sensitivity. This doesnt necessarily mean the results are incorrect, but more than just the magnitude is suspect. At low frequencies, straight filaments show solid-like behavior and look to be trending toward a second, low frequency, crossover point. The low frequency point at which the rheology transitions from solid-like to liquid-like represents the timescale at which it takes a filament to diffuse out of the cage of its neighbors into a new cage. This is often called the relaxation time, or reptation time. The results in Figure 4.13 show that this relaxation time is at most approximately 10^{-3} Hz, meaning a timescale of 1000 seconds. This is problematic because dynamics experiments like those in the previous section show that the time for straight filaments to diffuse out of their cage is a much shorter timescale [114].

Another type of rheology experiment used to study the properties of the microstructure of the sample consists of changing the strain while keeping the frequency constant. This strain sweep shows a plateau at low strain values (Figure 4.14). This is called the linear regime and is the range of strain over which the deformations are small enough that they do not significantly alter the structure of the network. All frequency sweep measurements are measured in this linear regime so as not to change the network through the act of measuring it. As strain increases past the linear regime, straight filaments show a drop in G' followed at a slightly higher strain by a drop in G''. This type of behavior is known as strain thinning and is typically caused by the alignment of microstructures in the solution with the

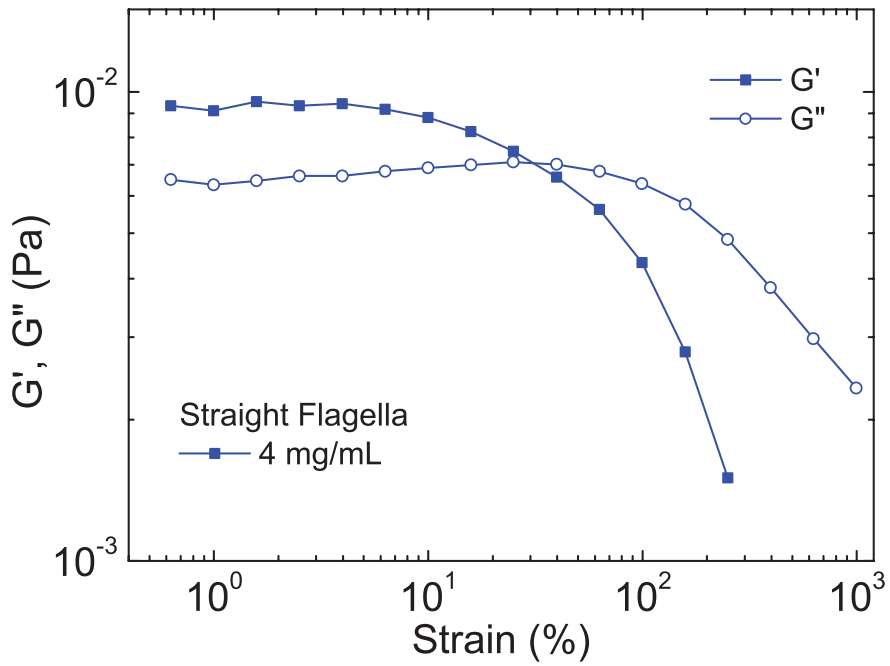

Figure 4.14: Strain dependent rheology for straight filaments. The plateau at small strains defines the linear regime in which oscillations of this magnitude do not considerably change the properties of the flagella network. The behavior at large strain is indicative of strain thinning and typically occurs due to particles aligning with the locally induced flow resulting from the applied strain [120].

direction of flow [120]. This seems a likely cause for the strain thinning in straight flagella as the concentrations measured are near the nematic transition and flow induced nematic ordering is observed through actions such as pipetting straight flagella.

4.3.3 Rheology of Suspensions of Helices

Rheological measurements of helical filaments provide a way to directly measure the effect of particle geometry on the material properties of a suspension of flagella. A larger range of flagella concentrations can be investigated with normal flagella from the wild type SJW 1103 because the helical shape prevents a liquid crystal forming until 17 mg/ml [121]. Frequency sweeps show clear viscoelastic behavior and three different frequency regimes (Figure 4.15). At very high frequencies, similar to straight filaments, the rheology is dominated by G'' and the response is liquid-like for the same reasons discussed above for straight filaments. Intermediate frequencies show solid-like behavior where G' is dominant over G''. This frequency represents the time scales over which the helical flagella remain caged by the nearest neighbors. Strains are applied fast enough that the filaments are unable to reptate out of the cage fast enough to relax the stress. Finally for low frequencies, liquid-like behavior is dominant again. These time scales are greater than the relaxation time of the flagella network and are therefore able to relax applied strain through reptation and behave more fluid-like.

Another significant difference in the frequency dependent rheology of normal flagella as compared to straight flagella is that the normal suspensions have both loss and storage moduli are an order of magnitude greater in magnitude. For 6 mg/ml flagella, straight filaments have moduli at 0.1 Hz on the order of 10^{-2} Pa whereas normal filaments are roughly 10^{-1} Pa. As the concentration of normal filaments increases, the moduli increase quite dramatically.

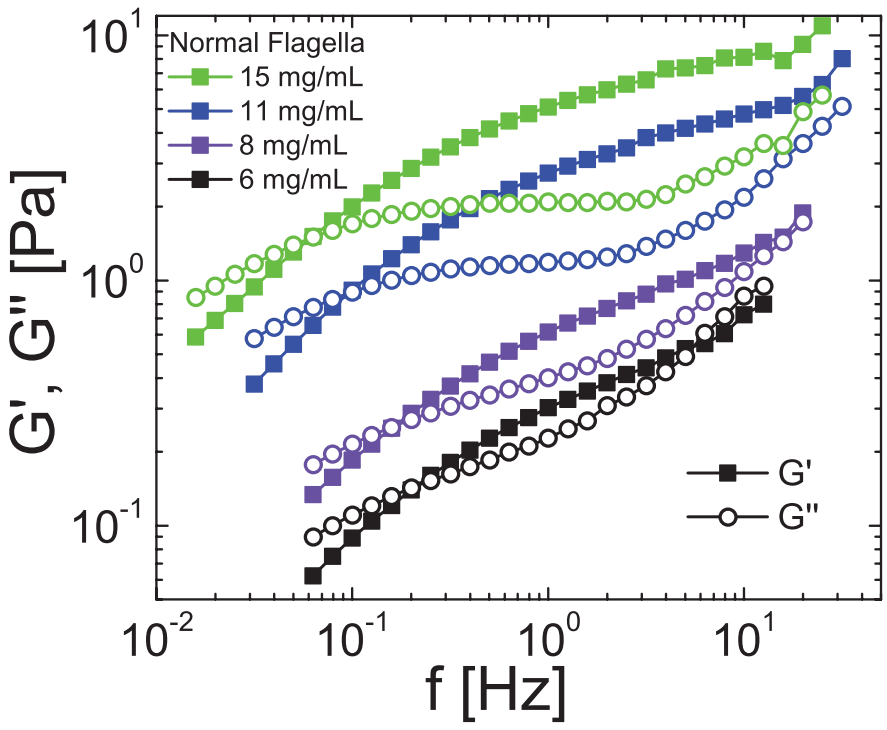

Figure 4.15: Frequency dependent bulk rheological measurements for a range of concentrations of 1103 flagella in the normal conformation. Intermediate regimes show solid-like behavior while high and low frequencies show a liquid-like response. The low frequency point at which G' and G'' are equal is equal to the inverse of the relaxation time for the network.

Increasing the concentration by a factor of 2.5, from 6 to 15, causes the moduli to increase by over an order of magnitude. This is in contrast with straight filaments which showed very small differences with a changing concentration. The high frequency crossover point follows a similar trend to the straight flagella in that higher concentrations cause the solid-like regime to extend to higher frequencies. Concentration also changes the low frequency crossover point, or relaxation time of the sample. Higher concentrations of flagella cause the relaxation time to increase. Effectively, this means that the higher the concentration of normal flagella, the broader the frequency range over which the sample is solid-like in response to applied strain. The inverse of the lower crossover point has similar values to the measured subdiffusive timescale for angular diffusion from filament tracking experiments (Figure 4.16).

Looking at the large magnitude strain results for normal filaments, there is a broad linear regime similar to straight filaments (Figure 4.17). However, at high enough strain rates, there is a pronounced increase and local maxima of G'' before both G' and G'' fall off in magnitude sharply. This type of behavior is named weak strain overshoot and can arise for a wide variety of reasons that are very system dependent, but is most commonly found in soft glassy materials [120, 122]. In general, the weak strain overshoot is due to the formation and destruction of small scale structure or interactions as the sample undergoes large changes in structure due to the large amplitude of applied strain. Weak strain overshoot behavior is observed for all concentrations of normal helical flagella measured.

The normal flagella purified from bacteria have an average length of 2.89 ± 0.03 µm. As discussed in Chapter 2, it is possible to use *in vitro* polymerization techniques to alter this average length by altering the amount of seeds used in a seeded growth procedure. Figure 4.18 shows a comparison between purified normal filaments at a concentration of 6 mg/ml and normal filaments that were polymerized with a 5% seed concentration. These

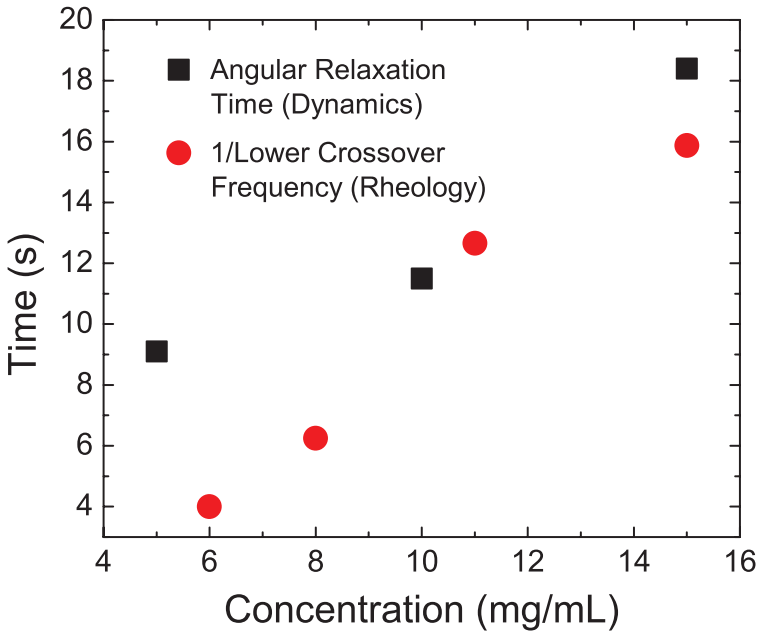

Figure 4.16: Comparison of experimental measures of relaxation of suspensions of normal filaments. Black squares show the timescale over which the filaments are subdiffusive in the angular direction measured by particle tracking filaments in a dense suspension. Red circles show the inverse of the low crossover frequency in frequency dependent bulk rheology on normal flagella suspensions. The two methods of measurement show similar trends, but diverge for lower concentrations.

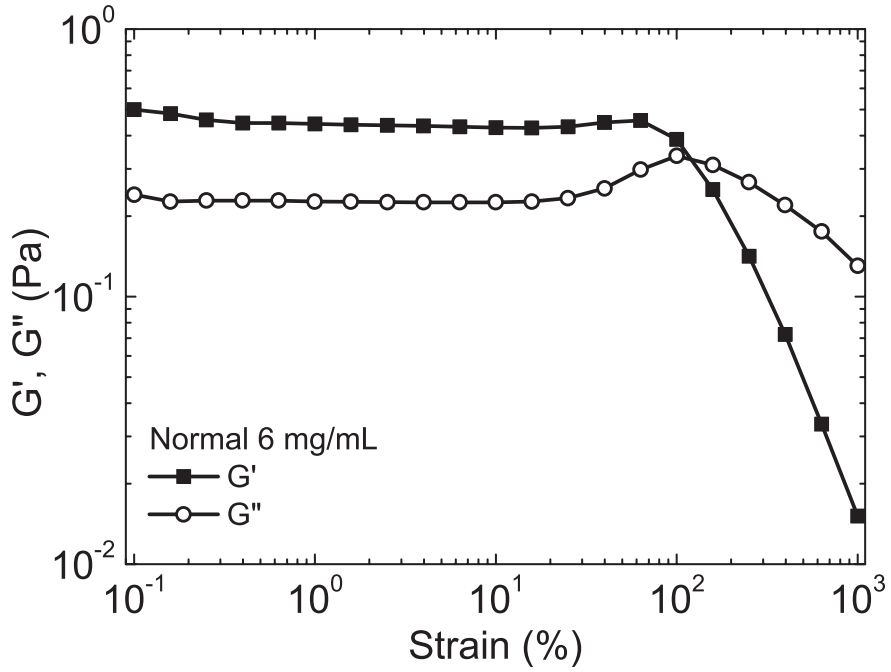

Figure 4.17: Strain dependent rheology for normal flagella at 6 mg/ml. The linear regime is clearly visible for small applied strain. As the strain increases, the loss modulus increases to reach a local maximum while the storage modulus quickly decreases in value. This behavior is called weak strain overshoot and is typical in soft glassy materials [122].

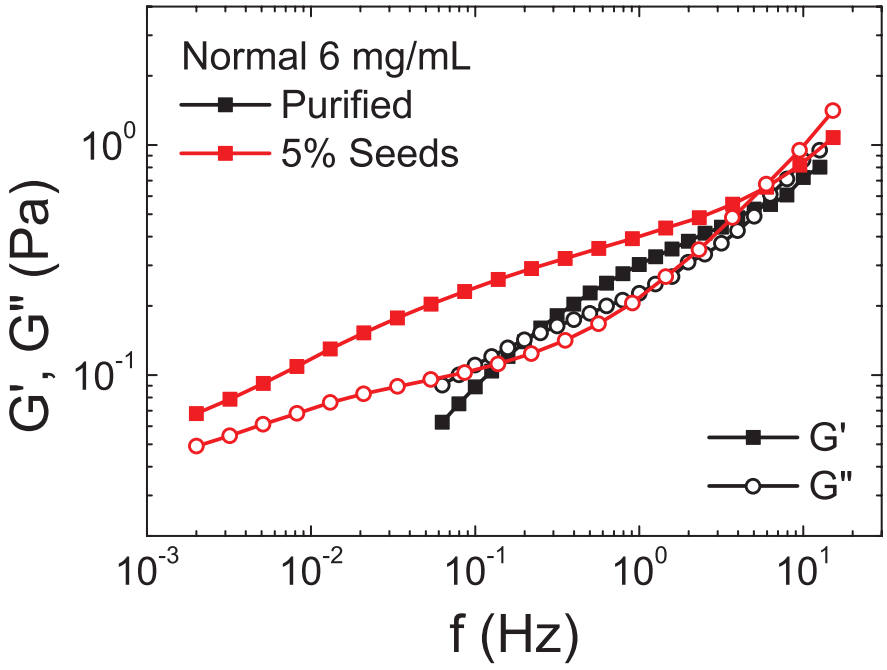

Figure 4.18: Frequency dependent bulk rheology for purified filaments (black) and polymerized filaments that are on average over twice as long. The high frequency behavior is consistent for both samples. However, the longer filaments have an enhanced elasticity and a much longer relaxation time.

polymerized filaments are, on average, 7.2 ± 0.2 µm. The results show that the two samples are mostly identical for high frequencies. The high frequency crossover point is lined up for both samples. Also, the magnitude of both G' and G'' agree between the two samples in this high frequency regime. This intuitively is consistent with the discussion earlier about the high crossover point pertaining to straight flagella. This crossover point would primarily be concentration dependent and the moduli would primarily be determined by the background fluid rather than the network of flagella.

The main difference between purified filaments and the long, polymerized filaments happens at intermediate and low frequencies. Purified filaments see the value of G' drop in magnitude much faster as the frequency decreases as compared to the polymerized filaments. This causes the longer filaments to show a much greater separation between G' and G'' than for the purified filaments. This also causes the lower crossover frequency to happen at a much lower frequency; such a low frequency that experimentally, we could not observe the lower crossover frequency with our apparatus. This means that the relaxation time of the sample, or the time it takes to reptate out of a cage into another, is a much longer timescale for long filaments as compared to shorter filaments. This is consistent with what reptation theory would predict; the longer a molecule, the longer the reptation time [34]. It is logical that long flagella would produce a greater elastic modulus because elastic behavior arises from neighboring helices becoming entangled. Long filaments have more filament-filament contacts, each of which contributes to the entanglement of the flagella network.

In addition to changing the length of the normal helical filaments, the many different helical forms of bacteria enable the study of differently shaped helical particles. In particular, we performed rheological experiments on flagella in the coiled state. This was accomplished by preparing SJW 1103 filaments in a 55% v/v ethylene glycol solution. A direct comparison between normal and coiled flagella at the same concentration is shown in Figure 4.19. It is

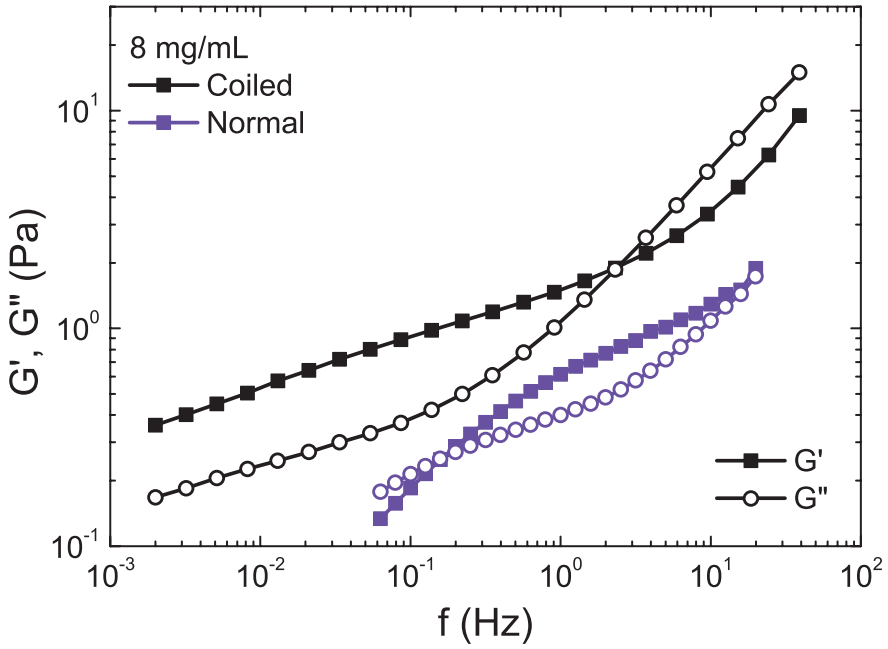

Figure 4.19: Frequency dependent bulk rheology measurements for 1103 filaments in the coiled state compared with filaments in the normal state. The coiled filaments show a much larger elastic modulus and a greatly increased relaxation time compared to normal filaments. However, the high frequency crossover point at which the sample becomes liquid-like occurs at a lower frequency in coiled filaments than normal filaments.

clear that the different helical shape causes significantly different rheological properties.

Coiled flagella have a much larger helical radius than normal, but correspondingly have a much shorter end to end length since the average contour length between the two samples is identical. The overlap concentration is therefore changed significantly with the different shape, increasing to about 0.4 mg/ml.The coiled filaments have a high frequency crossover point at a lower frequency than that of normal filaments. This may be due to the fact that ethylene glycol has a higher viscosity than water, causing G'' to have a more significant impact on the high frequency results than for normal filaments with a simple potassium phosphate buffer solvent. More importantly, the elastic modulus for coiled filaments show that the different shape enhances the elasticity in the flagella network as compared to the normal

shape. In addition, there does not appear to be clear evidence of a low frequency crossover point. This means that even for very long timescales, the coiled filaments will exhibit solid-like behavior. Clearly, the difference in shape greatly enhances the entanglement of the flagella for coiled filaments compared to the normal type flagella.

4.3.4 Block Copolymer Gelation

The *in vitro* polymerization techniques discussed in Chapter two enable the study of another shape of flagella consisting of part helix, part straight rod called block copolymers. Previously in this chapter, block copolymer dynamics were investigated in suspensions and it was found that the geometry of this type of filament caused subdiffusive behavior in both the long axis and transverse axis even for very long timescales (Figures 4.8 and 4.9). Because flagella suspensions relax applied strain through the diffusion of the filaments, it would therefore be expected that block copolymer suspensions would have an extremely long or nonexistent relaxation time. This would manifest itself in the rheology through a solid-like regime that extends to infinitely low frequencies (long timescales). This type of behavior is most commonly associated with solids and gels; materials that have chemical crosslinks that prevent constituent molecules from diffusing to relax applied strain. In the case of block copolymers, the unique shape of the filaments would essentially act as a way to create a gel that has no crosslinks or inter-particle interactions necessary.

Figure 4.20 shows the frequency dependent rheology of block copolymer solutions at varying concentrations. The elastic modulus plateau at low frequencies is a clear indication of gel-like behavior in which there is no relaxation time. These results suggest that this type of gel can be formed from any material in which it is possible to synthesize particles in this type of shape. There does seem to be a critical concentration necessary for gel-like behavior

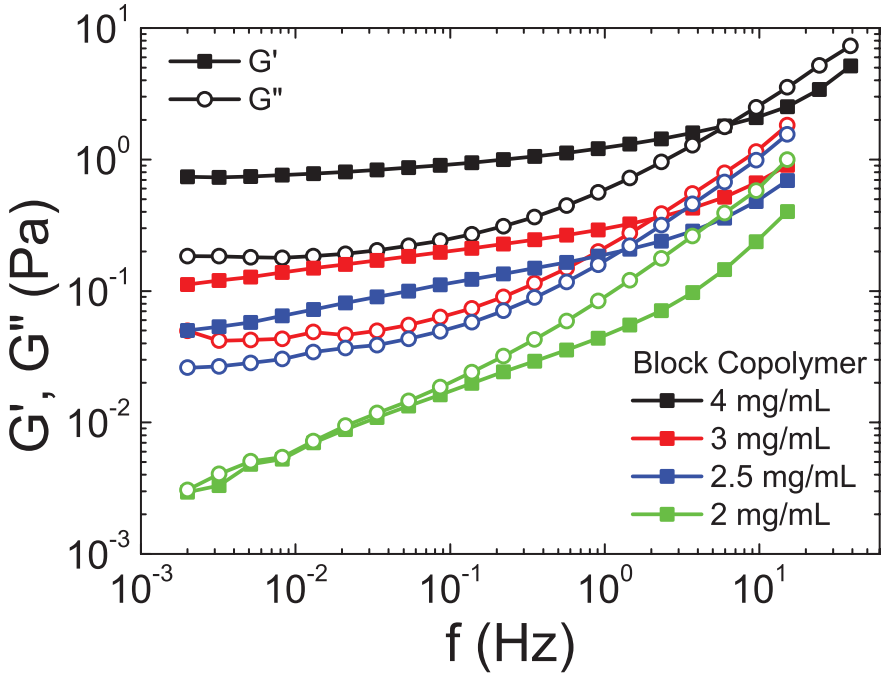

Figure 4.20: Frequeny dependent bulk rheology measurements for block copolymer filaments at different concentrations. The plateau of solid-like behavior at low frequency indicates the material is behaving as a gel in that there is no relaxation time for the flagella network. This plateau disappears if the concentration is too low as evidenced by the 2 mg/ml concentration.

to exist. At 2.5 mg/ml concentration, block copolymers show gel-like behavior while at 2.0 mg/ml, the low frequencies are no longer G' dominated and the gel ceases to exist. This must be a low enough concentration that there are not enough block copolymers in the solution to form an entangled network that spans the sample volume.

Another significant feature of the block copolymer frequency dependent rheology is that the magnitude of the elastic modulus is significantly greater than that of other morphologies of flagella. This can be attributed to the reduced angular diffusion of block copolymer filaments. Doi shows that the complex viscosity, defined as the complex modulus (G^*) divided by the angular frequency (ω), in semidilute solutions is equal to

$$\eta^*(\omega) = \frac{3\rho RT}{5M}\frac{\tau}{1+\mathrm{i}\omega\tau} \tag{4.7}$$

with

$$\tau = \frac{1}{6D_r} \tag{4.8}$$

where ρ is the mass of the particles per unit volume, R is a constant, T is the temperature, M is the molecular weight of the polymers, ω is the angular frequency of the oscillating shear, and D_r is the rotational diffusion coefficient [16]. This relationship implies a frequency dependence that we do not observe, especially for low frequency oscillations where the moduli are largely frequency independent, but does reinforce that the angular diffusion coefficient is an important parameter in determining the rheological properties of suspensions. At a concentration of only 4 mg/ml, block copolymer flagella exhibit a G' value on the order of 10^0; similar in magnitude to coiled filaments at a concentration of 8 mg/ml, double the concentration of the block copolymers. This is also an order of magnitude greater than normal flagella at a concentration of 6 mg/ml and three orders of magnitude larger than a straight flagella concentration of 4 mg/ml. This means that, through shape alone, it is

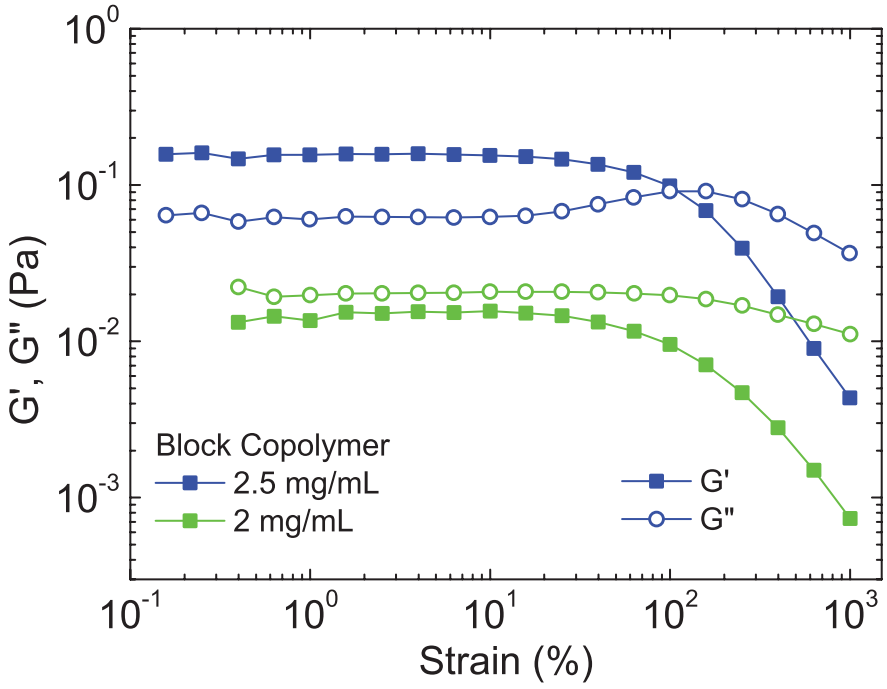

Figure 4.21: Strain dependent rheological measurements of block copolymer filaments both just above and below the critical concentration for gelation. In the gel-like sample at 2.5 mg/ml, weak strain overshoot is observed due to the local maximum present in G''. However, this goes away and only strain thinning is observed below the gel transition.

possible to modify the elastic modulus of the sample a full three orders of magnitude.

To further illustrate the concentration dependent gel transition in block copolymers, strain dependent rheology can be used. At concentrations of 2.5 mg/ml and higher, block copolymer solutions show a clear local maximum in G'' indicating weak strain overshoot behavior (Figure 4.21). This indicates that flagella are being brought in close enough proximity under the applied strain, that the hydrodynamic effects of filaments in close proximity causes an increased loss of energy to viscous dissipation. In contrast to this, at a concentration of 2 mg/ml, block copolymers no longer show the local maximum in G'' at high strain. This is the same behavior exhibited by straight flagella, strain thinning. This is a sign that the constituent particles are aligning with the local flow as the strain is applied. In order

to be able to align with the local flow, block copolymer flagella must be sufficiently free of nearest neighbors with which they are entangled to allow for this angular motion. This lack of entanglement is what causes the elastic plateau in the frequency dependent rheology to disappear as well.

4.3.5 Dynamic Rheology of Polymorphic Samples

In chapter three, we explored the phase diagrams of flagella in response to changing environmental conditions. Also, we showed that it was possible to induce changes in the conformation of flagellar filaments with changing temperature. Earlier in this chapter, we explored the material properties of different shapes of flagella and the ways in which the shape of flagella impacts the material properties of the resulting dense suspension. In this section, we will present results in which we are able to induce shape changes to flagella as in chapter three and be able to measure the resulting changing bulk material properties.

In order to measure the rheological properties of a sample undergoing a conformational change, samples were repeatedly measured with the same frequency and strain over an extended period of time. Choosing a frequency of 1 Hz and a strain of 5% allows for a measurement of G' and G'' every approximately 13 seconds. If there is a conformational change in the flagella as the temperature is changed, it will manifest as a significant change in G', G'', or both. Sample temperature was controlled via a Convection Temperature Device (Anton Paar CTD 180).

A typical experiment to induce these transitions in SJW 1660 filaments begins with loading the sample into the rheometer and making sure the oil trap is in place to prevent evaporation. The sample is initially at room temperature in the straight state. We first cool the sample to 10°C and allow the temperature to equilibrate. The temperature probe in the

sample chamber records changes in temperature much faster than the sample experiences temperature changes, so it is important to wait long enough that the viscous and elastic moduli are no longer changing in time (they increase with lower temperatures). During this cooling, the flagella are still in a straight conformation. After temperature equilibration, the temperature is quickly changed to 40°C to induce a transition.

Figure 4.22 shows rheological results for a 6 mg/ml sample of SJW 1660 filaments undergoing the experiment described above. Point a marks the point in time when the temperature of the sample is raised. The temperature probe responds rapidly to the new temperature, but the sample solvent (63% v/v ethylene glycol, 800 mM Tris pH 8.0, 10 mM potassium phosphate) lags behind. The drop in moduli at point b in Figure 4.22, with increasing temperature is both due to a lower viscosity at higher temperature and flagella depolymerization occurring in these conditions. As discussed in chapter three, 1660 filaments in high ethylene glycol concentrations are less stable in the straight conformation than the normal conformation. After the sample reaches some critical temperature at point c, the elastic modulus of the sample increases rapidly, marking the effect of the filaments transitioning to a normal state.

This experiment with 1660 filaments shows that flagella can be made into a material that transitions from a very liquid-like solution (straight filaments) to a solid-like solution (normal filaments). These results are just at a single frequency and strain, but by changing the shape of the constituent particles, the entire rheological profile of the flagellar suspension changes. In this way, bacterial flagella could prove a useful model system for studying materials in which one or more components changes structure, therefore changing the material properties.

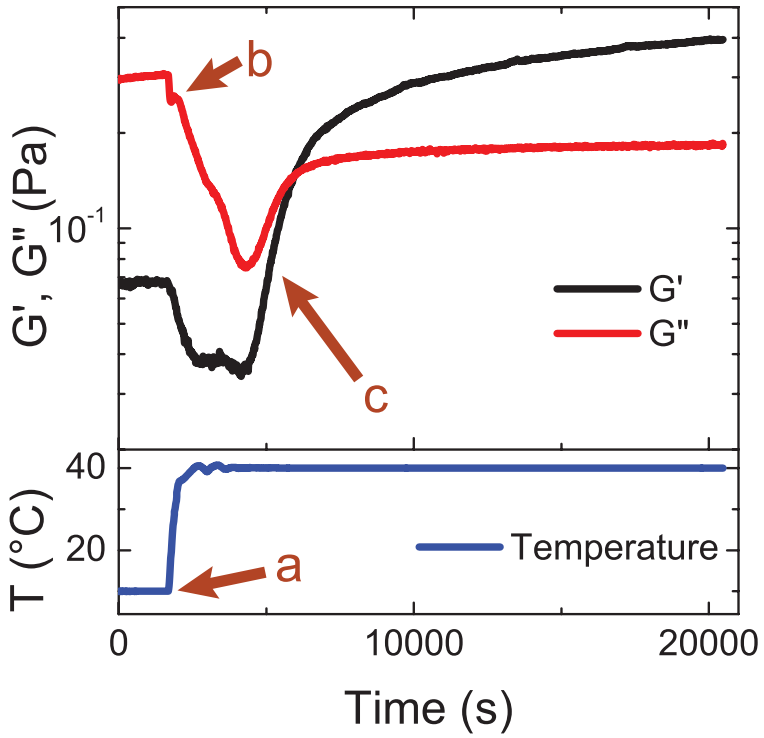

Figure 4.22: LA sample of 1660 flagellar filaments initially the straight conformation. At point a, the sample is heated from 10 to 40°C. Point b marks when the rise in temperature causes a sharp drop in the moduli due to viscosity change but potentially aided by flagella depolymerization. The temperature lags behind that of the temperature probe and when a critical temperature of the sample is reached, the flagella transition to a normal conformation. Point c marks the effect of this transition on the elastic modulus, a sudden increase.

4.3.6 Rheology of Crosslinking Solutions

Not all transitions that show changes in rheology are caused by polymorphic transitions. Another transition that can occur in bacterial flagella depending on solvent conditions is aggregation. This typically occurs in samples that are very near depolymerization, either because of a high concentration of a denaturant such as ethylene glycol, or a high temperature. When in these conditions, flagella that come into contact will irreversibly join, essentially crosslinking. This does not need to occur at the ends of the filament, crosslinking can occur anywhere along the contour length where two filaments are in close enough proximity. Also, unlike a previous study that introduced chemical crosslinkers [90], the flagella do not need to be aligned when they crosslink, but can have any orientation with respect to one another.

To investigate the effect of crosslinking on the rheology of flagella, samples containing SJW 1655 straight flagella at a concentration of 6 mg/ml were measured with a parallel plate tool geometry. To prepare the filaments for crosslinking, the flagella was put into a solution containing 62% v/v ethylene glycol, 400 mM Tris pH 8.0, 35 mM NaCl, and 10 mM potassium phosphate and the gap between the parallel plates was 50 µm. Samples were sheared with a strain of 1% and a frequency of 1 Hz so that data could be collected approximately every 10 seconds. Figure 4.23 shows the result of the aggregation of 1655 filaments. Initially at point a, the sample is kept at room temperature after being loaded on the rheometer. At point b, the temperature starts to rise, reaching a peak of about 27°C. This causes a drop in G' and G''. While the temperature is raised, the flagella can crosslink. However, the filaments are also extremely close to depolymerization.

If the crosslinks were able to bind and hold in the conditions after point b, it would be expected that the elastic modulus would increase dramatically. Because G' actually shows

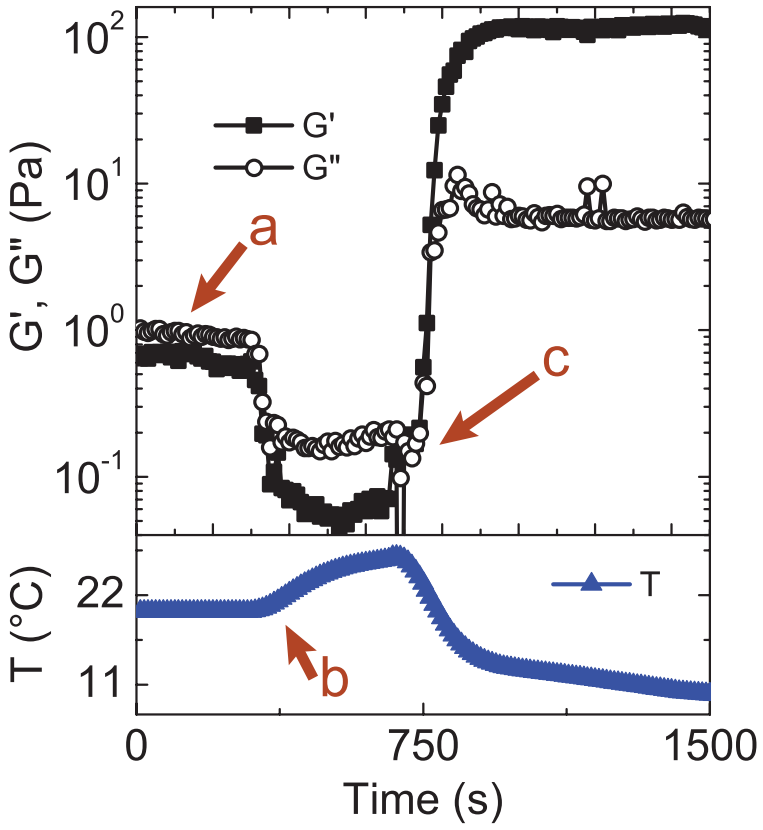

Figure 4.23: A sample of 1655 straight filaments initially at room temperature (a) is heated, triggering a decrease in the moduli but also starting to cause flagella to crosslink (b). Point c marks the temperature decreasing and the large difference in the moduli before and after the hot cycle due to the crosslinking that occurred while the temperature was raised.

a decrease while crosslinking is occurring is a sign that the flagella at this point are able to depolymerize if there is too much shear put on them. Essentially, the network is unable to store any elastic energy because as soon as strain is placed on a filament-filament connection, it simply breaks through depolymerization rather then deform the filaments. Point c marks when the temperature is lowered once again. After the temperature drop, the moduli for the sample have increased significantly. The loss modulus increases by an order of magnitude while the elastic modulus increases by two orders. This is the effect of the crosslinking that occurs at the elevated temperature. As the temperature decreases, enough crosslinks survive the high temperature long enough to become stable in the lower temperature regime and provide elasticity to the new network.

4.4 One Point Microrheology

4.4.1 Theory

Bulk rheology is an excellent tool to measure the material properties of a viscoelastic sample but it suffers from several limitations. The first limitation is that samples that are very low viscosity or extremely weakly elastic are extremely difficult to measure accurately. In a strain controlled rheometer, the torque on the detecting tool is the quantity that is measured, and are on the order of 10^{-8} Nm for most samples. Flagella samples at low concentrations and straight flagella samples simply dont provide enough of a torque to be reliably measured on bulk rheometers. One method for overcoming this problem is to increase the surface are of the measuring tool by using a different tool geometry such as the double gap. However, this only exacerbates the second drawback of bulk rheology, requiring a large sample volume. Using a cone plate tool with a diameter of 50 mm requires a sample volume of $\sim$ 800 µm.

For some experimental systems, this may be a trivial amount of sample to prepare, but for some types of flagella, it can be difficult to prepare this much sample at a high enough concentration to be measured. Specifically, block copolymer and long, polymerized filaments are difficult to prepare in bulk.

To circumvent these issues, we have used one point microrheology to supplement our bulk measurements. This technique involves doping a sample with a large number of fluorescent tracer particles that are non-interacting with the flagella. For bacterial flagella samples, we used 1 µm polystyrene beads impregnated with a fluorescein dye and typically diluted them into our sample so that between 100 and 200 beads were visible in any given field of view. Instead of an experimental apparatus to apply stress and/or strain to the sample like a rheometer, microrheology instead relies on the Brownian motion of the tracer particles and flagella background to apply very small strains to the network [123]. Because the force imparted on the network by the particle due to Brownian motion is very small, it is guaranteed to fall within the linear regime of rheology. To extract the rheological information, the tracer particles must have their position tracked over time and the mean squared displacement measured [124].

In a purely viscous sample, it is expected that the mean squared displacement of the tracer particles would grow linearly with time:

$$\left\langle r^2(t) \right\rangle = 4Dt \tag{4.9}$$

where D is the diffusion coefficient of the tracer particle as given by the Stokes-Einstein equation and the position is only measured in two dimensions. Likewise, if the particle was in a purely elastic material, it would not be able to diffuse, but would fluctuate in position around an equilibrium position with a spring-like potential [125]. The MSD would therefore

be given by

$$\left\langle r^2(t) \right\rangle = \frac{2k_{\mathrm{B}}T}{3\pi a G_0} \tag{4.10}$$

where a is the tracer particle radius, T is the temperature, and G_0 is the elastic modulus of the material [123]. In a viscoelastic material, the response can be frequency dependent and must therefore be generalized to a frequency dependent viscosity for both viscous and elastic moduli:

$$\left\langle \tilde{r}^2(s) \right\rangle = \frac{2k_{\mathrm{B}}T}{3\pi a s \tilde{G}(s)} \tag{4.11}$$

where s is the Laplace frequency, $\langle \tilde{r}^2(s) \rangle$ is the Laplace transform of the MSD, and $\tilde{G}(s)$ is the Laplace transform of the complex shear modulus, $G^*(\omega) = G'(\omega) + iG''(\omega)$. Equation 4.11 enables measuring G' and G'' by measuring the MSD of a diffusing tracer particle if the tracer particle is large enough to experience a homogenous sample [126]. In the case of a flagella solution, this means that the concentration must be high enough so that the average pore size in the network is smaller than the radius of the tracer particles.

4.4.2 Results

Microrheology is especially useful for working with low viscosity samples and samples with a small elastic modulus [123]. For bacterial flagella suspensions, straight filament samples and samples at a low concentration satisfy these conditions and benefit the most from using microrheology techniques. All of the results presented in this section were obtained by tracking 1 µm polystyrene microspheres impregnated with a fluorescent dye. The MSD for the beads and resulting rheological moduli were calculated using slightly modified MATLAB routines published by Kilfoil [127].

Microrheology results for straight filaments are shown in Figure 4.24. These results show that concentrations 4 mg/ml and higher, there is a solid-like regime at the high end of the

frequencies able to be measured with our apparatus. The high frequency cutoff in the data is limited by the frame rate of the camera used to acquire the images. Both 6 and 4 mg/ml then transition to a liquid-like regime at lower frequencies. This behavior is consistent with the dynamics experiments which showed that the straight filaments could reptate in the longitudinal direction unimpeded and therefore had a relatively short-lived cage lifetime. The results for 2 mg/ml show a liquid-like material at high frequencies. This suggests that 2 mg/ml is an insufficiently high concentration to form a spanning network of flagella able to elastically respond to deformation. The 2 mg/ml results do show a region of solid-like behavior at lower frequencies, but this result is a weak effect and would need to be replicated before concluding it is a real effect.

The magnitudes of the moduli measured with microrheology are approximately an order of magnitude greater than those measured with bulk rheology. It is unclear why this may be the case as the bulk measurements are made in the linear regime of strain at concentrations below the isotropic-nematic transition point. One potential source of error would be tracer bead-flagella interactions that could cause an artificial increase in the elastic modulus in microrheology, so different surface chemistries and compositions could be tested to see if results are reproducible. Conversely, if the flagella in bulk rheolgy experiments were to be in a nematic phase rather than the assume isotropic, the measured elastic modulus would be much lower than expected.

Experimental results for normal flagella are shown in Figure 4.25. Similar to straight filaments, normal flagella show high frequency solid-like behavior for higher concentrations. Both 6 and 15 mg/ml show this solid-like regime at high frequencies and liquid-like behavior at lower frequencies. The relaxation time of these suspensions follow a similar trend to the bulk measurements in that the higher the concentration, the longer the relaxation time. At lower concentrations of normal flagella, the response is entirely liquid-like over the measurable

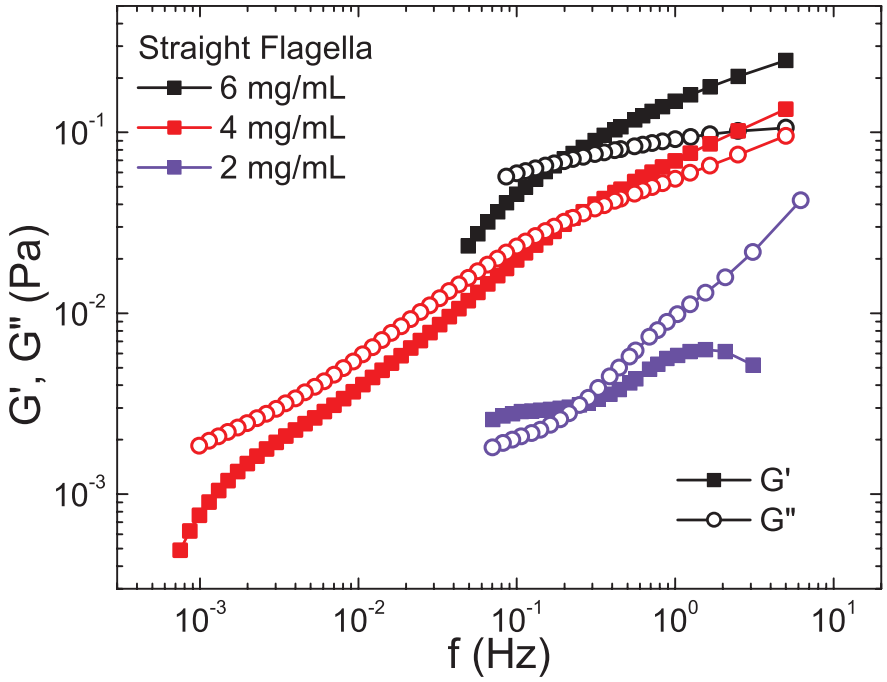

Figure 4.24: Microrheology results for straight filaments measured by tracking 1 µm polystyrene spheres as they diffuse through the network of flagella. Both 6 and 4 mg/ml samples show a high frequency solid-like regime and a low frequency liquid-like regime. The 2 mg/ml sample is mostly liquid like due to the extremely low concentration preventing the flagella network from responding elastically in response to deformation.

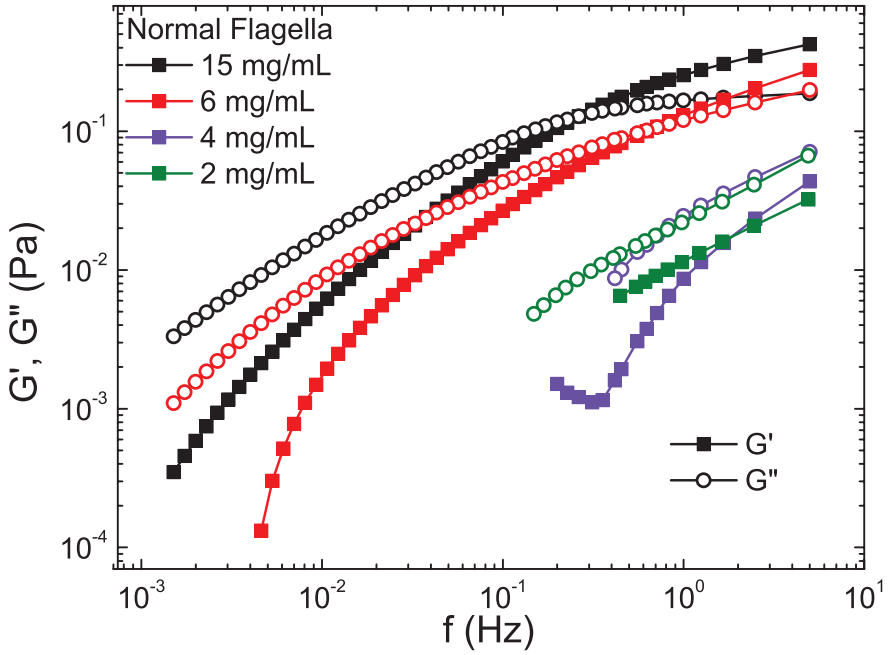

Figure 4.25: Microrheology results for normal filaments with a range of concentrations. Like straight filaments, the higher concentration samples show a high frequency solid-like response and a low frequency liquid-like response. At lower concentrations, such as 2 and 4 mg/ml, the concentration is insufficient to create an elastic response and the samples are fully liquid-like.

frequency range. This is another indication that low concentrations of flagella are unable to make a spanning entangled network that can respond elastically to deformation. Unlike straight flagella, 4 mg/ml is also liquid-like in normal samples. This may be due the shorter end to end distance of helical filaments as opposed to straight filaments with identical contour lengths. The shorter end to end distance may limit the number of nearest neighbors it is possible to become entangled with for normal filaments.

Another noteworthy result of normal flagella microrheology is that the magnitudes of the moduli for the 15 mg/ml sample are significantly less than that of bulk rheology. The order of magnitude difference between micro and bulk rheology may be due to the different ways helical flagella can respond elastically to deformation. It has been shown experimentally using optical tweezers that helical flagella, when stretched within the linear regime, act

effectively as a Hookean spring [81]. Another way that flagella can respond to deformation is through rigid rod buckling. Through buckling experiments, it has been shown that a strain of about 10% can be applied to the filament by a force of only 1 pN. However, in order to extend a filament a similar amount without the help of polymorphic transitions, it would take dramatically more force [81]. It is possible that using 1 µm diameter tracer beads is an insufficient size to properly probe this mode of elastic storage. The helical radius for normal filaments is rougly 0.2 µm, meaning peak to peak amplitude of the filament is 0.4 µm, a significant fraction of the size of our tracer particles. This could be alleviated by using larger tracer beads in future experiments.

The results of microrheological experiments performed on coiled flagella suspensions in 55% ethylene glycol are shown in Figure 4.26. Like normal filaments, with a sufficiently high concentration, solid-like response is observed at higher frequencies. The magnitude of the elastic modulus is similar in magnitude to that of normal filaments while the frequency range over which the response is solid-like extends to much lower frequencies. This much lower crossover frequency, corresponding to a much longer relaxation time for coiled filaments as compared to normal filaments. This is consistent with the results from bulk rheology which showed that coiled filaments had a very long relaxation time compared to normal flagella. The larger helical radius and shorter pitch must allow the coiled filaments to entangle very effectively with a sufficient concentration, making it difficult for the filament to reptate out of the cage of its nearest neighbors.

A feature of coiled microrheology results is that, similar to other flagella morphologies, once below a critical concentration, the sample behaves liquid-like over the entire frequency range. Coiled filaments are like normal filaments in this regard in that at 4 mg/ml the suspension behaves liquid-like and at 6 mg/ml the suspension is viscoelastic. Unlike normal filaments though, the 10 and 6 mg/ml results are very similar, with the 6 mg/ml sample being

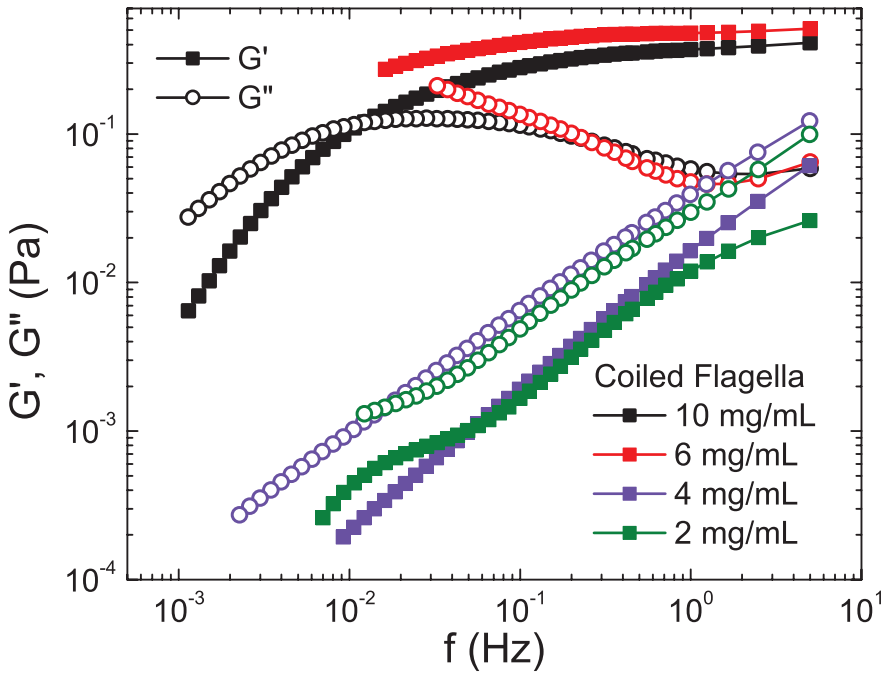

Figure 4.26: Microrheology results for 1103 filaments in the coiled state. Like normal filaments, high frequencies show a solid-like response while low frequencies show a liquid-like response. Coiled filaments have a much wider range of frequencies over which they are solid-like and therefore a much longer relaxation time. Again, if the concentration is too low, the samples are purely liquid-like such as 2 and 4 mg/ml in coiled samples.

slightly more elastic than the 10 mg/ml sample. This may be the result of experimental error in preparing samples. Because microrheology samples are just tens of µl in volume, a small error in combining components can make a significant difference in the final mixture. It is easy to incorrectly measure an amount of flagella when working with high concentrations due to the high viscosity of the sample. These experiments will need to be replicated in order to determine more accurately how the rheology of coiled filaments depends on concentration.

4.5 Conclusion

In conclusion, observing flagella dynamics showed how the shape of a filament affects the allowed type of diffusive motion. Straight filaments diffuse primarily in the longitudinal direction through direct translation in accordance with reptation theory. Conversely, normal filaments also diffuse in the longitudinal direction but, because of their helical shape, are unable to translate and instead must rotate around the long axis of the filament in order to affect a movement in the long axis. Block copolymer dynamics show that, due to the filaments geometry, it is mostly unable to reptate beyond the cage defined by the nearest neighbor filaments. The long axis of the helical side of the filament does not align with the long axis of the straight side of the filament, preventing either from diffusing along that axis. A block copolymer network with a sufficiently high concentration essentially is crosslinked due to the suppression of long scale diffusion.

Bulk rheology measurements show that straight flagella suspensions are very weakly elastic and have a very low viscosity as well. Normal helical flagella show very concentration dependent viscoelasticity. The relaxation time of the network of helical filament increased as the concentration increased, as did the storage and loss moduli. Another parameter of the shape of the flagella found to impact the rheology is the average length of helical filaments.

Longer normal filaments made through in vitro polymerization have a significantly longer relaxation time than purified filaments but maintained identical high frequency behavior. Additionally, changing the helical shape parameters proved to change the rheological properties. Comparing filaments in the coiled state and the normal state showed that the coiled filaments had a much longer relaxation time as well as a much higher elastic modulus than the normal flagella. Finally, bulk rheology measurements showed that block copolymer filaments have no measurable relaxation time until the sample concentration is lowered below 2.5 mg/ml. This is because reptation is suppressed as observed in the dynamics observations and the network is unable to rearrange to relax an applied strain. The block copolymers also showed a clear gel transition in both the frequency dependent and large strain rheology.

Finally, microrheology experiments were performed on several differently shaped flagellar filaments. Because of the low viscosity and elasticity in straight flagella networks, microrheology is an ideal way to measure rheological properties of these suspensions. Microrheology showed that the straight filament suspensions had viscoelastic properties where the higher measurable frequencies had a solid-like response and lower frequencies had a liquid-like response. Below a critical concentration, the flagella behaved strictly liquid-like because the flagellar network is sparse enough that filaments are not entangled and therefore provide little to no elasticity. The magnitude of the moduli for straight flagella are much greater than for bulk measurements. This could be due either to bead-flagella interactions causing increased elastic moduli or potential nematic ordering in the bulk samples, lowering the elastic modulus.

Normal filaments show a similar trend in that high frequencies are solid-like and lower frequencies liquid-like. The relaxation time also increases with concentration like bulk measurements. Also, like straight filaments, normal flagella samples below a critical concentration are purely liquid-like. The magnitude of the moduli are lower than bulk rheology measu-

rements, potentially due to the added size scales of the flagella (helical radius and pitch) necessitating a larger sized tracer particle so that it can experience a more isotropic local environment. Coiled filament measurements show this same reduction in modulus magnitude with microrheology as opposed to bulk measurements. Because this reduction is present in both helical forms of flagella, it may be a general feature of helical colloidal particles that these extra size considerations must be taken into account when selecting tracer particles. Coiled filaments also show an enhanced elasticity compared to normal filaments as well as a much longer relaxation time; both in agreement with bulk measurements.

In this chapter, we have explored ways in which the properties of bacterial flagella create a unique colloidal particle in suspension. Flagella are an excellent model of a helical particle because they are large enough to study individual dynamics while being small enough to create bulk viscoelastic materials. We have shown that changing the shape of the filaments can dramatically change the material properties of the resulting suspensions. These changes range from changing the moduli by orders of magnitude, changing the relaxation time, and changing the particle shape of a sample by changing an environmental condition such as temperature. Future work with bacterial flagella could include studying temperature induced transitions using microrheology, embedding flagella into a gel and inducing shape changes to change the gel behavior or size, or investigating mixtures of more than one shape of flagella into a suspension. Going forward, bacterial flagella can be used as a model system for helical colloidal particles that can be used to create new materials with adjustable material properties.

Bibliography

[1] X.-F. Tang, Z.-G. Yang, and W.-J. Wang, Colloids and Surfaces A: Physicochemical and Engineering Aspects **360**, 99 (2010).

[2] F. Pichot, J. R. Pitts, and B. A. Gregg, Langmuir **16**, 5626 (2000).

[3] G. C. Barker and M. J. Grimson, Food Hydrocolloids **3**, 345 (1989).

[4] E. Dickinson, Advances in Colloid and Interface Science **165**, 7 (2011).

[5] H. Goff, International Dairy Journal **7**, 363 (1997).

[6] N. El-Labban, Journal of Periodontal Research **5**, 315 (1970).

[7] C. V. Taylor, Journal of Experimental Zoology **37**, 259 (1923).

[8] W. C. K. Poon, *Colloidal Suspensions* (Clarendon Press, Oxford, 2012).

[9] L. Jaeken, IUBMB Life **59**, 127 (2007).

[10] R. C. Weisenberg, Science **177**, 1104 LP (1972).

[11] K. C. Neuman and A. Nagy, Nature Methods **5**, 491 (2008).

[12] D. A. Fletcher and R. D. Mullins, Nature **463**, 485 (2010).

[13] A. Ward, F. Hilitski, W. Schwenger, D. Welch, A. W. C. Lau, V. Vitelli, L. Mahadevan, and Z. Dogic, Nature Materials **14**, 583 (2015).

[14] L. D. Landau, E. M. Lifshitz, and L. E. Reichl, Physics Today **34**, 74 (1981).

[15] K. A. Dill and S. Bromberg, *Molecular Driving Forces: Statistical Thermodynamics in Biology, Chemistry, Physics, and Nanoscience*, 2nd ed. (Garland Science, 2010) p. 784.

[16] M. Doi and S. F. Edwards, *The Theory of Polymer Dynamics* (Clarendon Press, 1986).

[17] C. G. Baumann, S. B. Smith, V. A. Bloomfield, and C. Bustamante, Proceedings of the National Academy of Sciences **94**, 6185 (1997).

[18] F. Gittes, B. Mickey, J. Nettleton, and J. Howard, Journal of Cell Biology **120**, 923 (1993).

[19] X. Wang, P. Montero Llopis, and D. Z. Rudner, Nature Reviews. Genetics **14**, 191 (2013).

[20] T. W. Traut, Molecular and Cellular Biochemistry **140**, 1 (1994).

[21] P. G. de Gennes, The Journal of Chemical Physics **55**, 572 (1971).

[22] M. Doi and S. F. Edwards, Journal of the Chemical Society, Faraday Transactions 2: Molecular and Chemical Physics **74**, 1789 (1978).

[23] P.-G. De Gennes, *Scaling Concepts in Polymer Physics* (Cornell University Press, 1979).

[24] D. E. Smith, T. T. Perkins, and S. Chu, Physical Review Letters **75**, 4146 (1995).

[25] T. C. B. McLeish, Advances in Physics **51**, 1379 (2002).

[26] T. G. Mason, A. Dhople, and D. Wirtz, Macromolecules **31**, 3600 (1998).

[27] X. Zhu, B. Kundukad, and J. R. C. Van Der Maarel, Journal of Chemical Physics **129**, 1 (2008).

[28] D. T. N. Chen, Q. Wen, P. A. Janmey, J. C. Crocker, and A. G. Yodh, Annual Review of Condensed Matter Physics **1**, 301 (2010).

[29] G. J. Doherty and H. T. McMahon, Annual Review of Biophysics **37**, 65 (2008).

[30] S. Burlacu, P. A. Janmey, and J. Borejdo, American Journal of Physiology - Cell Physiology **262**, C569 (1992).

[31] C. P. Brangwynne, G. H. Koenderink, E. Barry, Z. Dogic, F. C. MacKintosh, and D. A. Weitz, Biophysical Journal **93**, 346 (2007).

[32] A. Ott, M. Magnasco, A. Simon, and A. Libchaber, Physical Review E **48**, R1642 (1993).

[33] S. Kaufmann, J. Käs, W. Goldmann, E. Sackmann, and G. Isenberg, FEBS Letters **314**, 203 (1992).

[34] J. Käs, H. Strey, and E. Sackmann, Nature **368**, 226 (1994).

[35] J. Käs, H. Strey, J. Tang, D. Finger, R. Ezzell, E. Sackmann, and P. Janmey, Biophysical Journal **70**, 609 (1996).

[36] K. R. Ayscough, Current Opinion in Cell Biology **10**, 102 (1998).

[37] J. H. Hartwig and D. J. Kwiatkowski, Current Opinion in Cell Biology **3**, 87 (1991).

[38] T. D. Pollard and J. A. Cooper, Annual Review of Biochemistry **55**, 987 (1986).

[39] B. Hinner, M. Tempel, E. Sackmann, K. Kroy, and E. Frey, Physical Review Letters **81**, 2614 (1998).

[40] R. Tharmann, M. M. A. E. Claessens, and A. R. Bausch, Physical Review Letters **98**, 8 (2007).

[41] F. C. MacKintosh, J. Käs, and P. A. Janmey, Physical Review Letters **75**, 4425 (1995).

[42] R. B. Maccioni and V. Cambiazo, Physiological Reviews **75**, 835 (1995).

[43] E. Mandelkow and E. M. Mandelkow, Current Opinion in Cell Biology **7**, 72 (1995).

[44] Y.-C. Lin, G. H. Koenderink, F. C. Mackintosh, and D. A. Weitz, Macromolecules **40**, 7714 (2007).

[45] H. C. Berg, Nature **245**, 380 (1973).

[46] H. C. Berg and D. A. Brown, Nature **239**, 500 (1972).

[47] R. Kamiya and S. Asakura, Journal of Molecular Biology **106**, 167 (1976).

[48] M. D. Manson, P. Tedesco, H. C. Berg, F. M. Harold, and C. Van der Drift, Proceedings of the National Academy of Sciences **74**, 3060 (1977).

[49] E. Purcell, American Journal of Physics **45**, 3 (1977).

[50] E. M. Purcell, Proceedings of the National Academy of Sciences **94**, 11307 (1997).

[51] L. Turner, W. S. Ryu, and H. C. Berg, Journal of Bacteriology **182**, 2793 (2000).

[52] M. Silverman and M. Simon, Journal of Bacteriology **118**, 750 (1974).

[53] M. Kim, J. C. Bird, A. J. Van Parys, K. S. Breuer, and T. R. Powers, Proceedings of the National Academy of Sciences **100**, 15481 (2003).

[54] M. Kim and T. R. Powers, Physical Review E **69**, 1 (2004).

[55] H. Flores, E. Lobaton, S. Méndez-Diez, S. Tlupova, and R. Cortez, Bulletin of Mathematical Biology **67**, 137 (2005).

[56] S. Kudo, Y. Magariyama, and S. Aizawa, Nature **346**, 677 (1990).

[57] H. C. Berg, Biophysical Journal **68**, 163S (1995).

[58] H. C. Berg and L. Turner, Biophysical Journal **65**, 2201 (1993).

[59] R. Vogel and H. Stark, Physical Review Letters **110**, 158104 (2013).

[60] R. Vogel and H. Stark, The European Physical Journal. E, Soft Matter **35**, 15 (2012).

[61] L. Onsager, Annals of the New York Academy of Sciences **51**, 627 (1949).

[62] M. P. Lettinga, Z. Dogic, H. Wang, and J. Vermant, Langmuir **21**, 8048 (2005).

[63] Y. Yang, E. Barry, Z. Dogic, and M. F. Hagan, Soft Matter **8**, 707 (2012).

[64] A. Kuijk, A. Van Blaaderen, and A. Imhof, Journal of the American Chemical Society **133**, 2346 (2011).

[65] L. Zhang, J. J. Abbott, L. Dong, B. E. Kratochvil, D. Bell, and B. J. Nelson, Applied Physics Letters **94**, 064107 (2009).

[66] L. Zhang, E. Ruh, D. Grützmacher, L. Dong, D. J. Bell, B. J. Nelson, and C. Schönenberger, Nano Letters **6**, 1311 (2006).

[67] J. T. Pham, J. Lawrence, D. Y. Lee, G. M. Grason, T. Emrick, and A. J. Crosby, Advanced Materials **25**, 6703 (2013).

[68] B. H. Oliveira, M. R. Silva, C. J. M. Braga, L. M. Massis, L. C. S. Ferreira, M. E. Sbrogio-Almeida, and M. Takagi, Brazilian Journal of Chemical Engineering **28**, 575 (2011).

[69] C. R. Calladine, Nature **255**, 121 (1975).

[70] C. Calladine, Journal of Molecular Biology **118**, 457 (1978).

[71] C. R. Calladine, B. F. Luisi, and J. V. Pratap, Journal of Molecular Biology **425**, 914 (2013).

[72] A. Ghosh and P. Fischer, Nano Letters **9**, 2243 (2009).

[73] K. Hasegawa, I. Yamashita, and K. Namba, Biophysical Journal **74**, 569 (1998).

[74] S. Kanto, H. Okino, S. Aizawa, and S. Yamaguchi, Journal of Molecular Biology **219**, 471 (1991).

[75] E. O'Brien and P. M. Bennett, Journal of Molecular Biology **70**, 133 (1972).

[76] K. Yonekura, S. Maki-Yonekura, and K. Namba, Nature **424**, 643 (2003).

[77] K. Namba and F. Vonderviszt, Quarterly Reviews of Biophysics **30**, 1 (1997).

[78] I. Yamashita, K. Hasegawa, H. Suzuki, F. Vonderviszt, Y. Mimori-Kiyosue, and K. Namba, Nature Structural and Molecular Biology **5**, 125 (1998).

[79] S. E. Spagnolie and E. Lauga, Physical Review Letters **106**, 058103 (2011).

[80] E. Lauga and T. R. Powers, Reports on Progress in Physics **72**, 96601 (2009).

[81] N. C. Darnton and H. C. Berg, Biophysical Journal **92**, 2230 (2007).

[82] H. HOTANI, "Micro-Video Study of Moving Bacterial Flagellar Filaments .3. Cyclic Transformation Induced by Mechanical Force," (1982).

[83] R. Kamiya and S. Asakura, "Flagellar Transformations at Alkaline pH," (1976).

[84] E. Hasegawa, R. Kamiya, and S. Asakura, Journal of Molecular Biology **160**, 609 (1982).

[85] H. Hotani, BioSystems **12**, 325 (1980).

[86] M. Seville, T. Ikeda, and H. Hotani, BioSystems **332**, 260 (1993).

[87] S. Asakura, G. Eguchi, and T. Iino, Journal of Molecular Biology **10**, 42 (1964).

[88] T. Ikeda, S. Asakura, and R. Kamiya, Journal of Molecular Biology **209**, 109 (1989).

[89] T. Ikeda, S. Asakura, and R. Kamiya, Journal of Molecular Biology **184**, 735 (1985).

[90] H. Kondoh and M. Yanagida, Journal of Molecular Biology **96**, 641 (1975).

[91] S. Asakura and T. Iino, Journal of Molecular Biology **64**, 251 (1972).

[92] J. DeChancie and K. N. Houk, Journal of the American Chemical Society **129**, 5419 (2007).

[93] S. M. Block, K. a. Fahrner, and H. C. Berg, Journal of Bacteriology **173**, 933 (1991).

[94] H. Hotani, Journal of Molecular Biology **106**, 151 (1976).

[95] R. Chakrabarti and C. E. Schutt, Gene **274**, 293 (2001).

[96] M. Jackson and H. H. Mantsch, Biochimica et Biophysica Acta (BBA)/Protein Structure and Molecular **1078**, 231 (1991).

[97] T. Arakawa, Y. Kita, and S. N. Timasheff, Biophysical Chemistry **131**, 62 (2007).

[98] A. Kaiser, O. Ismailova, A. Koskela, S. E. Huber, M. Ritter, B. Cosenza, W. Benger, R. Nazmutdinov, and M. Probst, Journal of Molecular Liquids **189**, 20 (2014).

[99] R. Vogel and H. Stark, The European Physical Journal. E, Soft Matter **33**, 259 (2010).

[100] G. Gomori, Proceedings of the Society for Experimental Biology and Medicine Society for Experimental Biology and Medicine New York NY **62**, 33 (1946).

[101] R. G. Bates and H. B. Hetzer, Journal of Physical Chemistry **65**, 667 (1961).

[102] C. A. Vega, R. A. Butler, B. Perez, and C. Torres, Journal of Chemical & Engineering Data **30**, 376 (1985).

[103] R. N. Goldberg, N. Kishore, and R. M. Lennen, Journal of Physical and Chemical Reference Data **31**, 231 (1999).

[104] N. E. Good, G. D. Winget, W. Winter, T. N. Connolly, S. Izawa, and R. M. M. Singh, Biochemistry **5**, 467 (1966).

[105] N. Watari and R. G. Larson, Biophysical Journal **98**, 12 (2010).

[106] F. Z. Temel and S. Yesilyurt, in *2011 IEEE International Conference on Mechatronics* (Ieee, 2011) pp. 342–347.

[107] J. T. Pham, J. Lawrence, G. M. Grason, T. Emrick, and A. J. Crosby, Physical Chemistry Chemical Physics **16**, 10261 (2014).

[108] J. T. Pham, A. Morozov, A. J. Crosby, A. Lindner, and O. du Roure, Physical Review E **92**, 1 (2015).

[109] M. Lattuada and T. A. Hatton, Nano Today **6**, 286 (2011).

[110] T. Sanchez, D. T. N. Chen, S. J. Decamp, M. Heymann, and Z. Dogic, Nature **491**, 431 (2012).

[111] T. Sanchez, D. Welch, D. Nicastro, and Z. Dogic, Science **333**, 456 (2011).

[112] M. Doi and S. F. Edwards, Journal of the Chemical Society, Faraday Transactions 2: Molecular and Chemical Physics **74**, 918 (1978).

[113] Y. Han, A. M. Alsayed, M. Nobili, J. Zhang, T. C. Lubensky, and A. G. Yodh, Science **314**, 626 (2006).

[114] S. Yardimci, *Networks Formed by Rigid Filaments of Tunable Shape*, Ph.D. thesis, Brandeis University (2014).

[115] P. Herh, J. Tkachuk, S. Wu, M. Bernzen, and B. Rudolph, American Laboratory **30**, 12 (1998).

[116] D. D. Braun and M. R. Rosen, *Rheology Modifiers Handbook: Practical Use and Applilcation* (Elsevier Science, 2013).

[117] A. Rao, *Rheology of Fluid and Semisolid Foods: Principles and Applications*, Food Engineering Series (Springer US, 2010).

[118] P. F. G. Banfill, Rheology Reviews **2006**, 61 (2006).

[119] M. A. Meyers and K. K. Chawla, *Mechanical behavior of materials*, Vol. 2 (Cambridge University Press, Cambridge, 2009).

[120] K. Hyun, S. H. Kim, K. H. Ahn, and S. J. Lee, Journal of Non-Newtonian Fluid Mechanics **107**, 51 (2002).

[121] E. Barry, Z. Hensel, Z. Dogic, M. Shribak, and R. Oldenbourg, Physical Review Letters **96**, 1 (2006).

[122] K. Hyun, M. Wilhelm, C. O. Klein, K. S. Cho, J. G. Nam, K. H. Ahn, S. J. Lee, R. H. Ewoldt, and G. H. McKinley, Progress in Polymer Science **36**, 1697 (2011).

[123] P. Cicuta and A. M. Donald, Soft Matter **3**, 1449 (2007).

[124] J. Xu, V. Viasnoff, and D. Wirtz, Rheologica Acta **37**, 387 (1998).

[125] T. Mason and D. A. Weitz, Physical Review Letters **74**, 1250 (1995).

[126] M. Bellour, M. Skouri, J.-P. Munch, and P. Hébraud, The European Physical Journal E **8**, 431 (2002).

[127] V. Pelletier, N. Gal, P. Fournier, and M. L. Kilfoil, Physical Review Letters **102**, 100 (2009).